The role of mTOR complex 1 in skeletal muscle

Inauguraldissertation

zur

Erlangung der Würde eines Doktors der Philosophie

vorgelegt der

Philosophisch-Naturwissenschaftlichen Fakultät

der Universität Basel

von

Klaas Emilio Antonius Anna Romanino

aus Frauenfeld (TG), Belgien und Italien

Biozentrum der Universität Basel

Basel, September 2012

Genehmigt von der Philosophisch-Naturwissenschaftlichen Fakultät

auf Antrag von

Prof. Dr. Markus A. Rüegg

Prof. Dr. Christoph Handschin

Basel, den 18.09.2012

Prof. Dr. Jörg Schibler

Dekan der Philosophisch-Naturwissenschaftlichen Fakultät

creative commons

Namensnennung-Keine kommerzielle Nutzung-Keine Bearbeitung 2.5 Schweiz

---

Sie dürfen:

das Werk vervielfältigen, verbreiten und öffentlich zugänglich machen

Zu den folgenden Bedingungen:

Namensnennung. Sie müssen den Namen des Autors/Rechteinhabers in der von ihm festgelegten Weise nennen (wodurch aber nicht der Eindruck entstehen darf, Sie oder die Nutzung des Werkes durch Sie würden entlohnt).

Keine kommerzielle Nutzung. Dieses Werk darf nicht für kommerzielle Zwecke verwendet werden.

Keine Bearbeitung. Dieses Werk darf nicht bearbeitet oder in anderer Weise verändert werden.

- Im Falle einer Verbreitung müssen Sie anderen die Lizenzbedingungen, unter welche dieses Werk fällt, mitteilen. Am Einfachsten ist es, einen Link auf diese Seite einzubinden.
- Jede der vorgenannten Bedingungen kann aufgehoben werden, sofern Sie die Einwilligung des Rechteinhabers dazu erhalten.
- Diese Lizenz lässt die Urheberpersönlichkeitsrechte unberührt.

Quelle: http://creativecommons.org/licenses/by-nc-nd/2.5/ch/ Datum: 3.4.2009

I dedicate this work to
my mother and my father,
for their endless support
in the past and the present.

TABLE OF CONTENTS

ABSTRACT

An important factor in energy and nutrient pathways is the mammalian target of rapamycin complex 1 (mTORC1). The multiprotein complex, with the central component mTOR, regulates cell growth and survival. Mice with muscle-specific inactivation of mTORC1 die after 4-6 months of respiratory failure caused by a progressive myopathy. Next to structural changes, like fiber atrophy, the deficiency of mTORC1 in muscle also causes metabolic alterations. Muscles of mTORC1-deficient mice show a decrease in oxidative capacity and fatty acid metabolism, caused by a reduced transcription of several mitochondrial genes. This is due to a reduced transcription of the master regulator of mitochondrial biogenesis, PGC-1α. Interestingly, transgenic or pharmacological increase of PGC-1α levels restores mitochondrial function in mice with ablated mTORC1 activity, but does not prevent the myopathy.

Additional metabolic changes in mTORC1-deficient muscle include glucose metabolism. Mice with inactivated mTORC1 in muscle show accumulations of glycogen, accompanied by a significant reduction of glucose uptake and glycolysis. The glycogen content is regulated through the activation of PKB/Akt, independently of PGC-1α. The reduction of glucose metabolism, in turn, correlates with an upregulation of the class II HDACs.

Besides inefficient nutrient uptake, mice lacking muscle mTORC1 increase their energy expenditure, which might be due to an upregulation of UCPs. Together, these metabolic changes lead to a protection against diet-induced obesity and hepatic steatosis. Thus, the mTORC1 is a central hub of metabolic pathways in skeletal muscle affecting systemic energy homeostasis.

INTRODUCTION

Rapamycin is a metabolite of the bacteria *Streptomyces hygroscopicus*, which were discovered in a soil sample from one of the Easter Islands in 1965 (Vezina et al., 1975). The compound was named after the small island Rapa Nui where the said sample was taken from. At first, rapamycin was only described for having an antifungal effect (Sehgal et al., 1975). However, the first description set in motion a cascade of events that resulted into an immunosuppressive drug that has been on the market for several years. The molecular target of rapamycin is a protein called TOR (target of rapamycin). It is a serine/threonine protein kinase and is evolutionary highly conserved from yeast to humans. Its mammalian counterpart is called mTOR (mammalian target of rapamycin) and can assemble into two distinct protein complexes (Wullschleger et al., 2006). mTOR complex 1 (mTORC1) is rapamycin sensitive and is composed of mTOR, regulatory-associated protein of mTOR (raptor), mLST8 and the later identified partners PRAS40 and DEPTOR (Figure 1) (Peterson et al., 2009; Thedieck et al., 2007). Originally, the second protein complex mTOR complex 2 (mTORC2) was described as rapamycin-insensitive, as acute treatment with rapamycin did not affect its activity. Yet, later studies have shown that in certain cell types chronic rapamycin exposure inhibits the new assembly of the complex, while not affecting pre-existing mTORC2 (Sarbassov et al., 2006). mTORC2 is formed out of mTOR, rapamycin-insensitive companion of mTOR (rictor), mLST8, DEPTOR, mSIN1 and protor1/2 (Laplante and Sabatini, 2012).

Substrates regulated by the mTOR complexes

Initially, TOR in yeast was found to regulate cell size and later mTOR was discovered to also regulate growth in mammalian cells (Wullschleger et al., 2006). The physiological importance of mTOR became apparent by the fact that mice deficient for mTOR or raptor die shortly after implantation at E5.5-6.5 (Gangloff et al., 2004; Guertin et al., 2006; Murakami et al., 2004).

Similarly, mice deficient for mTORC2 activity by the knockout of rictor or mSIN1, also die embryonically but slightly later at E11.5 (Guertin et al., 2006; Jacinto et al., 2006; Shiota et al., 2006). Next to the developmental importance, over the years the number of cellular processes dependent on mTOR signalling increased dramatically and it was discovered that the two mTOR complexes each signal via distinct effector pathways. mTORC1 is involved in protein synthesis, cell growth, autophagy, cell cycle progression and energy metabolism. mTORC2 is shown to affect mainly cytoskeletal organization and cell survival (Laplante and Sabatini, 2012).

mTORC2 phosphorylates a key regulator of cell survival, Protein kinase B (PKB, also known as Akt), at the serine site S473 (Sarbassov et al., 2005). Phosphorylation of S473 stimulates PKB/Akt phosphorylation at the threonine residue T308 by phosphoinositide-dependent protein kinase-1 (PDK1) and results in full PKB/Akt activation. Two additional kinases regulated by mTORC2 are serum- and glucocorticoid-induced protein kinase 1 (SGK1) and protein kinase C α (PKCα) (Figure 1). SGK1 affects ion transport and growth in different cell lines (Garcia-Martinez and Alessi, 2008). PKCα is known to control cytoskeletal organization by regulating actin dynamics *in vitro* (Sarbassov et al., 2004). However, so far the effect of mTORC2 on actin organization was not yet confirmed *in vivo*.

The two best-characterized substrates of the mTORC1 are eIF4E-binding protein 1 (4E-BP1) and ribosomal protein S6 kinase (S6K). Both regulate mRNA translation, hence promote protein synthesis, and are directly phosphorylated by mTORC1 (Ma and Blenis, 2009). These two effectors are believed to be the principal pathway through which mTORC1 promotes growth in all cells. On top of translational regulation, S6K has a second crucial role in mTOR signaling. Constitutive activation of mTORC1 induces a negative feedback loop over S6K to attenuate phosphoinositide 3-kinase (PI3K) via inhibition of insulin receptor substrate 1 (IRS1) (Figure 1)

(Harrington et al., 2004). In particular, S6K was shown to directly phosphorylate IRS1 and indirectly also regulate its transcription (Um et al., 2004).

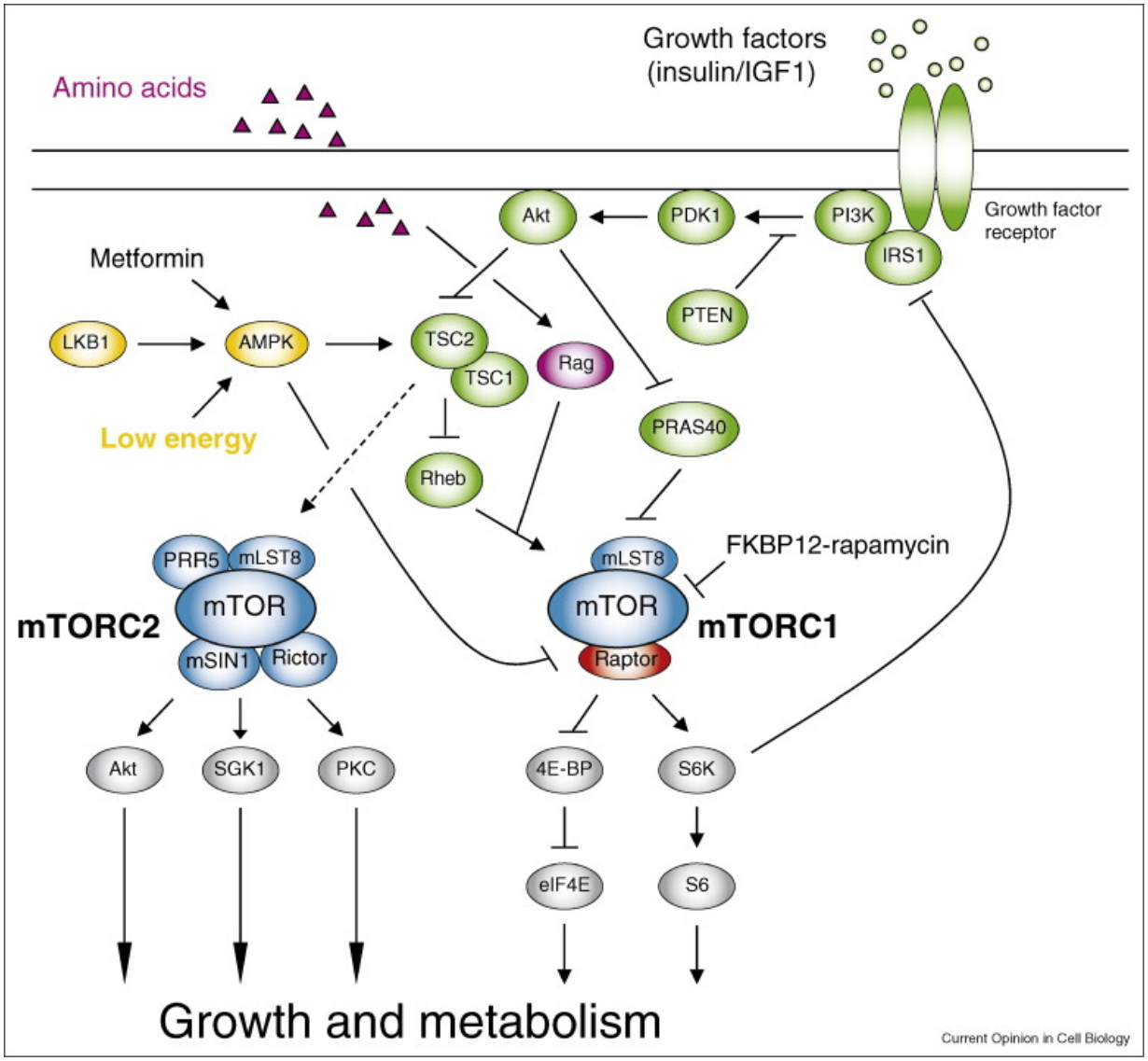

Figure 1. The mTOR signaling pathway. (Polak and Hall, 2009)

Next to activating the translational regulators, mTORC1 also influences growth by inhibiting autophagy, the central degradation process in cells. In most cell types, mTORC1 directly phosphorylates and supresses a kinase complex called Ulk1/Atg13/FIP200, which is required to initiate autophagy (Hosokawa et al., 2009; Kim et al., 2011). Through this complex, mTORC1

regulates the formation of autophagosomes that then engulf cytoplasmic proteins or organelles and fuse to lysosomes, leading to their degradation.

Over the last decade several other targets of mTORC1 were discovered. Of particular interest is that mTORC1 controls mitochondrial gene expression and function (Schieke et al., 2006). Recent work demonstrates that mTORC1 interacts indirectly with the main mitochondrial gene regulator, peroxisome proliferator-activated receptor γ coactivator 1α (PGC-1α) over the transcription factor yin-yang 1 (YY1) (Blattler et al., 2012b; Cunningham et al., 2007).

Peroxisome proliferator-activated receptor gamma coactivator-1α (PGC-1α)

PGC-1α is the best characterized member of the PGC-1 family, which is composed of two additional members: PGC-1β and PGC-1 related coactivator (PRC) (Lin et al., 2005). PGC-1α is found in all mammals and was originally identified in brown adipose tissue (BAT) (Puigserver et al., 1998). In general, PGC-1α is highly expressed in tissues with high energy requirements like skeletal muscle, heart, liver, brain, pancreas, kidney and white adipose tissue (WAT). Across the different tissues, stressors such as exercise, cold or fasting are supposed to lead to PGC-1α activation (Handschin and Spiegelman, 2006). Its role is best studied in skeletal muscle, where PGC-1α was demonstrated to be highly expressed in oxidative slow-twitch (type I) muscles (Lin et al., 2002). PGC-1α was shown to be a transcriptional co-activator that controls different processes including mitochondrial biogenesis, skeletal muscle fiber-type determination, angiogenesis and fatty acid oxidation. Its most prominent role, however, is to regulate a large number of transcription factors, including, among other, PPARα, PPARγ, ERRα, NRF-1 and 2, GABP, TFAM, all implicated in mitochondrial biogenesis and oxidative phosphorylation (Fernandez-Marcos and Auwerx, 2011).

Like mTOR, PGC-1α is thought to be a central integrator of external signals. It is known to be regulated on a transcriptional and a post-transcriptional level (Fernandez-Marcos and Auwerx,

2011). The PGC-1α promoter contains binding sites for MEF2, FOXO1, ATF2 and CREB. They are, in turn, modulated by different signaling pathways, such as insulin, cytokines, exercise, cold and glucagon. Post-transcriptionally, PGC-1α was demonstrated to be regulated by phosphorylation, acetylation, methylation and ubiquitination. AMPK and p38 MAPK are the best-characterized protein kinases known to target PGC-1α (Jager et al., 2007; Puigserver et al., 2001). An additional kinase which was shown to inhibit PGC-1α activity, is PKB/Akt, downstream of the insulin pathway (Li et al., 2007). Binding of PGC-1α to SIRT1 leads to its deacetylation and its subsequent activation (Canto et al., 2009). Silent information regulator 1 (SIRT1) is a newly discovered deacetylase that seems to play an important role in aging and cancer induction in mice (Gerhart-Hines et al., 2007).

Regulation of the mTOR pathway

One important function of mTORC1 is to sense growth factors to regulate cell growth (Polak and Hall, 2009). In particular, binding of insulin or insulin-like growth factors (IGFs) to their receptors leads to recruitment and phosphorylation of IRS-1 and activation of the PI3K signaling pathway (Figure 1) (Martin and Hall, 2005). At the cell membrane, PI3K controls the activity of PDK1, the kinase of PKB/Akt. Upon activation, PKB/Akt also translocates to the membrane where is gets phosphorylated and subsequently signals to mTORC1 as described below. Thus with regard to the ability of mTORC2 to phosphorylate PKB/Akt, PKB/Akt acts both up- and downstream of mTORC1. Activation of PKB/Akt triggers the inhibition of the tuberous sclerosis complex 1 (TSC1) and tuberous sclerosis complex 2 (TSC2). Subsequently, the TSC1/TSC2 complex releases its inactivation of the small GTPase ras homolog enriched in brain (Rheb). Rheb is a direct activator of mTORC1 (Figure 1) (Inoki et al., 2003; Long et al., 2005). Next to inhibition of the TSC complex, PKB/Akt also regulates mTORC1 in a TSC-independent manner. In response to growth factors, PKB/Akt inhibits Proline-rich Akt substrate 40kDa (PRAS40) by phosphorylating it. PRAS40, in turn, binds raptor and thereby directly inhibits the mTORC1

(Sancak et al., 2007; Thedieck et al., 2007). Besides insulin and IGF-1, the energy state of a cell also influences mTOR activity. Cells with low energy levels show a high AMP/ATP ratio. This activates the adenosine monophosphate-activated protein kinase (AMPK). AMPK influences mTORC1 activity in two different ways. First, it can phosphorylate TSC2 which results in an increase of its GAP activity towards Rheb, thus inhibiting mTORC1 (Inoki et al., 2003). Secondly, it directly inhibits mTORC1 by the phosphorylation of raptor (Figure 1) (Sancak et al., 2008). Amino acids were identified to stimulate the kinase activity of mTORC1 over the Rag GTPases (Figure 1). The Rag proteins do not directly regulate mTORC1 activity, but seem to promote the intracellular localization of mTOR to a compartment that also contains its activator Rheb (Sancak et al., 2008).

mTORC1 signaling in skeletal muscle

Skeletal muscle is an organ in which cell size is highly dynamic and of key importance for its function. The size of a muscle adapts rapidly in response to external stimuli, age or pathological situations. To elucidate the function of the mTOR pathway specifically in skeletal muscle several transgenic mouse lines have been developed over the last few years. The two most important publications focusing on the mTOR pathway in skeletal muscle used the Cre-loxP recombination system. LoxP sites were either introduced into the *mTOR* or the *rptor* locus, respectively, and the mice carrying these floxed genes were crossed with mice transgenically expressing Cre under the human skeleton actin (HSA) promotor. HSA is specifically expressed in myotubes and has a temporal expression onset just after myotube fusion (Schwander et al., 2003). Therefore, skeletal muscle-specific knockout mice for mTOR (Risson et al., 2009) or raptor (called RAmKO mice, Bentzinger et al., 2008, see appendix) were obtained upon such a breeding scheme. Both transgenic mouse lines are undistinguishable from their control littermates at birth but suffer from progressive atrophy and die after 4-6 months. Next to the myopathy both mouse models with skeletal muscle-specific inactivation of mTORC1 show different metabolic changes in their

muscles. The oxidative capacity is dramatically impaired and they accumulate significant amounts of glycogen.

The goal of this study is to further characterize mTORC1 signaling in skeletal muscle. In a recent publication we could show that the reduced oxidative capacity in different mouse models with inactivated mTORC1 is due to the reduced transcription of PGC-1α (see publication 1). In a second part, we analyzed the systemic metabolic changes that result from the specific inactivation of mTORC1 in skeletal muscle (see publication 2). Finally, in order to solve the open question of the premature death of RAmKO mice we carried out metabolic analysis of their blood (see additional findings). In addition to the confirmation of the importance of mTORC1 in muscle physiology, this work reveals interesting new details on the role of muscle mTORC1 in mitochondrial activity and whole body metabolism.

Myopathy caused by mammalian target of rapamycin complex 1 (mTORC1) inactivation is not reversed by restoring mitochondrial function

Klaas Romanino[a], Laetitia Mazelin[b], Verena Albert[a], Agnès Conjard-Duplany[c], Shuo Lin[a], C. Florian Bentzinger[a,1], Christoph Handschin[a], Pere Puigserver[d,e], Francesco Zorzato[f,g], Laurent Schaeffer[b], Yann-Gaël Gangloff[b], and Markus A. Rüegg[a,2]

[a]Biozentrum, University of Basel, 4056 Basel, Switzerland; [b]Centre National de la Recherche Scientifique, Unité Mixte de Recherche 5239, École Normale Supérieure de Lyon, Laboratoire de Biologie Moléculaire de la Cellule, Equipe Différenciation Neuromusculaire, Université Lyon 1; Lyon, France; [c]Laboratoire de Biochimie et Physiopathologie Métaboliques, Equipe d'Accueil Universitaire, Faculté de Médecine Lyon Est, Université de Lyon, La Buire, 69372 Lyon Cedex 8, France; [d]Dana Farber Cancer Institute and [e]Department of Cell Biology, Harvard Medical School, Boston, MA 02115; and Departments of [f]Anesthesia and [g]Biomedicine, Basel University Hospital, 4031 Basel, Switzerland

Edited* by Kevin P. Campbell, University of Iowa Carver College of Medicine, Iowa City, IA, and approved November 15, 2011 (received for review July 15, 2011)

Mammalian target of rapamycin complex 1 (mTORC1) is central to the control of cell, organ, and body size. Skeletal muscle-specific inactivation of mTORC1 in mice results in smaller muscle fibers, fewer mitochondria, increased glycogen stores, and a progressive myopathy that causes premature death. In mTORC1-deficient muscles, peroxisome proliferator-activated receptor gamma coactivator 1-α (PGC-1α), which regulates mitochondrial biogenesis and glucose homeostasis, is strongly down-regulated. Here we tested whether induction of mitochondrial biogenesis pharmacologically or by the overexpression of PGC-1α is sufficient to reverse the phenotype of mice deficient for mTORC1. We show that both approaches normalize mitochondrial function, such as oxidative capacity and expression of mitochondrial genes. However, they do not prevent or delay the progressive myopathy. In addition, we find that mTORC1 has a much stronger effect than PGC-1α on the glycogen content in muscle. This effect is based on the strong activation of PKB/Akt in mTORC1-deficient mice. We also show that activation of PKB/Akt not only affects glycogen synthesis but also diminishes glycogen degradation. Thus, our work provides strong functional evidence that mitochondrial dysfunction in mice with inactivated mTORC1 signaling is caused by the down-regulation of PGC-1α. However, our data also show that the impairment of mitochondria does not lead directly to the lethal myopathy.

Adaptations of skeletal muscle to changes in the environment have been shown to depend on insulin-like growth factor (IGF), PKB/Akt, and mammalian target of rapamycin (mTOR) signaling (1). mTOR is a highly conserved protein kinase that is known for its central role in the control of cell size through the regulation of protein synthesis (2). It is found in two distinct multiprotein complexes, mTOR complex 1 (mTORC1) and mTOR complex 2 (mTORC2). Mice with skeletal muscle-specific deletion of *mTOR* or *rptor*, essential components of mTORC1, suffer from progressive myopathy that causes premature death at the age of 4–6 mo (3, 4). Importantly, muscles of mTOR$^-$ (mTOR muscle-knockout) and raptor muscle-knockout (RAmKO) mice show impaired mitochondrial function and increased glycogen content. Moreover, both mTOR$^-$ and RAmKO mice show a striking increase in the phosphorylation of PKB/Akt at threonine 308 and serine 473; this increase most likely is based on the lack of feedback inhibition onto insulin receptor substrate 1 by S6 kinase (5). Although the increase in glycogen correlates with an increased inhibition of the PKB/Akt target glycogen synthase kinase 3β (GSK3β), the mitochondrial phenotype correlates with the strong reduction of peroxisome proliferator-activated receptor-γ (PPARγ) coactivator α (PGC-1α), which regulates mitochondrial biogenesis and glucose homeostasis in skeletal muscle and has been shown to associate with mTOR (6–8). Interestingly, similar to RAmKO and mTOR$^-$ mice, deletion of *PGC-1α* in skeletal muscle results in a myopathy (9), and overexpression of PGC-1α in *mdx* mice, a mouse model of Duchenne muscular dystrophy, has been shown to ameliorate the disease phenotype (10). These data suggest that both the mitochondrial and the myopathic phenotype of mTOR$^-$ and RAmKO mice could be based on a deregulation of PGC-1α.

In the current study, we tested this hypothesis by applying the PPAR pan-agonist bezafibrate and by transgenic overexpression of PGC-1α. We find that both experimental paradigms improve mitochondrial function but do not prevent the progressive myopathy in either mTOR$^-$ or RAmKO mice. In addition, we find that the increase in glycogen in both mTOR$^-$ and RAmKO mice is dominated by the activation of PKB/Akt and not by changes in PGC-1α.

Results

Bezafibrate Partially Restores Mitochondrial Function In Muscles in the Absence of mTOR. Among the most striking phenotypes of mTOR$^-$ and RAmKO mice is a decrease in oxidative capacity and morphological changes of mitochondria (3, 4). In both mouse models, these phenotypes correlated with a decrease in the transcript levels of PGC-1α. Additionally, it has been demonstrated that mTORC1 controls mitochondrial gene expression through direct modulation of the transcriptional complex consisting of PGC-1α and yin-yang 1 (YY1) in vitro (8). PGC-1α in turn has been demonstrated to control its own expression through a feed-forward loop (11). These data suggest that the muscle pathology of mTOR$^-$ and RAmKO mice might be caused by mTORC1's effect on the expression of PGC-1α. To test this notion, we first used bezafibrate, a PPAR pan-agonist that activates the PPAR/PGC-1α pathway (12, 13). Administration of bezafibrate increases expression of PPARα and -δ and the coactivator PGC-1α in skeletal muscle (14). Importantly, the improvement of mitochondrial function by bezafibrate is sufficient to alleviate the progressive myopathy in mice deficient in cytochrome *c* oxidase (14). mTOR$^-$ mice were fed a diet containing 0.5% bezafibrate for 20 wk starting at age 5 wk. Quantitative real-time PCR (qRT-PCR) analysis showed that bezafibrate treatment significantly increased

Author contributions: K.R., C.F.B., Y.-G.G., and M.A.R. designed research; K.R., L.M., V.A., A.C.-D., and S.L. performed research; C.H., P.P., F.Z., L.S., and Y.-G.G. contributed new reagents/analytic tools; K.R., S.L., and Y.-G.G. analyzed data; and K.R. and M.A.R. wrote the paper.

The authors declare no conflict of interest.

*This Direct Submission article had a prearranged editor.

[1]Present address: The Sprott Centre for Stem Cell Research, Regenerative Medicine Program, Ottawa Health Research Institute, Ottawa, ON, Canada K1H 8L6.

[2]To whom correspondence should be addressed. E-mail: markus-a.ruegg@unibas.ch.

This article contains supporting information online at www.pnas.org/lookup/suppl/doi:10.1073/pnas.1111448109/-/DCSupplemental.

transcript levels of PGC-1α (Fig. 1*A*). Bezafibrate increased the expression of several mitochondrial genes, including medium-chain acyl coenzyme A dehydrogenase (MCAD), long chain acyl-coenzyme A dehydrogenase (LCAD), cytochrome c oxidase I and IV (COX I and IV), citrate synthase and muscle carnitine palmitoyltransferase I (mCPT1) (Fig. 1*B*), which are all known targets of PGC-1α (6). Most importantly, bezafibrate partially restored the activity of oxidative enzymes as shown by staining muscle cross-sections for succinate dehydrogenase (SDH) and cytochrome oxidase (COX) activities (Fig.1*C* and Fig. S1*A*). Significantly increased oxidative capacity of mTOR$^-$ muscles was confirmed further by measuring SDH activity directly (Fig. 1*D*).

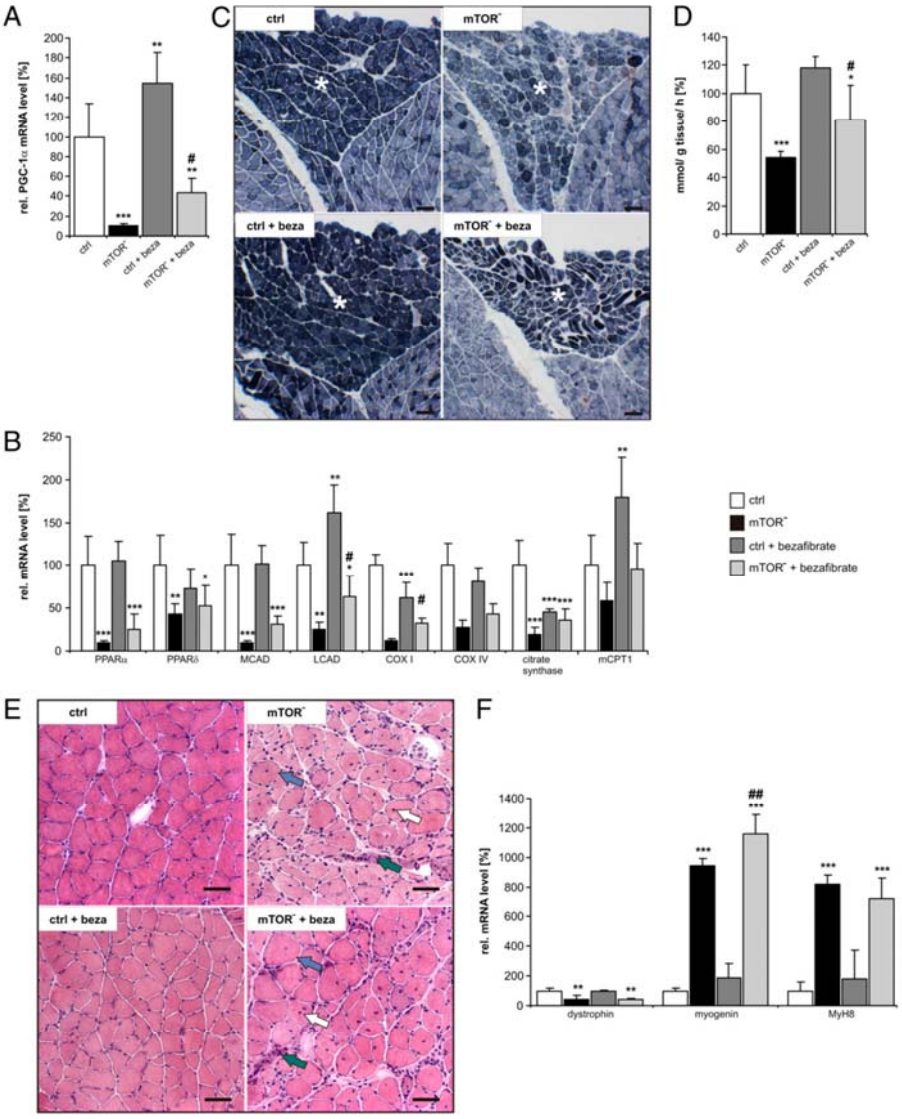

Fig. 1. Bezafibrate partially restores mitochondrial function in muscles in the absence of mTOR but does not prevent the myopathy. (*A*) Relative mRNA levels of PGC-1α were determined by qRT-PCR in control (ctrl), mTOR-deficient (mTOR$^-$), and bezafibrate-treated control (ctrl + beza) and mTOR$^-$ (mTOR$^-$ + beza) soleus muscle. Data represent mean ± SEM ($n \geq 3$ mice). (*B*) Relative mRNA levels of PPARα and PPAR δ, MCAD, LCAD, COX I and COX IV, citrate synthase and mCPT1 in the soleus muscle of indicated mice. Note that bezafibrate increases expression of most genes. Data represent mean ± SEM ($n \geq 3$ mice). (*C*) Oxidative properties of hind leg muscle increase upon bezafibrate treatment. Pictures show representative cross-sections stained for SDH activity (dark blue). The soleus muscle is marked by an asterisk. (Scale bar, 100 μm.) (*D*) Quantification of SDH activity as detected by an enzymatic assay (for details see *SI Materials and Methods*). Data represent mean ± SD ($n \geq 5$ mice). (*E*) H&E staining of cross-sections of soleus muscle. In the muscle of mTOR$^-$ and mTOR$^-$ + beza mice, some large (blue arrows) but also small fibers are present. Both groups of mice also show centralized nuclei (white arrows) and many mononuclear cells (green arrows). (Scale bar, 50 μm.) (*F*) Relative mRNA levels of the indicated proteins in soleus muscle as determined by qRT-PCR. Data represent mean ± SEM ($n \geq 3$ mice). In all experiments shown, mice were 20-wk-old males. Significant differences between control and experimental groups are indicated by *; significant changes between mTOR$^-$ and mTOR$^-$ + beza mice are indicated by $^{\#}$. $^{*/\#}P < 0.05$; $^{**/\#\#}P < 0.01$; $^{***/\#\#\#}P < 0.001$.

Improved Mitochondrial Function Does Not Reverse Myopathy in mTOR⁻ Mice. Mice deficient for mTORC1 display muscle atrophy and progressive myopathy resulting in early death (3, 4). Thus, we tested whether treatment with bezafibrate would ameliorate the myopathy in the mTOR⁻ mice. H&E staining of muscle cross-sections showed that the myopathy was still present after bezafibrate treatment (Fig. 1*E*). In addition, expression of dystrophin, which is reduced in mTOR⁻ mice (3), was still low, and expression of two markers for muscle regeneration, myogenin and the perinatal form of myosin heavy-chain MyH8, were still increased (Fig. 1*F*). Moreover, bezafibrate decreased rather than increased muscle mass and total force in both fast- (tibialis anterior, TA) and slow-twitch (soleus) muscles (Table S1) of 140-d-old mTOR⁻ mice. Finally, kyphosis in mTOR⁻ mice was not prevented or delayed by bezafibrate (Fig. S1*B*).

Transgenic Overexpression of PGC-1α Restores Mitochondrial Function in RAmKO Mice. Because our results show that bezafibrate improved mitochondrial function but not the myopathy in mTOR⁻ mice, we next tested directly whether overexpression of PGC-1α would be beneficial for the mutant mice. Indeed, PGC-1α was shown to improve the muscular dystrophy in mdx mice, a mouse model for Duchenne muscular dystrophy (10), and has been implicated in preventing muscle atrophy upon denervation (15) and during aging (16). For our experiments, we used PGC-1α transgenic mice that overexpress the protein specifically in skeletal muscle using the muscle creatine kinase (MCK) promoter (17). These mice were mated with RAmKO mice (4), which have largely the same phenotype as mTOR⁻ mice (3) but allow any contribution of mTORC2 to be ruled out. The resulting RAmKO mice that also are transgenic for PGC-1α (herein called "RAmKO-PGC1α-TG") expressed increased levels of PGC-1α mainly in the fast-twitch extensor digitorum longus (EDL) muscle (Fig. 2*A*). Expression of PGC-1α in RAmKO-PGC1α-TG mice also was increased in the slow-twitch soleus muscle (Fig. S2*A*), although at considerably lower extent, consistent with much greater activity of the MCK promoter in fast- as compared with slow-twitch muscle fibers (17). Therefore we used the fast-twitch EDL and TA muscles in the subsequent analysis. Like the mRNA, the protein level of PGC-1α in EDL was lower in RAmKO and was strongly increased in PGC-1α-TG mice. Interestingly, despite the overexpression, PGC-1α protein levels were only doubled compared with controls (Fig. S2*B* and quantification in Fig. 2*B*).

To estimate whether PGC-1α affected mitochondria number in the mice, we used qRT-PCR to determine the copy number of mtDNA (D-loop region) relative to the amount of genomic DNA [using sequences for NADH dehydrogenase (ubiquinone) flavoprotein 1 (*Ndufv1*)] (18). As expected, the ratio between mtDNA

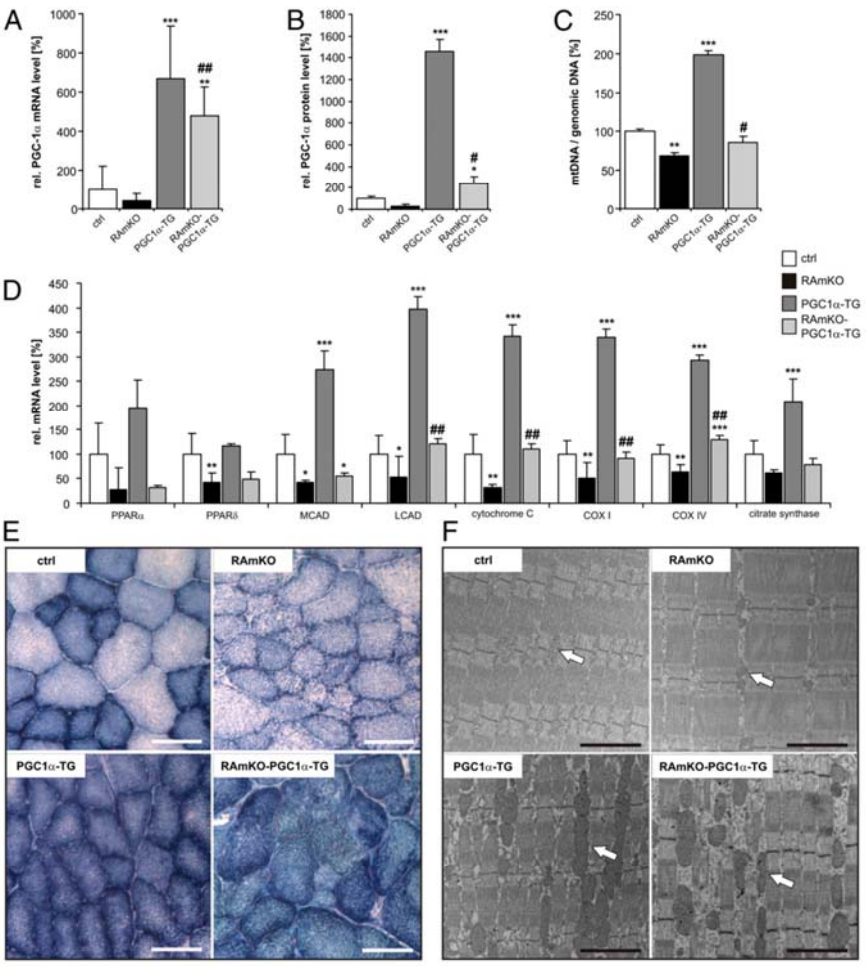

Fig. 2. Transgenic expression of PGC-1α in RAmKO mice normalizes mitochondrial properties. (*A*) Relative mRNA levels of PGC-1α in EDL muscle of 90-d-old mice of different genotypes as determined by qRT-PCR ($n \geq 3$ mice). (*B*) Quantification of PGC-1α protein levels. Western blot analysis was performed from lysates of EDL muscle from 80-d-old mice. Values represent average of gray values ($n \geq 3$ mice; see also Fig. S2*B*). (*C*) Ratio between mtDNA and genomic DNA in EDL muscle of 140-d-old mice as determined by qRT-PCR ($n \geq 2$ mice). (*D*) Relative mRNA levels of the indicated genes in EDL muscle of 90-d-old mice as determined by qRT-PCR ($n \geq 3$ mice). Abbreviations are as described in the legend of Fig. 1. (*E*) Activity of oxidative enzymes examined by NADH-TR staining (blue precipitate) in TA muscle of 130-d-old mice. (Scale bar, 100 μm.) (*F*) Electron micrographs of longitudinal sections of EDL muscle of 140-d-old mice. (Scale bar, 200 nm.) Mitochondria are indicated by white arrows. Values in *A–D* represent mean ± SD. Significant differences between control and genetically modified mice are indicated by *; significant changes between RAmKO and RAmKO-PGC1α-TG mice are indicated by #. $^{*/\#}P < 0.05$; $^{**/\#\#}P < 0.01$; $^{***/\#\#\#}P < 0.001$.

and genomic DNA was decreased in RAmKO and increased in PGC1α-TG mice (Fig. 2*C*). Importantly, the ratio was restored to wild-type levels in RAmKO-PGC1α-TG mice (Fig. 2*C*). A restoration of mitochondrial function in RAmKO-PGC1α-TG mice also was indicated by the normalization of transcripts encoding mitochondrial proteins (Fig. 2*D*). These data thus show that in RAmKO-PGC1α-TG mice the expression and the function of PGC-1α are restored to control levels. The measurement of the oxidative property of skeletal muscle by NADH-tetrazolium reductase (NADH-TR) confirmed the improvement of mitochondrial function (Fig. 2*E*). Finally, examination of the muscle by electron microscopy showed that the shape and size of the mitochondria in RAmKO-PGC-1α-TG mice was similar to that in PGC-1α-TG mice and was clearly distinct from RAmKO mice (Fig. 2*F*). These results therefore are strong evidence that overexpression of PGC-1α is sufficient to restore mitochondrial function in RAmKO mice to that of control mice.

mTORC1 Regulates Glycogen Content Independently of PGC-1α Through PKB/Akt. Recent evidence has implicated PGC-1α in the regulation of glucose metabolism in muscle (7). Because RAmKO and mTOR^{-} mice have an approximately fivefold increase in glycogen in skeletal muscle (3, 4), we also investigated whether PGC-1α expression would affect this parameter. To do so, we stained muscle cross-sections with periodic acid-Schiff (PAS) and quantified the amount of glycogen by an enzymatic assay. As described previously (4, 7), the glycogen content was increased in RAmKO and PGC1α-TG mice (Fig. 3 *A* and *B*), but the increase was much more pronounced in RAmKO than in PGC1α-TG mice. Interestingly, the effect of PGC-1α overexpression and *rptor* deletion were additive (RAmKO-PGC1α-TG mice; Fig. 3*B*), suggesting that the two factors affect independent signaling pathways controlling glycogen storage. One mechanism responsible for the high levels of glycogen in RAmKO mice might be activation of PKB/Akt attested by the hyperphosphorylation of the T308 and S473 sites (Fig. 3*C* and quantification in Table S2). Surprisingly, overexpression of PGC-1α increased the total amount of PKB/Akt, but this increase did not affect phosphorylation at T308 or S473 (Fig. 3*C* and Table S2).

A well-described target of PKB/Akt is GSK3β, which inhibits glycogen synthase (19). As a consequence of increased PKB/Akt signaling, inhibitory phosphorylation of GSK3β was increased in mTORC1-deficient muscle (Fig. 3*C* and Table S2). Thus, inhibition of GSK3β leads to higher synthesis of glycogen in the mutant mice. It has been suggested that the increase in glycogen stores in the PGC1α-TG mice is caused by a down-regulation of glycogen phosphorylase (7). Indeed, the levels of glycogen phosphorylase were lower at the mRNA and protein level in PGC1α-TG mice (Fig. 3 *C* and *D* and Table S2). Strikingly, the same down-regulation of glycogen phosphorylase also was seen in RAmKO mice although the levels of PGC-1α are low in those mice (Fig. 3 *C* and *D* and Table S2). In summary, these data indicate that hyperactivation of PKB/Akt is sufficient to regulate both glycogen synthesis and degradation independently of PGC-1α.

Increased PGC-1α Expression Does Not Prevent Myopathy of RAmKO Mice. To exclude the possibility that the failure of bezafibrate to ameliorate the myopathy in mTOR^{-} mice resulted from insufficient activation of PGC-1α, we also examined whether muscle mass and integrity were restored in the RAmKO-PGC1α-TG mice. However, the loss in muscle mass of the RAmKO mice was not prevented (Table S3), nor was the significant reduction of the whole-body weight (Fig. 4*A*). Moreover, H&E staining of muscle cross-sections of RAmKO-PGC1α-TG mice detected clear signs of myopathy (Fig. 4*B*). For example, the muscles contained more small fibers (blue arrows in Fig. 4*B*), as reflected in the doubling of the number of fibers that have a mean fiber feret between 20 and 30 μm in RAmKO and RAmKO-PGC1α-TG mice compared with controls (Fig. 4*C*). Additionally, mononuclear cells were found

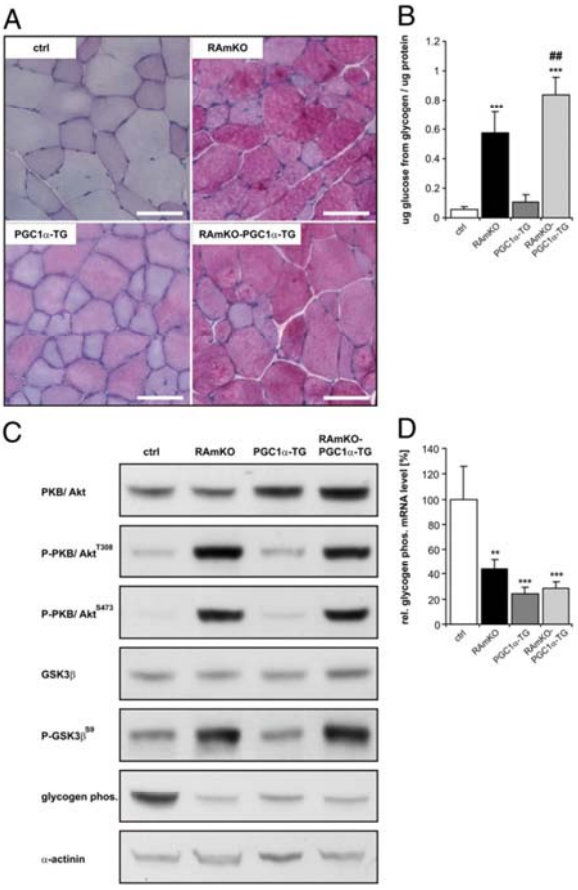

Fig. 3. Glycogen content is increased in all genetically modified mouse models. (*A*) PAS staining of cross-sections of TA muscle of 90-d-old mice. The reaction product (magenta color) is indicative of the amount of glycogen in the tissue. (Scale bar, 50 μm.) (*B*) Quantification of the glycogen concentration in TA muscle from 90-d-old mice as determined by an enzymatic assay (for details see *SI Materials and Methods*). (*C*) Western blot analysis of EDL muscle from 80-d-old mice using antibodies directed against the proteins indicated. An equal amount of protein was loaded in each lane. An antibody against α-actinin was used as loading control. For quantification see Table S2. (*D*) Relative mRNA levels of glycogen phosphorylase in EDL muscle of 90-d-old mice as determined by qRT-PCR ($n \geq 3$ mice). Values in *B* and *D* represent mean ± SD. Significant differences between control and genetically modified mice are indicated by *; significant changes between RAmKO and RAmKO-PGC1α-TG mice are indicated by #. $^{*/\#}P < 0.05$; $^{**/\#\#}P < 0.01$; $^{***/\#\#\#}P < 0.001$.

(green arrows in Fig. 4*B*), as were centralized nuclei in several muscle fibers (white arrows in Fig. 4*B* and quantification in Fig. 4*D*). Expression of PGC-1α also did not affect muscle force in RAmKO mice (Table S4). There also was no significant improvement in the physical activity of the RAmKO mice by the overexpression of PGC-1α (Fig. 4*E*), and the mice still developed a kyphosis (Fig. 4*F*). In fact, we did not detect a significant change in the mean age of onset of the kyphosis (RAmKO: 15 ± 2 wk; RAmKO-PGC1α-TG: 15 ± 3 wk; mean ± SD, $n = 7$ for each genotype). Finally, the age at which the disease became so severe that the mice needed to be killed was similar for RAmKO and RAmKO-PGC1α-TG mice. These results show that an increase in PGC-1α levels, despite the restoration of mitochondrial function and number, fails to rescue the myopathy of RAmKO mice.

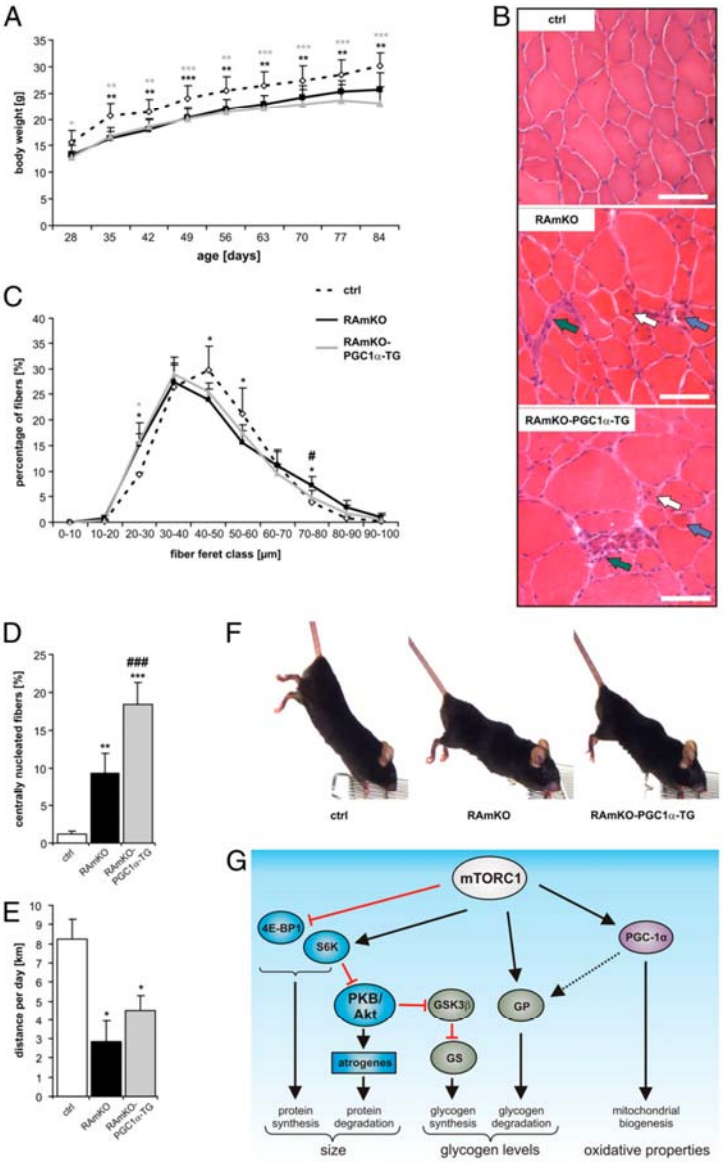

Fig. 4. Increased PGC-1α levels do not prevent progressive myopathy in RAmKO mice. (*A*) Mice of each genotype were weighed every week ($n \geq 5$ mice). (*B*) H&E staining of cross-sections of TA muscle of 130-d-old mice. In the muscle of RAmKO and RAmKO-PGC1α-TG mice some large (blue arrows) but also small fibers are present. Both genotypes also show centralized nuclei (white arrows) and many mononuclear cells (green arrows). (*C*) Distribution of fiber size in the TA muscle of 14-d-old mice ($n = 2$ for control; $n = 4$ for RAmKO; $n = 5$ for RAmKO-PGC-1α-TG mice). (*D*) Percentage of muscle fibers with centralized nuclei in TA muscle of 90-d-old mice ($n \geq 5$ mice). All fibers (~2,000) of one midbelly cross-section were analyzed in experiments shown in *C* and *D*. (*E*) Average distance run voluntarily per day between the ages of 95 d and 105 d ($n \geq 3$ mice). (*F*) Photographs of 140-d-old littermates. The RAmKO and RAmKO-PGC1α-TG mice are leaner and suffer from a kyphosis. (*G*) Proposed model for the contribution of different signaling pathways to the disease phenotype in mTORC1-deficient skeletal muscle. The balance between protein synthesis [via eIF4E-Binding Protein 1 (4E-BP1) and S6 kinase (S6K)] and protein degradation contributes to muscle size (*Left*). The balance between glycogen synthesis [via PKB/Akt; GSK3β, and glycogen synthase (GS)] and glycogen degradation [via glycogen phosphorylase (GP)] regulates glycogen levels (*Center*). PGC-1α has only a minor contribution to the glycogen levels but is the main regulator of the oxidative properties (*Right*). Values in *A*, *C*, *D*, and *E* represent mean ± SD. Significant differences between control and genetically modified mice are indicated by *; significant changes between RAmKO and RAmKO-PGC1α-TG mice are indicated by #. $*/\#P < 0.05$; $**/\#\#P < 0.01$; $***/\#\#\#P < 0.001$.

Discussion

This work provides direct evidence that the mitochondrial deficits in mTOR$^-$ and RAmKO mice are the consequence of decreased expression of PGC-1α (Fig. 4*G*). Furthermore, our study shows that both the high glycogen content and the severe myopathy observed in mTORC1-deficient mice are not strongly affected by restoring PGC-1α function (Fig. 4*G*). We chose to examine this question by using (*i*) bezafibrate, because it reaches all muscles, and (*ii*) mice transgenic for PGC-1α (17), where the transgene is driven by the MCK promoter that is expressed mainly in fast-twitch muscle fibers. Bezafibrate is used in clinical trials and was used successfully in the Δcox10 mouse model to delay the onset of the mitochondrial myopathy (14). The PGC-1α–mediated rescue of mitochondrial function in mTORC1-deficient muscles, characterized by a normalization of the mtDNA content, increased levels of key mitochondrial enzymes and of tissue oxidative capacity. However, despite the normalization of the oxidative capacity in RAmKO-PGC1α-TG mice, overall running activity was still low, similar to that of RAmKO mice. This result suggests that the myopathic pathology, but not the metabolic changes in RAmKO muscle, prevents the mice from running as far as control littermates.

mTORC1 influences the expression of PGC-1α and therefore mitochondrial biogenesis through formation of a complex with PGC-1α and the transcription factor YY1. Inhibition of mTORC1 disrupts the interaction between YY1 and PGC-1α, thereby decreasing the expression of mitochondrial target genes including PGC-1α itself (8). Interestingly, our data revealed that the function of PGC-1α in driving mitochondrial biogenesis does not require functional mTORC1. However, we noted that the expression levels of PGC-1α and its downstream targets, such as MCAD,

LCAD, COX I and IV, and cytochrome *c*, were consistently lower in RAmKO-PGC1α-TG than in PGC1α-TG mice. Our data indicate that both mRNA and protein expression of PGC-1α are less efficient in mTORC1-deficient than in wild-type muscle, because the levels always were much lower in RAmKO-PGC1α-TG than in PGC1α-TG mice. Another reason for the lower activity of PGC-1α in mTORC1-deficient muscle could be the hyperactivation of PKB/Akt, which was shown to inhibit PGC-1α directly by phosphorylation in liver (20).

The amount of glycogen stored in the muscles was 2–15 times higher in all the genetically modified mice studied than in controls. We also found that PGC-1α-TG and RAmKO-PGC1α-TG mice had increased levels of glycogen compared with their littermate controls, a finding that is in agreement with the finding that PGC-1α inhibits the transcription of glycogen phosphorylase (7). However, in the RAmKO mice, glycogen phosphorylase levels are low despite the low levels of PGC-1α. Most likely, these low levels are the result of the strong inhibitory effect by activated PKB/Akt, as demonstrated in hepatocytes (21). In addition, our data also show that hyperactivation of PKB/Akt in RAmKO mice is sufficient to overrule the effect of PGC-1α on glycogen phosphorylase. Activated PKB/Akt also regulates glycogen synthase through inhibition of GSK3β (19). Thus, the pronounced glycogen accumulation in muscles of mTORC1-deficient mice probably is based on the simultaneous stimulation of glycogen synthesis and inhibition of glycogen degradation by PKB/Akt (Fig. 4*G*).

Finally, our data show that increased levels of PGC-1α and improved mitochondrial function are not sufficient to reverse any aspects of the severe myopathy in mTORC1-deficient mice. It has been reported that PGC-1α counteracts denervation-induced atrophy and age-related muscle loss (15, 16). However, we could not observe a beneficial effect of higher PGC-1α levels on muscle mass in the atrophic mTORC1-deficient mice. Of course, PGC-1α may ameliorate only certain types of muscle pathologies. In addition, although PGC-1α is increased in RAmKO-PGC1α-TG mice, the disruption of the mTORC1/YY1/PGC-1α complex may prevent the restoration of muscle in the mTORC1-deficient mice.

Because restoration of mitochondrial function does not affect the myopathy in mTORC1-deficient muscle, a possible scenario is that alterations in the balance between protein synthesis and protein degradation are responsible for this pathology. Such changes might involve proteasomal and autophagic protein degradation and overall protein synthesis (Fig. 4*G*). Indeed, recent evidence shows that such a shift in the catabolic–anabolic balance can result in muscle pathology. For example, inactivation of autophagy directly or by chronic hyperactivation of PKB/Akt results in severe muscle phenotypes that cause the death of the animals at the age of approximately 1 y (22, 23). Thus, a change in the homeostasis between protein synthesis and degradation as observed in RAmKO and mTOR^{-} mice is likely to affect the health of skeletal muscle.

In summary, our data show that mTORC1 regulates mitochondrial activity through PGC-1α and regulates glycogen levels through PKB/Akt. Intriguingly, the lethal myopathy resulting from the loss of mTORC1 is independent of mitochondrial activity and the PGC-1α pathway.

Materials and Methods

Mice. RAmKO, mTOR^{-}, and PGC1α-TG mice have been described previously (3, 4, 17). The RAmKO-PGC1α-TG mice were generated by crossing RAmKO with PGC1α-TG mice. Mice were maintained in a conventional facility with a fixed light–dark cycle. Body weight was measured weekly. Moribund mice were killed before natural death. Studies were carried out according to criteria outlined for the care and use of laboratory animals and with approval of the Swiss (for experiments with RAmKO, PGC1α-TG, and RAmKO-PGC1α-TG mice) and French (for experiments with mTOR^{-} mice) authorities, respectively.

Statistics. All data are expressed as mean ± SD or mean ± SEM as indicated. One-way ANOVA and a priori-defined contrast analysis were performed for statistical comparisons of the different groups except in Tables S1 and S4, where Student's *t* tests were used.

ACKNOWLEDGMENTS. We thank Arnaud Ferry from the Université Pierre et Marie Curie-Paris for measurement of muscle force of the mTOR^{-} mice. We are indebted to the animal (Le Plateau de Biologie Expérimental de la Souris) and microscopy (Plateau Technique Imagerie/Microscopie) facilities of the Institut Fédératif de Recherche 128 Biosciences. This work was supported by grants from the Cantons of Basel-Stadt and Baselland, the Swiss Foundation for Research on Muscle Disease, and Swiss Life (to M.A.R.) and from the Association Française Contres les Myopathies (to M.A.R., L.S., and Y.-G.G.) and the Agence Nationale de la Recherche (to L.S. and Y.-G.G.).

1. Glass DJ (2005) Skeletal muscle hypertrophy and atrophy signaling pathways. *Int J Biochem Cell Biol* 37:1974–1984.
2. Wullschleger S, Loewith R, Hall MN (2006) TOR signaling in growth and metabolism. *Cell* 124:471–484.
3. Risson V, et al. (2009) Muscle inactivation of mTOR causes metabolic and dystrophin defects leading to severe myopathy. *J Cell Biol* 187:859–874.
4. Bentzinger CF, et al. (2008) Skeletal muscle-specific ablation of raptor, but not of rictor, causes metabolic changes and results in muscle dystrophy. *Cell Metab* 8: 411–424.
5. Um SH, et al. (2004) Absence of S6K1 protects against age- and diet-induced obesity while enhancing insulin sensitivity. *Nature* 431:200–205.
6. Wu Z, et al. (1999) Mechanisms controlling mitochondrial biogenesis and respiration through the thermogenic coactivator PGC-1. *Cell* 98:115–124.
7. Wende AR, et al. (2007) A role for the transcriptional coactivator PGC-1alpha in muscle refueling. *J Biol Chem* 282:36642–36651.
8. Cunningham JT, et al. (2007) mTOR controls mitochondrial oxidative function through a YY1-PGC-1alpha transcriptional complex. *Nature* 450:736–740.
9. Handschin C, et al. (2007) Skeletal muscle fiber-type switching, exercise intolerance, and myopathy in PGC-1alpha muscle-specific knock-out animals. *J Biol Chem* 282: 30014–30021.
10. Handschin C, et al. (2007) PGC-1alpha regulates the neuromuscular junction program and ameliorates Duchenne muscular dystrophy. *Genes Dev* 21:770–783.
11. Lin J, Handschin C, Spiegelman BM (2005) Metabolic control through the PGC-1 family of transcription coactivators. *Cell Metab* 1:361–370.
12. Bastin J, Aubey F, Rötig A, Munnich A, Djouadi F (2008) Activation of peroxisome proliferator-activated receptor pathway stimulates the mitochondrial respiratory chain and can correct deficiencies in patients' cells lacking its components. *J Clin Endocrinol Metab* 93:1433–1441.
13. Tenenbaum A, Motro M, Fisman EZ (2005) Dual and pan-peroxisome proliferator-activated receptors (PPAR) co-agonism: The bezafibrate lessons. *Cardiovasc Diabetol* 4:14.
14. Wenz T, Diaz F, Spiegelman BM, Moraes CT (2008) Activation of the PPAR/PGC-1alpha pathway prevents a bioenergetic deficit and effectively improves a mitochondrial myopathy phenotype. *Cell Metab* 8:249–256.
15. Sandri M, et al. (2006) PGC-1alpha protects skeletal muscle from atrophy by suppressing FoxO3 action and atrophy-specific gene transcription. *Proc Natl Acad Sci USA* 103:16260–16265.
16. Wenz T, Rossi SG, Rotundo RL, Spiegelman BM, Moraes CT (2009) Increased muscle PGC-1alpha expression protects from sarcopenia and metabolic disease during aging. *Proc Natl Acad Sci USA* 106:20405–20410.
17. Lin J, et al. (2002) Transcriptional co-activator PGC-1 alpha drives the formation of slow-twitch muscle fibres. *Nature* 418:797–801.
18. Amthor H, et al. (2007) Lack of myostatin results in excessive muscle growth but impaired force generation. *Proc Natl Acad Sci USA* 104:1835–1840.
19. Sakamoto K, Goodyear LJ (2002) Invited review: Intracellular signaling in contracting skeletal muscle. *J Appl Physiol* 93:369–383.
20. Li X, Monks B, Ge Q, Birnbaum MJ (2007) Akt/PKB regulates hepatic metabolism by directly inhibiting PGC-1alpha transcription coactivator. *Nature* 447:1012–1016.
21. Aiston S, Hampson LJ, Arden C, Iynedjian PB, Agius L (2006) The role of protein kinase B/Akt in insulin-induced inactivation of phosphorylase in rat hepatocytes. *Diabetologia* 49:174–182.
22. Grumati P, et al. (2010) Autophagy is defective in collagen VI muscular dystrophies, and its reactivation rescues myofiber degeneration. *Nat Med* 16:1313–1320.
23. Masiero E, et al. (2009) Autophagy is required to maintain muscle mass. *Cell Metab* 10:507–515.

Supporting Information

Romanino et al. 10.1073/pnas.1111448109

SI Materials and Methods

Quantitative Real-Time PCR. Total RNA was isolated (SV Total RNA Isolation System; Promega), and equal amounts of RNA were reverse transcribed using a mixture of oligodT and random hexamer primers (iScript cDNA Synthesis Kit; Bio-Rad). Quantitative real-time PCR (qRT-PCR) was performed using SYBR Green (PowerSYBR Green Master Mix; Applied Biosystems) and StepOne Software 2.1. (Applied Biosystems). Expression levels for each gene of interest were normalized to the mean cycle number using qRT-PCR for the housekeeping gene GAPDH. All data were confirmed with β-actin as another housekeeping gene. For the qRT-PCR data of the mTOR^{-} mice the housekeeping genes cyclophilin B and hypoxanthine phosphoribosyltransferase (HPRT) were used.

For qRT-PCR the following primers were used: GAPDH (forward: CAT CGT GGA AGG GCT CAT GAC, reverse: CTT GGC AGC ACC AGT GGA TG); cyclophilin B (forward: GAT GGC ACA GGA GGA AAG AG, reverse: AAC TTT GCC GAA AAC CAC AT); β-actin (forward: CAG CTT CTT TGC AGC TCC TT, reverse: GCA GCG ATA TCG TCA TCC A); peroxisome proliferator-activated receptor gamma coactivator 1-α (PGC-1α; forward: TGA TGT GAA TGA CTT GGA TAC AGA CA, reverse: GCT CAT TGT TGT ACT GGT TGG ATA TG); peroxisome proliferator-activated receptor α (PPARα; forward: GCG TAC GGC AAT GGC TTT AT, reverse: ACA GAA CGG CTT CCT CAG GTT); PPARδ (forward: GCA AGC CCT TCA GTG ACA TCA, reverse: CCA GCG CAT TGA ACT TGA CA); medium-chain acyl CoA dehydrogenase (MCAD; forward: AAC ACT TAC TAT GCC TCG ATT GCA, reverse: CCA TAG CCT CCG AAA ATC TGA A); cytochrome *c* (forward: GCA AGC ATA AGA CTG GAC CAA A, reverse: TTG TTG GCA TCT GTG TAA GAG AAT C); cytochrome *c* oxidase IV(COX IV; forward: TAC TTC GGT GTG CCT TCG A, reverse: TGA CAT GGG CCA CAT CAG); citrate synthase (forward: CAA GCA GCA ACA TGG GAA GA, reverse: GTC AGG ATC AAG AAC CGA AGT CT); glycogen phosphorylase (GP; forward: CAC TTA CCA GCT GGG CTT GGA CAT, reverse: AAA GCA AGC TGC CAG GCG TC); COX I (forward: GGT CAA CCA GGT GCA CTT TT, reverse: TGG GGC TCC GAT TAT TAG TG); long-chain acyl-CoA dehydrogenase (LCAD; forward: ATG GCA AAA TAC TGG GCA TC, reverse: TCT TGC GAT CAG CTC TTT CA); muscle carnitine palmitoyltransferase I (mCPT1; forward: TGC CTT TAC ATC GTC TCC AA, reverse: AGA CCC CGT AGC CAT CAT C); dystrophin (forward: TGC GCT ATC AGG AGA CAA TG, reverse: TTC TTG GCC ATC TCC TTC AC); myogenin (forward: CTA CAG GCC TTG CTC AGC TC, reverse: AGA TTG TGG GCG TCT GTA GG); and myosin heavy-chain 8 (MyH8; forward: CAA GGA TGG AGG GAA AGT GA, reverse: GGT TCA TGG GGA AGA CTT GA).

For the quantification of mtDNA copy numbers the following primers were used: *D-loop* region (forward: GGT TCT TAC TTC AGG GCC ATC A, reverse: GAT TAG ACC CGT TAC CAT CGA GAT), NADH dehydrogenase (ubiquinone) flavoprotein 1 (*Ndufv1*; forward: CTT CCC CAC TGG CCT CAA G, reverse: CCA AAA CCC AGT GAT CCA GC).

Succinate Dehydrogenase Activity. Frozen muscles were homogenized in medium containing 50% glycerol, 20 mM phosphate buffer (pH 7.4), 5 mM β-mercaptoethanol, 0.5 mM EDTA, and 0.02% BSA at a dilution of 1:50 based on wet weight. Succinate dehydrogenase activity was determined at 37 °C in a two-step assay as described (1). In the first step, fumarate was allowed to accumulate from succinate for 60 min. In the second step, the amount of fumarate produced was measured with fumarase and a NAD-coupled reaction with malate dehydrogenase and the glutamate-oxaloacetate transaminase. The amount of NADH produced was measured by its fluorescence. Standards were processed the same way as the samples.

Histology. Muscles frozen in liquid nitrogen-cooled isopentane were cut into 12-μm cross-sections. General histology on cross-sections was performed using H&E (Merck). NADH staining was done as described (2). PAS staining was performed according to the manufacturer's instructions (Sigma). After staining, samples were dehydrated and mounted with DePex mounting medium (Gurr; BDH Chemicals, Ltd.). SDH and COX staining were carried out as described in refs. 3 and 4.

Quantification of mtDNA Copy Numbers. Total DNA was extracted and purified with a standard chloroform/ethanol precipitation after proteinase K digestion. DNA concentrations were determined photometrically, adjusted to 50 ng/μL, and used to quantify the amount of mtDNA in relation to the genomic DNA by qRT-PCR. For the quantification of the mtDNA, primers were used that are complementary to the *D-loop* region. Primers to quantify genomic DNA were directed against the single-copy nuclear gene *Ndufv1*.

Electron Microscopy. Transmission electron microscopy was performed as described in ref. 5.

Western Blotting Analysis, Glycogen Content, and Fiber Size Distribution. Western blotting, glycogen content, and fiber size distribution were performed as described earlier (6). For Western blots the following antibodies were used: anti–PGC-1 from Millipore; Pan-actin, Akt, phospho-Akt (Thr308), phospho-Akt (Ser473), glycogen synthase kinase 3β (GSK-3β), Phospho-GSK-3β (Ser9), and raptor from Cell Signaling; α-actinin from Sigma; and GP from Santa Cruz. The concentrations used were according to the manufacturers' instructions.

Voluntary Wheel Running. Mice were housed individually in cages equipped with a running wheel carrying a magnet. Wheel revolutions were registered by a reed sensor connected to an I-7053D Digital-Input module (Spectra), and the revolution counters were read by a standard laptop computer via an I-7520 RS-485-to-RS-232 interface converter (Spectra). Digitalized signals were processed by the "mouse running" software developed by Santhera Pharmaceuticals Ltd.

Physiological Studies. Measurements of muscle contractile properties of the soleus and tibialis anterior (TA) muscle (Table S1) were performed as described (7). Muscle force of extensor digitorum longus (EDL) muscles (Table S4) was measured as described previously (8) using a muscle-testing setup (Heidelberg Scientific Instruments). Tetanic force was recorded in response to 400-ms pulses at 150 Hz, and specific force was normalized to the muscle cross-sectional area [CSA = wet weight (mg)/length (mm) × 1.06 (density mg/mm^3)].

1. Chi MM, et al. (1983) Effects of detraining on enzymes of energy metabolism in individual human muscle fibers. *Am J Physiol* 244:C276–C287.
2. Dunant P, et al. (2003) Expression of dystrophin driven by the 1.35-kb MCK promoter ameliorates muscular dystrophy in fast, but not in slow muscles of transgenic mdx mice. *Mol Ther* 8:80–89.
3. Konieczny P, et al. (2008) Myofiber integrity depends on desmin network targeting to Z-disks and costameres via distinct plectin isoforms. *J Cell Biol* 181:667–681.
4. MacArthur DG, et al. (2007) Loss of ACTN3 gene function alters mouse muscle metabolism and shows evidence of positive selection in humans. *Nat Genet* 39:1261–1265.
5. Moll J, et al. (2001) An agrin minigene rescues dystrophic symptoms in a mouse model for congenital muscular dystrophy. *Nature* 413:302–307.
6. Bentzinger CF, et al. (2008) Skeletal muscle-specific ablation of raptor, but not of rictor, causes metabolic changes and results in muscle dystrophy. *Cell Metab* 8: 411–424.
7. Risson V, et al. (2009) Muscle inactivation of mTOR causes metabolic and dystrophin defects leading to severe myopathy. *J Cell Biol* 187:859–874.
8. Delbono O, et al. (2007) Loss of skeletal muscle strength by ablation of the sarcoplasmic reticulum protein JP45. *Proc Natl Acad Sci USA* 104:20108–20113.

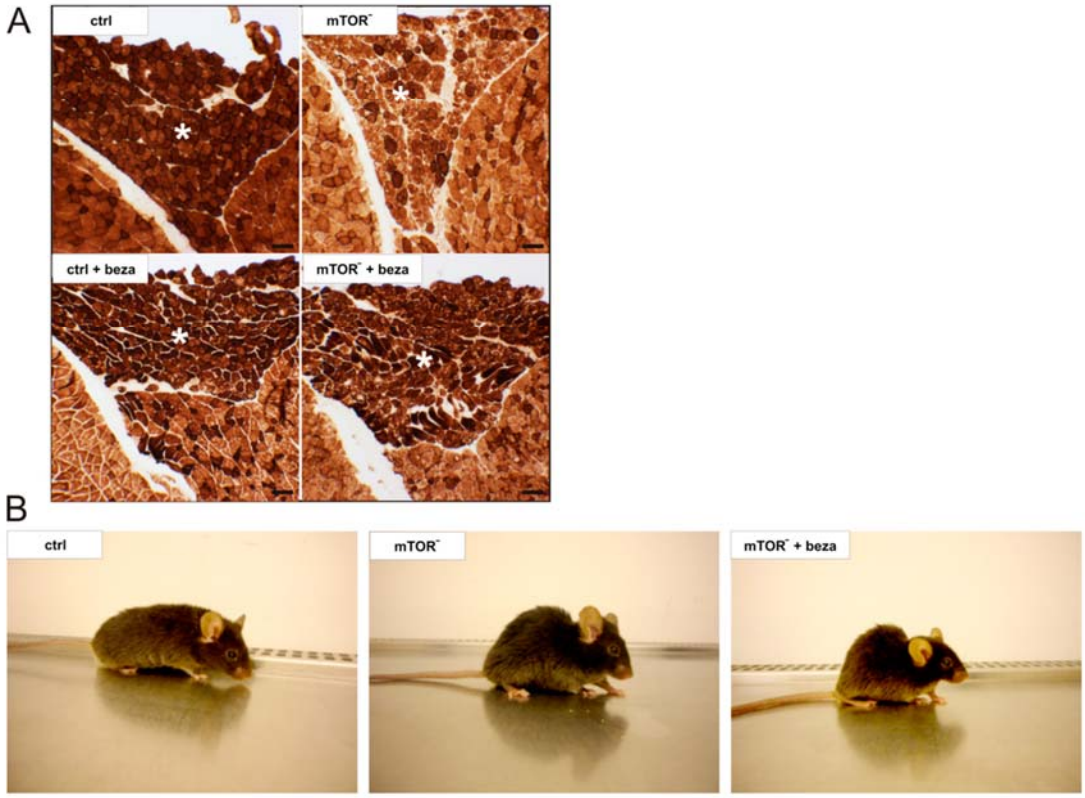

Fig. S1. Oxidative properties and myopathy in bezafibrate-treated control and mTOR⁻ mice. (*A*) COX staining in hind leg muscles. COX is the complex IV of the respiratory chain enzymes, and its activity is representative for the oxidative enzymes. The soleus muscle is marked by an asterisk. (Scale bar, 100 μm.) (*B*) Photographs of 140-d-old mice of indicated genotypes. Note that bezafibrate-treated mTOR⁻ mice still develop a severe kyphosis.

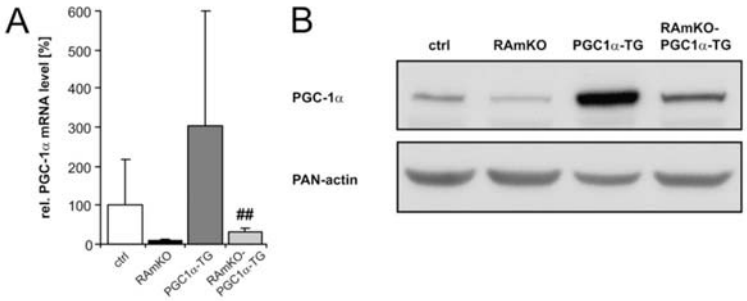

Fig. S2. Transgenic expression of PGC-1α in control and raptor muscle-knockout (RAmKO) mice. (*A*) Relative mRNA levels of PGC-1α in soleus muscle of 90-d-old mice as determined by qRT-PCR. Values represent mean ± SD ($n \geq 6$ mice). $^{\#\#}P < 0.01$, RAmKO vs. RAmKO mice that also are transgenic for PGC1α (RAmKO-PGC1α-TG mice). (*B*) Western blot of PGC-1α in EDL muscles from 80-d-old mice. Equal amounts of protein were loaded in each lane. An antibody against Pan-actin was used as loading control. For quantification, see Fig. 2*B*.

Table S1. Muscle contractile properties of 140-d-old mice were assessed by recording isometric forces in response to electrical stimulation

Muscle	Control	mTOR$^-$	mTOR$^-$ + beza
Soleus			
Mass (mg)	13.2 ± 1.6	9.7 ± 1***	7.0 ± 0.3*** ###
Po (mN)	224.2 ± 52.2	132.0 ± 19.9**	104.8 ± 9.7** #
sPo (mN/mm^2)	171.2 ± 40.2	130.6 ± 14.5*	140.0 ± 17.2*
TA			
Mass (mg)	61.5 ± 5.1	38.3 ± 6.9***	26.9 ± 2.3*** ##
Po (mN)	1137.3 ± 118.7	445.8 ± 118.4**	292.3 ± 75.8***
sPo (mN/mm^2)	18.5 ± 0.7	11.8 ± 1.1***	11.3 ± 2.4***
Pt (mN)	20.7 ± 3.3	7.2 ± 1.8***	3.3 ± 0.7*** ##

The following data were measured: muscle mass (Mass), absolute maximum tetanic force (Po), specific tetanic force (sPo), and peak twitch tension (Pt). Data represent mean ± SD ($n \geq 3$ mice). Significant differences between control and experimental groups are indicated by *; significant changes between mTOR$^-$ and bezafibrate mTOR$^-$ (mTOR$^-$ + beza) mice are indicated by #. *P* values were determined by Student's *t* test. $^{*/\#}P < 0.05$; $^{**/\#\#}P < 0.01$; $^{***/\#\#\#}P < 0.001$.

Table S2. Quantification of Western blot analysis for the proteins indicated

Protein	Control	RAmKO	PGC1α-TG	RAmKO-PGC1α-TG
Raptor	100.0 ± 63.9	0.9 ± 1.5**	44.2 ± 25.3	3.3 ± 2.7**
total PKB/Akt	100.0 ± 19.8	252.6 ± 43.9	318.8 ± 92.1	520.6 ± 205.5** #
P-PKB/Akt T308	100.0 ± 10.9	393.7 ± 14.2**	66.2 ± 44.6	236.5 ± 47.5**
P-PKB/Akt S473	100.0 ± 113.7	1192.7 ± 15.7**	52.5 ± 32.3	1696.9 ± 458.7**
GSK3β	100.0 ± 35.7	98.0 ± 0.7	58.1 ± 26.2	133.2 ± 40.5
P-GSK3β S9	100.0 ± 37.8	294.1 ± 159.2*	61.7 ± 37.3	233.4 ± 113.1*
GP	100.0 ± 47.5	4.5 ± 0.9**	20.1 ± 10.4*	7.7 ± 4.3**

Proteins analyzed were extracted from EDL muscle of 80-d-old mice ($n \geq 3$ mice). Numbers given represent mean gray value ± SD after subtraction of the background and normalization to α-actinin. Significant differences between control and genetically modified mice are indicated by *; significant changes between RAmKO and RAmKO-PGC1α-TG mice are indicated by #. $^{*/\#}P < 0.05$; $^{**/\#\#}P < 0.01$; $^{***/\#\#\#}P < 0.001$.

Table S3. Weight or length measured for different organs in 140-d-old mice

Muscle or organ	Control	RAmKO	PGC1α-TG	RAmKO-PGC1α-TG
Soleus (mg)	8.1 ± 0.6	6.6 ± 0.8*	8.6 ± 0.8	6.3 ± 0.6**
EDL (mg)	11.4 ± 1.2	10.6 ± 0.5	11.1 ± 1.3	9.8 ± 1.2
TA (mg)	48.4 ± 3.9	41.8 ± 4.5*	50.9 ± 3.9	35.2 ± 4.4** #
Heart (mg)	147.2 ± 16.4	126.9 ± 4.8	154.8 ± 11.9	136.3 ± 7.9
Liver (mg)	1281.2 ± 338.7	1212.3 ± 139.8	1345.3 ± 140.3	1183.9 ± 161.1
Tibia length (cm)	2.1 ± 0.1	2.1 ± 0.1	2.0 ± 0.1	2.0 ± 0.1

Values represent mean ± SD ($n \geq 6$ mice). Significant differences between control and genetically modified mice are indicated by *; significant changes between RAmKO and RAmKO-PGC1α-TG mice are indicated by #. $^{*/\#}P < 0.05$; $^{**/\#\#}P < 0.01$; $^{***/\#\#\#}P < 0.001$.

Table S4. Muscle contractile properties of EDL muscle of 90-d-old mice were assessed by recording isometric forces in response to electrical stimulation

EDL properties	Control	RAmKO	PGC1α-TG	RAmKO-PGC1α-TG
Mass (mg)	9.8 ± 2.1	9.2 ± 1.3	9.4 ± 2.2	8.2 ± 1.2
Po (mN)	282.3 ± 54.5	237.6 ± 47.9*	217.6 ± 47.2*	192.3 ± 8.9**
sPo (mN/mm^2)	358.4 ± 55.5	309.0 ± 72.6*	299.1 ± 52.3*	280.8 ± 27.7*
Pt (mN)	51.3 ± 14.0	43.8 ± 12.7	30.4 ± 11.5**	31.3 ± 7.4*

The following data were measured: muscle mass (Mass), absolute maximum tetanic force (Po), specific tetanic force (sPo), and peak twitch tension (Pt). Values represent mean ± SD ($n \geq 4$ muscles). In agreement with recent findings of others (1), EDL muscles from PGC-1α-TG mice are significantly weaker than EDL muscles from controls, Significant differences between control and genetically modified mice are indicated by *; significant changes between RAmKO and RAmKO-PGC1α-TG mice are indicated by #. *P* values were determined by Student's *t* test. $^{*/\#}P < 0.05$; $^{**/\#\#}P < 0.01$; $^{***/\#\#\#}P < 0.001$.

1. Summermatter S, et al. (2011) Remodeling of calcium handling in skeletal muscle through PGC-1{alpha}: Impact on force, fatigability and fiber type. *Am J Physiol Cell Physiol*.

Skeletal muscle mTORC1 regulates glucose uptake and systemic energy homeostasis

Klaas Romanino[1], Barbara Kupr[1], Verena Albert[1], C. Florian Bentzinger[1, 2], Thomas A. Lutz[3] and Markus A. Rüegg[1,*]

[1] Biozentrum, University of Basel, Klingelbergstrasse 70, Basel, 4056, Switzerland.

[2] Present address: The Sprott Centre for Stem Cell Research, Regenerative Medicine Program, Ottawa Health Research Institute, Ottawa, Ontario K1H 8L6, Canada.

[3] Institute of Veterinary Physiology, University of Zürich, Winterthurerstrasse 260, Zurich, 8057, Switzerland.

[*]Corresponding author:
Markus A. Rüegg, Ph.D.
Biozentrum, University of Basel
Klingelbergstrasse 70
4056 Basel
Switzerland
Phone: +41 61 267 2223
Email: markus-a.ruegg@unibas.ch

SUMMARY

The mammalian target of rapamycin complex 1 (mTORC1) is a central node in a complex net of signaling pathways that are involved in growth and survival of cells. The serine/threonine protein kinase integrates external signals and affects different nutrient pathways. Here we show that in skeletal muscle, inactivation of mTORC1 reduces diet-induced obesity and protects from hepatic steatosis. Mice with a muscle-specific inactivation of mTORC1 have increased energy expenditure, probably due to an upregulation of the uncoupling proteins. In addition to the elevated calorie consumption, the mice have a reduced transcription of fatty acid and glucose metabolism-regulating genes. The inefficient fatty acid metabolism is caused by a mitochondrial dysfunction mediated by reduced PGC-1α levels. Additionally, we demonstrate that skeletal muscle mTORC1 regulates HDAC4/5, which is the likely mediator of glucose uptake and glycolysis. Taken together, the mTORC1 is a central regulator of metabolic pathways in skeletal muscle and in addition affects systemic energy homeostasis.

Keywords: skeletal muscle; mTORC1; energy expenditure; HDAC, UCP

INTRODUCTION

The highly conserved serine/threonine protein kinase mammalian target of rapamycin (mTOR) is known to control numerous cellular processes related to cell growth (Wullschleger et al., 2006). mTOR can form two functionally distinct multiprotein complexes, the rapamycin-sensitive mTORC1, and mTORC2, which is only sensitive to prolonged rapamycin treatment (Sarbassov et al., 2006). mTORC1 is a central sensor of growth factors and nutrients in various cell types and was described to play an important role in different disease models like cancer, metabolic diseases and aging (Laplante and Sabatini, 2012). Thus, the interest on the mTOR pathway is growing extensively, especially with regard to type 2 diabetes and the obesity epidemic (Polak and Hall, 2009). mTORC1 is highly active in the liver and skeletal muscle of obese and high-fat-fed rodents (Khamzina et al., 2005; Um et al., 2004). Inhibition of mTOR signaling has been proposed to mimic calorie restriction, which is metabolically highly beneficial and extents lifespan (Selman et al., 2009). Paradoxically, prolonged treatment with the mTORC1-inhibitor rapamycin causes glucose intolerance and insulin resistance (Cunningham et al., 2007; Fraenkel et al., 2008; Houde et al., 2010). However, recent work demonstrates that the insulin resistance caused by chronic rapamycin treatment seems to be the result of the inactivation of mTORC2 and not mTORC1 and that this impact is uncoupled from the beneficial systemic effects of mTORC1 inhibition (Lamming et al., 2012).

It is difficult to distinguish the contribution of different tissues on the systemic effects of rapamycin treatment. To address this question, various mouse models with tissue-specific deletions of essential components of the mTORC1 were generated over the last years (Laplante and Sabatini, 2012). White adipose tissue (WAT)-specific deletion of raptor, a component essential for the activity of mTORC1, leads to improved insulin sensitivity and reduced adipocyte number and size (Polak et al., 2008). Inactivation of mTORC1 in the liver leads to resistance to hepatic steatosis and hypercholesteremia induced by a Western diet (Peterson et al., 2011).

Loss of functional mTORC1 in skeletal muscle leads to a progressive muscle atrophy and an early death (Bentzinger et al., 2008; Risson et al., 2009). In addition, mTORC1 deficiency in skeletal muscle causes a variety of tissue-specific metabolic changes. mTORC1 activity in muscle is necessary for the formation of a functional complex of YY1 with PGC-1α and by this means regulates PGC-1α levels itself and mitochondrial gene expression (Blattler et al., 2012b; Cunningham et al., 2007). Due to reduced PGC-1α levels, the oxidative capacity of mTORC1-deficient muscle is severely impaired (Romanino et al., 2011). Inactivation of mTORC1 in skeletal muscle also causes elevated levels of glycogen due to an increase of glycogen synthesis and a decrease of glycogen degradation (Bentzinger et al., 2008; Romanino et al., 2011).

Glucose uptake of peripheral tissue is an important factor in type 2 diabetes and skeletal muscle is a major site of glucose uptake in response to food intake and insulin. In this study we show that skeletal muscle mTORC1 regulates systemic energy homeostasis and that both fatty acid (FA) and glucose metabolism are dependent on proper mTORC1 signaling in skeletal muscle. In particular, we provide evidence that inactivation of mTORC1 in skeletal muscle leads to an upregulation of class II histone deacetylases (HDACs), correlating with a downregulation of glycolytic genes and a decrease of the glucose uptake.

RESULTS

Inactivation of mTORC1 in skeletal muscle reduces diet-induced obesity and protects from hepatic steatosis.

Mice with muscle-specific knock out of *rptor* (called RAmKO mice) suffer from a strongly reduced body weight, due to muscle atrophy that is accompanied by reduced weight of the epididymal fat pads (Bentzinger et al., 2008). To investigate whether the phenotype of RAmKO mice can be ameliorated by increased calorie intake, we fed the mice a high-fat (HFD) or a high-carbohydrate diet (HCD). After 14 weeks, the difference in body weight between RAmKO and control (ctrl) mice became apparent (Figure 1A, B and Table S1). Ctrl mice gained weight on a HCD and became severely obese on a HFD, whereas RAmKO mice were completely resistant to diet-induced obesity. Interestingly, the effect of muscle-specific inactivation of mTORC1 also affected other tissues than skeletal muscle itself. HFD induced an enlarged and paler liver in ctrl mice that was due to an accumulation of lipids (hepatic steatosis). In contrast, the liver of RAmKO mice which were on a HFD for the same time period showed a normal size and coloration (Figure 1C and Table S1). In contrast to the ctrls, liver sections stained with Oil Red O demonstrated no accumulation of lipids in RAmKO mice fed a HFD (Figure 1D). The inability to accumulate lipids and gain weight can be the result of altered feeding behavior or nutrient absorption. We analyzed the food intake of the RAmKO mice and found it to be unchanged (Figure 1E). Also the ability of the body to take up nutrients, as assessed by quantifying the amount of lipids in the feces, was not altered (Figure 1F). Because the activity of the RAmKO mice is strongly reduced due to their myopathic phenotype (Bentzinger et al., 2008), activity cannot be responsible for their leanness either. Using indirect calorimetry we investigated the energy expenditure of ctrl and RAmKO mice and found that the calorie consumption was significantly elevated in the latter (Figure 1G). The effect can be observed both in the dark and the light phase, again suggesting that the activity of the mice is not relevant. Together, these

results show that due to higher energy consumption RAmKO mice are resistant to diet-induced obesity and hepatic steatosis.

There is no shift in substrate utilization in RAmKO mice but fatty acid and glucose metabolism are reduced.

Oxygen and carbohydrate level measurements showed no difference of the respiratory exchange ratio (RER) of RAmKO compared to ctrl mice (Figure 2A). Hence, RAmKO mice show no change in the preference of either carbohydrates or fat as an energy source. This was unexpected, because RAmKO muscle has a reduced oxidative capacity and contains increased glycogen levels (Bentzinger et al., 2008), both indications of a shift in nutrient utilization. Interestingly, transcript levels of genes important for the transport of FA and β-oxidation were all significantly lower in RAmKO mice compared to ctrl littermates (Figure 2B). Because both processes take place in the mitochondria, this is likely due to the reduced number of mitochondria in RAmKO mice caused by PGC-1α reduction (Romanino et al., 2011). RAmKO muscle also expressed lower levels of glucose transporters (GLUT1 and GLUT4) and other glucose metabolism genes (Figure 2C). This confirms that there is no shift in substrate utilization in skeletal muscle after mTORC1 inactivation, but both FA and glucose metabolism are reduced. The fact that the levels of glucose transporters are reduced explains why the uptake of glucose is impaired in RAmKO mice as seen by a shift in the glucose tolerance curve (GTT) in our previous publication (Bentzinger et al., 2008). Fasting blood glucose levels were not significantly changed, but tended to be lower in RAmKO mice than ctrl mice (Figure 2D). However, compared to ctrl littermates, RAmKO mice exhibited significantly lower circulating insulin concentrations (Figure 2E). To directly assess whether the RAmKO mice are responsive to insulin, we carried out an insulin tolerance test (ITT) (Figure 2F). RAmKO mice showed a slightly delayed response to insulin, reflecting the reduced uptake of glucose in skeletal muscle.

The substantial effect of skeletal muscle-specific inactivation of mTORC1 on global energy homeostasis raises the question whether signaling in other metabolically active tissues, such as the liver, is also affected. Therefore, we analyzed the transcription of genes important for FA and glucose metabolism in the liver of the RAmKO mice. In both cases no changes in mRNA levels could be observed compared to ctrl animals (Figure S1A and S1B). In addition, the levels of two important metabolic regulators in the liver, PGC-1α and HNF4α were also unchanged (Figure S1C). In summary, our data show that glycogen storage and glucose usage are differentially regulated in muscles of RAmKO mice. Additionally, compared to ctrls there is no metabolic shift in mTORC1-inactivated skeletal muscle but both, glycolytic and FA oxidizing genes are significantly downregulated and there is no compensatory mechanism in the liver.

Skeletal muscle mTORC1 regulates HDAC4/5 and uncoupling proteins

Glycogen storage, glucose uptake and glycolysis are differentially regulated by mTORC1. The increase of the glycogen synthesis in RAmKO muscle is due to the hyperactivation of Akt/PKB and its target glycogen synthase kinase 3β (GSK3β) (Bentzinger et al., 2008). However, the reduced glucose uptake and glycolysis must have another mechanism, because activation of Akt/PKB in skeletal muscle has been shown to upregulate glycolytic proteins (Izumiya et al., 2008). Several alternative pathways have been described to regulate glycolytic proteins. *In vitro* mTORC1 has been shown to activate glucose uptake and glycolysis over the hypoxia-inducible factor-1α (HIF-1α) (Duvel et al., 2010). However, HIF-1α does not seem to be responsible for the reduction of the glycolytic proteins in skeletal muscle, as its protein level and prolyl hydroxylation were unchanged in RAmKO mice (Figure S2A). Next to HIF-1α, the class II histone deacetylases 4 and 5 (HDAC 4 and 5) were described to regulate glycolytic proteins in skeletal muscle (McGee et al., 2008; Tang et al., 2009). Indeed, the protein levels of HDAC 4 and 5 were upregulated in RAmKO mice (Figure 3A and quantification in Table S2). Secondly, Dach2 which is known to be inhibited by HDAC4 and 5 in skeletal muscle was reduced (Figure 3B), confirming

the increased activity of the HDACs. Dach2 is an inhibitor of myogenin, which was strongly upregulated in RAmKO mice (Figure 3C). It is well described that the HDACs and its downstream targets are regulated through activity and innervation (Moresi et al., 2010; Tang and Goldman, 2006). Especially in denervated muscle the HDAC-Dach2-myogenin signaling pathway has been shown to be differently regulated (Cohen et al., 2007). Interestingly, in RAmKO mice we could observe ectopic clusters in the diaphragm (Bentzinger et al., 2008) and an upregulation of acetylcholine receptor α and γ (AChRα, γ) in the soleus muscle (Figure S2B and S2C), all signs of destabilization of the neuromuscular junctions (NMJs).

Even though the HDACs are the likely cause of the downregulation of glycolytic genes in RAmKO muscle, the increased energy expenditure in RAmKO mice remains unexplained. Uncoupling proteins (UCPs) are key factors in the regulation of energy expenditure (Azzu and Brand, 2010). Through uncoupling of the proton gradient in the inner membrane of the mitochondria, the UCPs regulate the efficiency of ATP production and therefore the energy expenditure. mTORC1 has previously been described to regulate the UCPs in WAT (Polak et al., 2008). Therefore we decided to investigate the levels of UCPs in RAmKO mice. The levels of ubiquitously expressed UCP2 and the muscle-specific UCP3 were both increased in RAmKO muscle, as shown by qRT-PCR (Figure 3D) and western blot (Figure 3E and quantification in Table S2). The effect of skeletal muscle mTORC1 on energy expenditure again seems to be muscle-specific, as the UCPs in liver, white and brown adipose tissue (BAT) were not significantly increased (Figure S2D and S2E). Taken together, our data show that the decrease of the glycolytic genes correlates to an increase of HDAC4 and 5, and that like in the WAT, mTORC1 regulates the UCPs and energy expenditure.

DISCUSSION

The control of energy balance plays a central role in metabolic diseases such as type 2 diabetes and obesity. mTORC1 has been postulated to play an essential role in glucose homeostasis by fine tuning the insulin signaling and by controlling metabolic pathways in different tissues (Tremblay et al., 2005; Um et al., 2006). Skeletal muscle is a particularly important player in the regulation of energy balance in the body. Here we show that inactivation of mTORC1 in skeletal muscle reduces glucose uptake and glycolysis. Previous work has shown that glycogen stores are significantly increased in mTORC1-deficient muscle (Bentzinger et al., 2008). Our data thus show that glucose uptake and glycolysis and glycogen storage are regulated by distinct pathways.

Similar to RAmKO mice, treatment with the mTORC1-inhibitor rapamycin leads to a reduced glucose uptake (Blattler et al., 2012a). However, rapamycin-treated mice become insulin resistant, whereas RAmKO mice are insulin tolerant. Treatment with rapamycin affects several metabolically active tissues simultaneously and reduces mTOR signaling in skeletal muscle and in the liver (Blattler et al., 2012a). We could not observe differences in key metabolic signaling pathways in the liver of RAmKO mice. After rapamycin treatment in both skeletal muscle and in the liver PKB/Akt activity is reduced (Blattler et al., 2012a). In RAmKO mice a strong activation of PKB/Akt is observed, because of the inhibitory feedback loop of S6K (Bentzinger et al., 2008). This results in increased levels of IRS-1 and activation of the insulin pathway. Intriguingly, RAmKO mice are protected from metabolic effects of rapamycin on glucose tolerance (Blattler et al., 2012a). This suggests that the activation state of the insulin pathway and PKB/Akt determines whether the mice are susceptible to the development of diabetes or not.

RAmKO mice display a reduction in glycolytic proteins that coincides with the increase in class II HDACs. Although HDACs have been described to regulate the transcription of glycolytic

proteins, in skeletal muscle they have mostly been implicated in denervation signaling (Cohen et al., 2007). Denervation upregulates HDACs and through inhibition of Dach2 it activates the transcription of myogenin. The transcription of Dach2 and myogenin in RAmKO mice is significantly altered, confirming changes in HDAC activity. In addition, as indicated by the upregulation of the α and γ subunits of the AChR, RAmKO mice show signs of NMJ destabilization. Nevertheless, the overall morphology of the NMJ is not severely disturbed (Bentzinger et al., 2008). The underlying cause of the mild NMJ destabilization observed in RAmKO mice remains to be determined. Taken together, our study reveals that mTORC1 and class II HDACs regulate glycolytic proteins and glucose uptake in skeletal muscle, resulting in mild effect on glucose tolerance.

Next to a reduction of glucose metabolism, inactivation of mTORC1 also leads to a reduced transcription of FA metabolism genes. This phenotype is paralleled by a reduction of the oxidative capacity of the muscles and by a reduction of the number of mitochondria. Therefore, it is most likely due to the lower levels of PGC-1α in RAmKO muscle. These results suggest that by controlling FA and glucose metabolism, glycogen storage and the oxidative capacity, mTORC1 is a central controller of metabolic properties of muscle tissue. Moreover, since both FA oxidation and glucose metabolism are decreased in RAmKO mice, inactivation of mTORC1 does not cause a preference for utilization of a particular nutrient.

Similar to adipose tissue, deletion of raptor in skeletal muscle leads to an upregulation of UCPs and thereby probably increases the energy expenditure of the RAmKO mice. Unlike the adipose-specific knockout of raptor (Polak et al., 2008), in RAmKO mice uncoupling proteins in the other metabolically active tissues are not affected. Similar to RAmKO mice, mice overexpressing human UCP3 are hyperphagic but lean, show reduced weight gain upon HFD and display significantly higher total oxygen consumption compared to ctrl littermates (Clapham et al., 2000).

Nevertheless, it is not completely clear if the regulation of UCP2 and UCP3 directly correlates with UCP1 regulation. It is debated whether UCP2 and UCP3 need an additional activation signal to be fully functional, since mice in which UCP2 or UCP3 are knocked out show only weak phenotypes (Brand and Esteves, 2005; Harper and Himms-Hagen, 2001).

Here we show that skeletal muscle mTORC1 plays an essential role in whole body homeostasis and energy expenditure. mTORC1 controls the major metabolic pathways in skeletal muscle. Both FA and glucose metabolism are impaired in RAmKO mice and the expression of UCPs is increased. The inefficient nutrient utilization and the increased energy demand lead to beneficial systemic effects and to a resistance to diet-induced obesity. Our work is first to analyze the systemic metabolic consequences of mTORC1 inhibition specifically in skeletal muscle. Moreover, our data demonstrates that muscle mTORC1 is a significant controller of systemic energy demand and implies that the beneficial effects of rapamycin on systemic metabolism and longevity could be due to inhibition of mTORC1 in skeletal muscle.

EXPERIMENTAL PROCEDURES

Animals and Diet Treatments

RAmKO mice (described earlier (Bentzinger et al., 2008)) carry floxed alleles for *rptor* and express the Cre recombinase under the control of the muscle-specific human skeletal actin (HSA) promoter. The animals were maintained in a conventional facility with a fixed light cycle. Food intake and body weight were measured weekly. Four weeks after weaning RAmKO and ctrl mice were fed a HFD (60% fat, 20% protein, and 20% carbohydrates, Research Diets), HCD (10% fat, 20% protein, and 70% carbohydrates, Research Diets) or normal chow (Kliba Nafag) for 14 weeks. Studies were carried out according to criteria outlined for the care and use of laboratory animals and with approval of the authorities.

Histology

Livers frozen in liquid nitrogen-cooled isopentane were cut into 10 µm cross-sections. Sections were stained with hematoxylin (Merck) and Oil Red-O (Sigma-Aldrich) and mounted with glycerol gelatin (Sigma-Aldrich).

Indirect Calorimetry

Mice were acclimatized for two days (individual housing) followed by data acquisition over three days. Oxygen use and carbon dioxide production was measured and energy expenditure was calculated with the Weir equation. Respiratory exchange ratio (RER) was calculated as VCO_2/ VO_2. Data were normalized to body weight.

Metabolic Measurements

The amount of lipids in feces was determined by collecting feces over 24 hrs and then a standard methanol:chloroform extraction. Blood glucose was measured directly from the tail vein

with the OneTouch UltraMini glucometer (LifeScan). Plasma Insulin amount was determined according to the manufacturer's instruction with the ultra-sensitive mouse insulin ELISA kit (Crystal Chem).

IP Insulin Tolerance Test (ITT)

The mice were fasted for 6 hrs and 0.5 mU/g insulin was injected. Basal blood glucose was measured before the injection and at the indicated time points after intraperitoneal injection.

Quantitative Real-time PCR

Total RNA was isolated (SV Total RNA isolation System, Promega) and equal amounts of RNA reverse transcribed using a mixture of oligodT and random hexamer primers (iScript cDNA Synthesis Kit, Bio-Rad). Quantitative real-time PCR was performed using SYBR Green (Power SYBR Green Master Mix, Applied Biosystems) and StepOne^{TM} Software 2.1. (Applied Biosystems). Expression levels for each gene of interest were normalized to the mean cycle number using real-time PCR for the housekeeping protein β-actin. All experiments were performed in triplicates and the following primers were used:

CD36	fw: TGGCCTTACTTGGGATTGG	bw: CCAGTGTATATGTAGGCTCATCCA
FATP1	fw: GGCTCCTGGAGCAGGAACA	bw: ACGGAAGTCCCAGAAACCA
FATP4	fw: GGCTTCCCTGGTGTACTATGGAT	bw: ACGATGTTTCCTGCTGAGTGGTA
FABPpm	fw: AGCGGCTGACCAAGGAGTT	bw: GACCCCTGCCACGGAGAT
FABP3	fw: CCCCTCAGCTCAGCACCA	bw: CAGAAAAATCCCAACCCAAGAAT
CPT-1b	fw: GGTCGATTGCATCCAGAGAT	bw: GACTCCGGTGGAGAAGATGA
MTE-1	fw: TGGGAACACCATCTCCTACAA	bw: CCACGACATCCAAGAGACCA
GLUT 1	fw: CGAGGGACAGCCGATGTG	bw: TGCCGACCCTCTTCTTTCAT
GLUT 4	fw: GATGAGAAACGGAAGTTGGAGAGA	bw: GCACCACTGCGATGATCAGA
HK2	fw: CCCTGCCACCAGACGAAA	bw: GACTTGAACCCCTTAGTCCATGA
PK	fw: CGATCTGTGGAGATGCTGAA	bw: AATGGGATCAGATGCAAAGC
PFK	fw: CAGATCAGTGCCAACATAACCAA	bw: CGGGATGCAGAGCTCATCA
LDHA	fw: TGTCTCCAGCAAAGACTACTGT	bw: GACTGTACTTGACAATGTTGGGA
Dach2	fw: ACTGAAAGTGGCTTTGGATAA	bw: TTCAGACGCTTTTGCATTGTA
Myogenin	fw: TGGGCGTGTAAGGTGTGTAA	bw: GGCCTCATTCACCTTCTTGA
UCP2	fw: ACCAAGGGCTCAGAGCATGCA	bw: TGGCTTTCAGGAGAGTATCTTTG

UCP3	fw: ACTCCAGCGTCGCCATCAGGATTCT	bw: TAAACAGGTGAGACTCCAGCAACTT
β-actin	fw: CAGCTTCTTTGCAGCTCCTT	bw: GCAGCGATATCGTCATCCA

Western Blotting

Western blots were performed as described earlier (Bentzinger et al., 2008) using following antibodies: HDAC4 from Santa Cruz Biotechnology, HDAC5 from Cell Signaling, UCP2 from Millipore, UCP3 from Abcam and α-actinin from Sigma. The concentrations used were according to the manufacturer and to determine total protein levels a reducing agent compatible BCA Protein Assay (Pierce) was used. Quantifications were performed with the ImageJ software. Grey values were corrected for background.

Statistical Analysis

Compiled data are expressed as mean ± SD. For statistical comparisons the Student's t-test was used. The level of significance is indicated as follows: *** $p<0.001$, ** $p< 0.01$, * $p< 0.05$.

ACKNOWLEDGMENTS

We are indebted to Christoph Handschin from the Biozentrum Basel for his support. This work was supported by the Cantons of Basel-Stadt and Baselland, grants from the Swiss Foundation for Research on Muscle Disease, Swiss Life and the Association Française contres les Myopathies.

REFERENCES

Azzu, V., and Brand, M.D. (2010). The on-off switches of the mitochondrial uncoupling proteins. Trends Biochem Sci *35*, 298-307.

Bentzinger, C.F., Romanino, K., Cloetta, D., Lin, S., Mascarenhas, J.B., Oliveri, F., Xia, J., Casanova, E., Costa, C.F., Brink, M.*, et al.* (2008). Skeletal muscle-specific ablation of raptor, but not of rictor, causes metabolic changes and results in muscle dystrophy. Cell metabolism *8*, 411-424.

Blattler, S.M., Cunningham, J.T., Verdeguer, F., Chim, H., Haas, W., Liu, H., Romanino, K., Ruegg, M.A., Gygi, S.P., Shi, Y.*, et al.* (2012a). Yin Yang 1 deficiency in skeletal muscle protects against rapamycin-induced diabetic-like symptoms through activation of insulin/IGF signaling. Cell metabolism *15*, 505-517.

Blattler, S.M., Verdeguer, F., Liesa, M., Cunningham, J.T., Vogel, R.O., Chim, H., Liu, H., Romanino, K., Shirihai, O.S., Vazquez, F.*, et al.* (2012b). Defective mitochondrial morphology and bioenergetic function in mice lacking the transcription factor YY1 in skeletal muscle. Molecular and cellular biology.

Brand, M.D., and Esteves, T.C. (2005). Physiological functions of the mitochondrial uncoupling proteins UCP2 and UCP3. Cell metabolism *2*, 85-93.

Clapham, J.C., Arch, J.R., Chapman, H., Haynes, A., Lister, C., Moore, G.B., Piercy, V., Carter, S.A., Lehner, I., Smith, S.A.*, et al.* (2000). Mice overexpressing human uncoupling protein-3 in skeletal muscle are hyperphagic and lean. Nature *406*, 415-418.

Cohen, T.J., Waddell, D.S., Barrientos, T., Lu, Z., Feng, G., Cox, G.A., Bodine, S.C., and Yao, T.P. (2007). The histone deacetylase HDAC4 connects neural activity to muscle transcriptional reprogramming. The Journal of biological chemistry *282*, 33752-33759.

Cunningham, J.T., Rodgers, J.T., Arlow, D.H., Vazquez, F., Mootha, V.K., and Puigserver, P. (2007). mTOR controls mitochondrial oxidative function through a YY1-PGC-1alpha transcriptional complex. Nature *450*, 736-740.

Duvel, K., Yecies, J.L., Menon, S., Raman, P., Lipovsky, A.I., Souza, A.L., Triantafellow, E., Ma, Q., Gorski, R., Cleaver, S.*, et al.* (2010). Activation of a metabolic gene regulatory network downstream of mTOR complex 1. Mol Cell *39*, 171-183.

Fraenkel, M., Ketzinel-Gilad, M., Ariav, Y., Pappo, O., Karaca, M., Castel, J., Berthault, M.F., Magnan, C., Cerasi, E., Kaiser, N.*, et al.* (2008). mTOR inhibition by rapamycin prevents beta-cell adaptation to hyperglycemia and exacerbates the metabolic state in type 2 diabetes. Diabetes *57*, 945-957.

Harper, M.E., and Himms-Hagen, J. (2001). Mitochondrial efficiency: lessons learned from transgenic mice. Biochim Biophys Acta *1504*, 159-172.

Houde, V.P., Brule, S., Festuccia, W.T., Blanchard, P.G., Bellmann, K., Deshaies, Y., and Marette, A. (2010). Chronic rapamycin treatment causes glucose intolerance and hyperlipidemia by upregulating hepatic gluconeogenesis and impairing lipid deposition in adipose tissue. Diabetes *59*, 1338-1348.

Izumiya, Y., Hopkins, T., Morris, C., Sato, K., Zeng, L., Viereck, J., Hamilton, J.A., Ouchi, N., LeBrasseur, N.K., and Walsh, K. (2008). Fast/Glycolytic muscle fiber growth reduces fat mass and improves metabolic parameters in obese mice. Cell metabolism *7*, 159-172.

Khamzina, L., Veilleux, A., Bergeron, S., and Marette, A. (2005). Increased activation of the mammalian target of rapamycin pathway in liver and skeletal muscle of obese rats: possible involvement in obesity-linked insulin resistance. Endocrinology *146*, 1473-1481.

Lamming, D.W., Ye, L., Katajisto, P., Goncalves, M.D., Saitoh, M., Stevens, D.M., Davis, J.G., Salmon, A.B., Richardson, A., Ahima, R.S.*, et al.* (2012). Rapamycin-induced insulin resistance is mediated by mTORC2 loss and uncoupled from longevity. Science *335*, 1638-1643.

Laplante, M., and Sabatini, D.M. (2012). mTOR signaling in growth control and disease. Cell *149*, 274-293.

McGee, S.L., van Denderen, B.J., Howlett, K.F., Mollica, J., Schertzer, J.D., Kemp, B.E., and Hargreaves, M. (2008). AMP-activated protein kinase regulates GLUT4 transcription by phosphorylating histone deacetylase 5. Diabetes *57*, 860-867.

Moresi, V., Williams, A.H., Meadows, E., Flynn, J.M., Potthoff, M.J., McAnally, J., Shelton, J.M., Backs, J., Klein, W.H., Richardson, J.A.*, et al.* (2010). Myogenin and class II HDACs control neurogenic muscle atrophy by inducing E3 ubiquitin ligases. Cell *143*, 35-45.

Peterson, T.R., Sengupta, S.S., Harris, T.E., Carmack, A.E., Kang, S.A., Balderas, E., Guertin, D.A., Madden, K.L., Carpenter, A.E., Finck, B.N.*, et al.* (2011). mTOR complex 1 regulates lipin 1 localization to control the SREBP pathway. Cell *146*, 408-420.

Polak, P., Cybulski, N., Feige, J.N., Auwerx, J., Ruegg, M.A., and Hall, M.N. (2008). Adipose-specific knockout of raptor results in lean mice with enhanced mitochondrial respiration. Cell metabolism *8*, 399-410.

Polak, P., and Hall, M.N. (2009). mTOR and the control of whole body metabolism. Curr Opin Cell Biol *21*, 209-218.

Risson, V., Mazelin, L., Roceri, M., Sanchez, H., Moncollin, V., Corneloup, C., Richard-Bulteau, H., Vignaud, A., Baas, D., Defour, A.*, et al.* (2009). Muscle inactivation of mTOR causes metabolic and dystrophin defects leading to severe myopathy. The Journal of cell biology *187*, 859-874.

Romanino, K., Mazelin, L., Albert, V., Conjard-Duplany, A., Lin, S., Bentzinger, C.F., Handschin, C., Puigserver, P., Zorzato, F., Schaeffer, L.*, et al.* (2011). Myopathy caused by mammalian target of rapamycin complex 1 (mTORC1) inactivation is not reversed by restoring mitochondrial function. Proceedings of the National Academy of Sciences of the United States of America *108*, 20808-20813.

Sarbassov, D.D., Ali, S.M., Sengupta, S., Sheen, J.H., Hsu, P.P., Bagley, A.F., Markhard, A.L., and Sabatini, D.M. (2006). Prolonged rapamycin treatment inhibits mTORC2 assembly and Akt/PKB. Mol Cell *22*, 159-168.

Selman, C., Tullet, J.M., Wieser, D., Irvine, E., Lingard, S.J., Choudhury, A.I., Claret, M., Al-Qassab, H., Carmignac, D., Ramadani, F.*, et al.* (2009). Ribosomal protein S6 kinase 1 signaling regulates mammalian life span. Science *326*, 140-144.

Tang, H., and Goldman, D. (2006). Activity-dependent gene regulation in skeletal muscle is mediated by a histone deacetylase (HDAC)-Dach2-myogenin signal transduction cascade. Proceedings of the National Academy of Sciences of the United States of America *103*, 16977-16982.

Tang, H., Macpherson, P., Marvin, M., Meadows, E., Klein, W.H., Yang, X.J., and Goldman, D. (2009). A histone deacetylase 4/myogenin positive feedback loop coordinates denervation-dependent gene induction and suppression. Mol Biol Cell *20*, 1120-1131.

Tremblay, F., Gagnon, A., Veilleux, A., Sorisky, A., and Marette, A. (2005). Activation of the mammalian target of rapamycin pathway acutely inhibits insulin signaling to Akt and glucose transport in 3T3-L1 and human adipocytes. Endocrinology *146*, 1328-1337.

Um, S.H., D'Alessio, D., and Thomas, G. (2006). Nutrient overload, insulin resistance, and ribosomal protein S6 kinase 1, S6K1. Cell metabolism *3*, 393-402.

Um, S.H., Frigerio, F., Watanabe, M., Picard, F., Joaquin, M., Sticker, M., Fumagalli, S., Allegrini, P.R., Kozma, S.C., Auwerx, J.*, et al.* (2004). Absence of S6K1 protects against age- and diet-induced obesity while enhancing insulin sensitivity. Nature *431*, 200-205.

Wullschleger, S., Loewith, R., and Hall, M.N. (2006). TOR signaling in growth and metabolism. Cell *124*, 471-484.

Figure 1

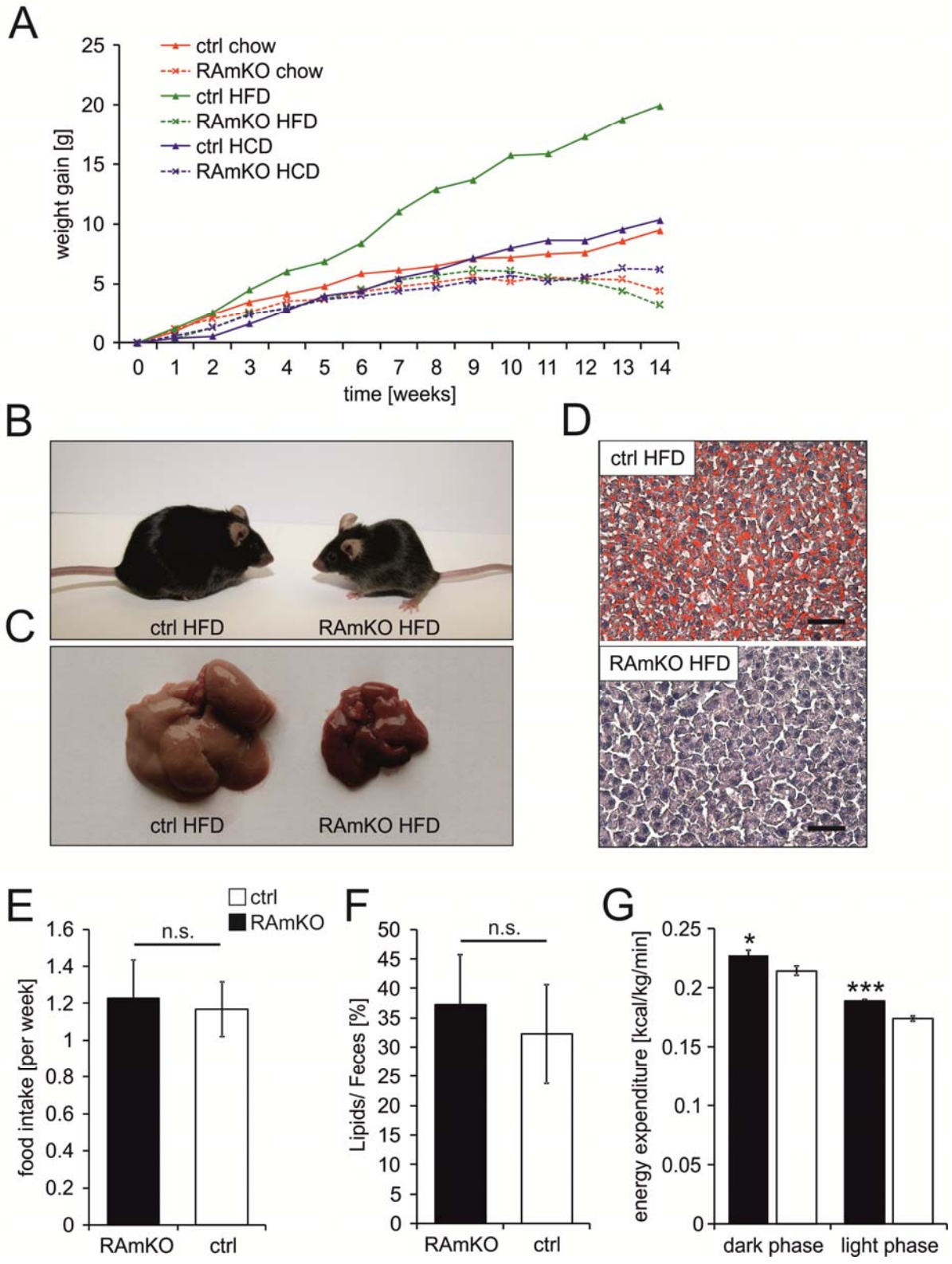
A
ctrl chow
RAmKO chow
ctrl HFD
RAmKO HFD
ctrl HCD
RAmKO HCD
weight gain [g]
time [weeks]
B
ctrl HFD
RAmKO HFD
C
ctrl HFD
RAmKO HFD
D
ctrl HFD
RAmKO HFD
E
ctrl
RAmKO
n.s.
food intake [per week]
RAmKO
ctrl
F
n.s.
Lipids/ Feces [%]
RAmKO
ctrl
G
*
***
energy expenditure [kcal/kg/min]
dark phase
light phase

Figure 1. RAmKO mice are resistant to diet-induced obesity and hepatic steatosis due to increased energy expenditure

(A) Raptor muscle-knockout (RAmKO) and control (ctrl) mice were reared with a normal chow diet, high-fat diet (HFD) or a high-carbohydrate diet (HCD) starting at the age of 6 weeks. Animals were weighed weekly. Starting at the age of 6 weeks, RAmKO mice weigh significantly less than ctrl mice on all three diets (n=5-8).

(B) Representative photograph showing mice that were on a HFD for 100 days. RAmKO mice compared to ctrl littermates clearly do not show the dramatic increase of body weight due to the diet.

(C) Picture shows representative livers of mice after 100 days on HFD. Muscle deficiency of raptor protects from HFD-induced hepatic steatosis, which is characterized by an enlarged liver containing a high number of vacuoles filled with triglycerides.

(D) Cross-sections of livers from mice that were on a HFD for 100 days stained with Oil Red O and hematoxylin. The red color is indicative for the lipid content in the tissue. Ctrl mice suffer from an accumulation of lipids after a HFD, RAmKO mice do not. Scale bar = 50 μm.

(E) Average daily food intake of normal chow measured over 100 days. Food intake of RAmKO mice is not changed compared to ctrl littermates. Data are normalized to body weight (n=5-8).

(F) Lipid absorption in the digestive system was measured by methanol:chloroform extraction in feces, that was collected over 24 hrs. No difference was found between RAmKO and ctrl mice. Weight of the extracted lipids is given as percentage of the total weight. Mice were around 12 weeks old (n=4-7).

(G) Energy expenditure measured by indirect calorimetry. Data are normalized to body weight. RAmKO mice burn in average 7% more calories. The difference is larger in the light phase when ctrl and RAmKO mice are less active. Mice were around 12 weeks old (n=8).

Values in E-G represent mean ± SD. p values are *$p < 0.05$, **$p < 0.01$, ***$p < 0.001$.

Figure 2

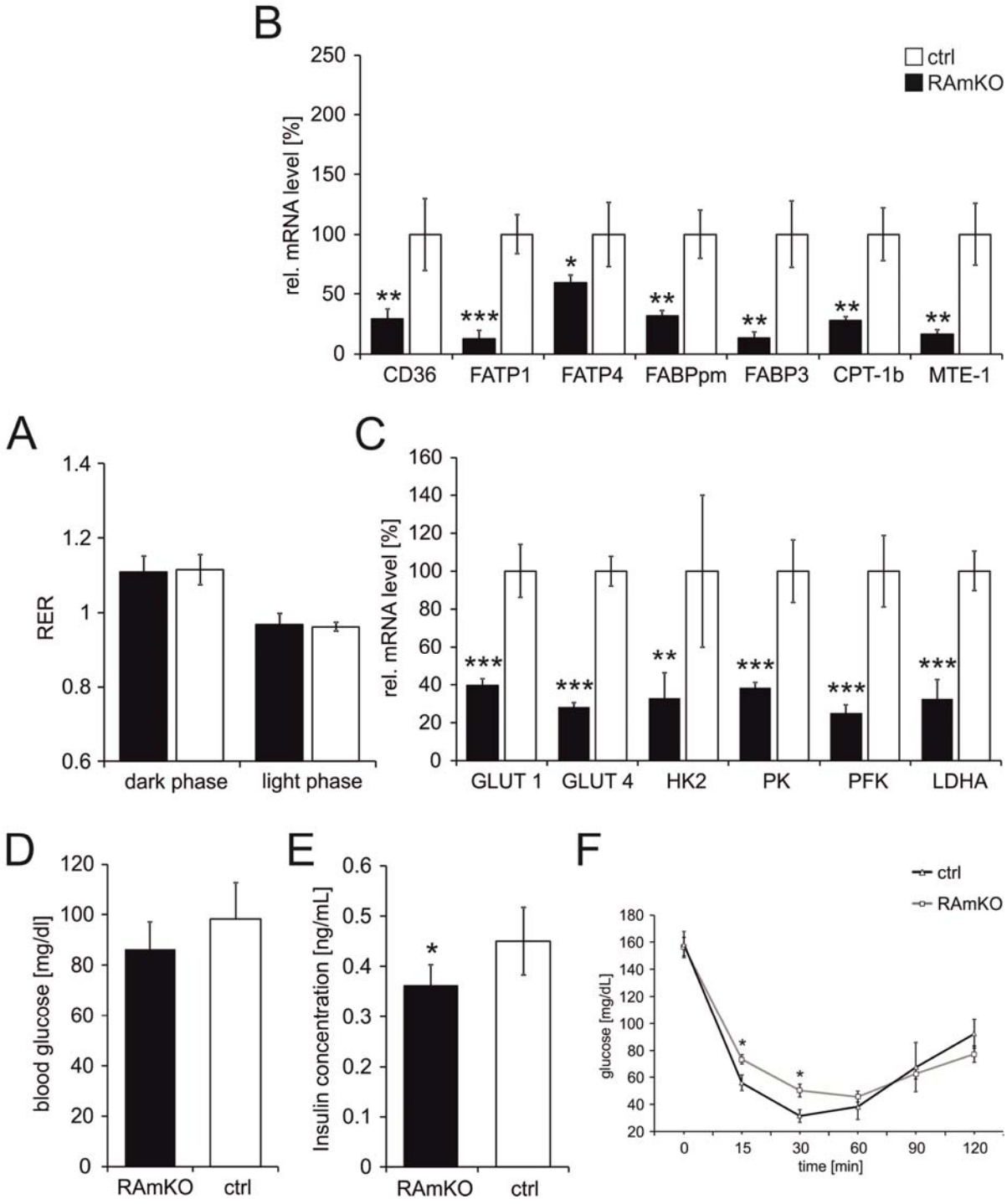
B
ctrl
RAmKO
rel. mRNA level [%]
250
200
150
100
50
0
**
***
*
**
**
**
**
CD36
FATP1
FATP4
FABPpm
FABP3
CPT-1b
MTE-1
A
RER
1.4
1.2
1
0.8
0.6
dark phase
light phase
C
rel. mRNA level [%]
160
140
120
100
80
60
40
20
0
***
***
**
***
***
***
GLUT 1
GLUT 4
HK2
PK
PFK
LDHA
D
blood glucose [mg/dl]
120
100
80
60
40
20
0
RAmKO
ctrl
E
Insulin concentration [ng/mL]
0.6
0.5
0.4
0.3
0.2
0.1
0
*
RAmKO
ctrl
F
ctrl
RAmKO
glucose [mg/dL]
180
160
140
120
100
80
60
40
20
*
*
0
15
30
60
90
120
time [min]

Figure 2. RAmKO mice show a reduction of fatty acid and glucose metabolism

(A) Respiratory exchange ratio (RER) measured by indirect calorimetry. Both in the light and the dark phase RAmKO and ctrl mice have the same turnover of oxygen to carbon dioxide, indicating that the mice metabolize the same fuel sources to supply the body with energy. Mice were around 12 weeks old (n=8).

(B) Relative mRNA levels of the indicated genes controlling fatty acid (FA) metabolism in soleus muscle of 12-week-old mice determined by qRT-PCR. RAmKO mice show a reduction in the mRNA levels of genes controlling FA uptake: CD36 (also known as fatty acid translocase), fatty acid transport protein 1 and 4 (FATP1, FATP4), plasma membrane-associated fatty acid binding protein (FABPpm). Gene controlling FA binding: fatty acid binding protein 3 (FABP3). Genes responsible for the activation of FA for β-oxidation: carnitine palmitoyltransferase 1 (CPT-1b) and mitochondrial thioesterase (MTE-1) (n=3-5).

(C) Relative mRNA levels of the indicated genes controlling glucose metabolism in soleus muscle of 12-week-old mice determined by qRT-PCR. RAmKO mice have lower mRNA levels of genes controlling glucose uptake: glucose transporter 1 and 4 (GLUT 1, 4) and several glycolytic genes: hexokinase 2 (HK2), pyruvate kinase (PK), phosphofructokinase (PFK), lactate dehydrogenase A (LDHA) (n=5-6).

(D) Blood glucose concentration after overnight fasting of 9-week-old RAmKO mice and control littermates. Glucose levels are unchanged in RAmKO mice, but have a tendency to be lower (n=8-11).

(E) Insulin concentration in the blood of 12-week-old RAmKO mice and control littermates. Insulin levels are slightly reduced in RAmKO mice (n=4-5).

(F) Insulin tolerance test (ITT). RAmKO mice are mildly insulin resistant (n=4-5).

Values in A-F represent mean ± SD. p values are *$p < 0.05$, **$p < 0.01$, ***$p < 0.001$.

Figure 3

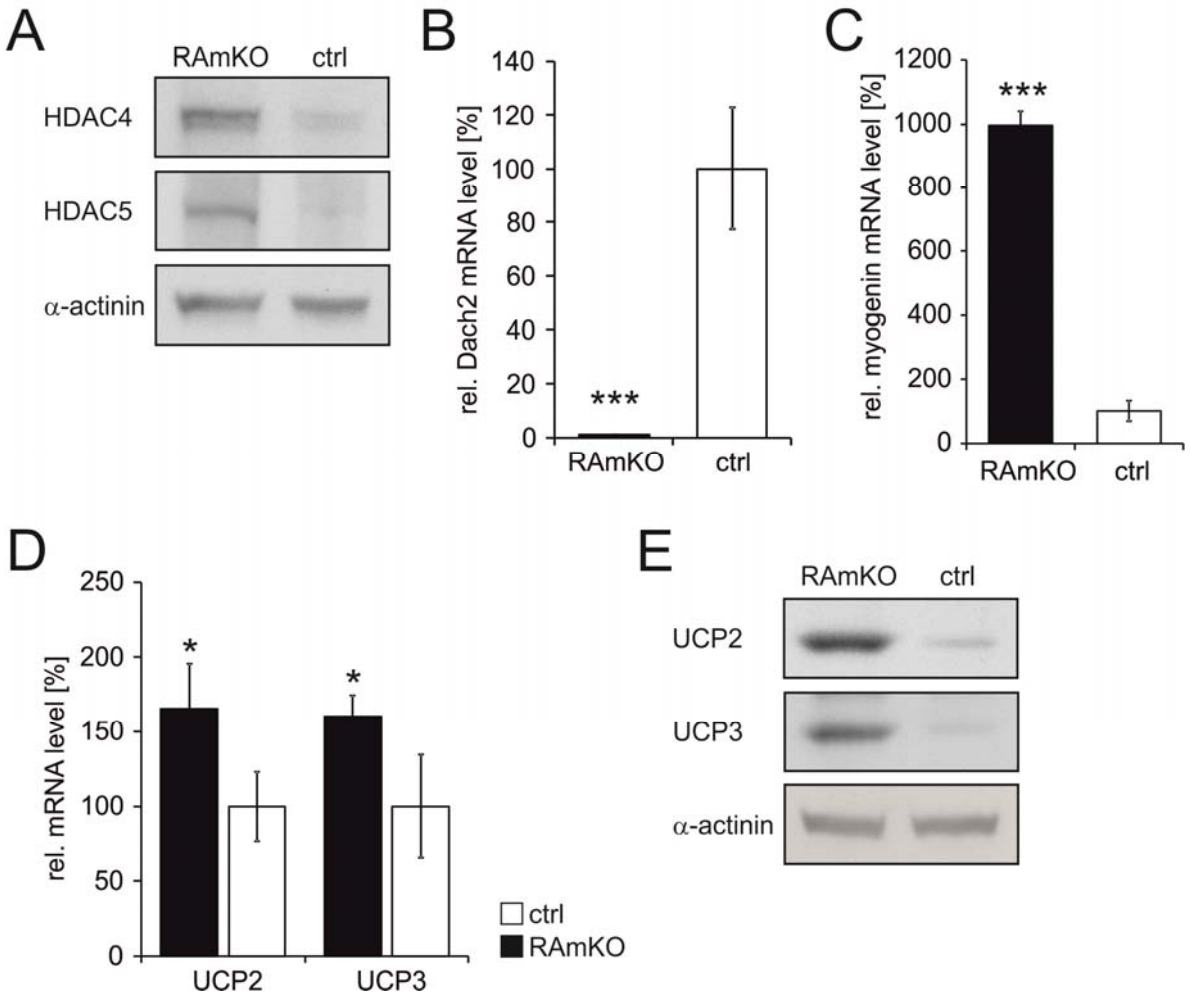

Figure 3. HDACs and UCPs are upregulated in RAmKO mice

(A) Representative western blot of soleus muscle lysates from 12-week-old mice using antibodies directed against the proteins indicated. The levels of histone deacetylases 4 and 5 (HDAC4, HDAC5) are elevated in RAmKO muscles. Equal amount of protein was loaded in each lane. An antibody against α-actinin was used as loading control. For quantification see Supplemental Table 1 (n=4-5).

(B, C) Relative mRNA levels of the HDAC targets, Dach2 and myogenin, in soleus muscle of 12-week-old mice as determined by qRT-PCR (n=5-6).

(D) Relative mRNA levels of the indicated genes in soleus muscle of 12-week-old mice as determined by qRT-PCR. The uncoupling proteins 2 and 3 (UCP2, UCP3) show a higher expression in the muscle of RAmKO mice (n=3-4).

(E) Representative western blot of soleus muscle lysates from 12-week-old mice using antibodies directed against the proteins indicated. The levels of the uncoupling proteins are elevated in RAmKO muscles. Equal amount of protein was loaded in each lane. An antibody against α-actinin was used as loading control. For quantification see Supplemental Table 1 (n=4-5).

Values in B, C and D represent mean ± SD. p values are *$p < 0.05$, **$p < 0.01$, ***$p < 0.001$.

Supplemental Data

SUPPLEMENTAL EXPERIMENTAL PROCEDURES

Quantitative Real-time PCR

Expression levels for each gene of interest were normalized to the mean cycle number using real-time PCR for the different housekeeping proteins. β-actin was used for the skeletal muscle and the liver samples. For the WAT polymerase (RNA) II polypeptide A (PolR2a) and for the BAT TATA Box binding protein (TBP) was used as a housekeeper. Following primers were used:

PPARα	fw: TGTTTGTGGCTGCTATAATTTGC	bw: GCAACTTCTCAATGTAGCCTATGTTT
Mttp	fw: CGTCCACATACAGCCTTGAC	bw: CCACCTGACTACCATGAAGC
CPT1a	fw: GGAGAGAATTTCATCCACTTCCA	bw: CTTCCCAAAGCGGTGTGAGT
Dgat1	fw: CATGCGTGATTATTGCATCC	bw: ACAGGTTGACATCCCGGTAG
MCAD	fw: TTTCGAAGACGTCAGAGTGC	bw: TGCGACTGTAGGTCTGGTTC
ACC-1	fw: ACCTTACTGCCATCCCATGTG	bw: GTGCCTGATGATCGACGAACAAA
SCD1	fw: CAAGCTGGAGTACGTCTGGA	bw: CAGAGCGCTGGTCATGTAGT
GLUT1	fw: CGAGGGACAGCCGATGTG	bw: TGCCGACCCTCTTCTTTCAT
GLUT2	fw: GTCCAGAAAGCCCCAGATACC	bw: GTGACATCCTCAGTTCCTCTTAG
GK	fw: CCCTGAGTGGCTTACAGTTC	bw: ACGGATGTGAGTGTTGAAGC
G6Pase	fw: CAGAATGGGTCCACCTTGACAC	bw: AGCGGAATGGGAGCAACTTG
PEPCK	fw: GCATAACTAACCCGAAGGCAAG	bw: CATCCAGGCAATGTCATCGC
PGC-1α	fw: TGATGTGAATGACTTGGATACAGACA	bw: GCTCATTGTTGTACTGGTTGGATATG
HNF4α	fw: CCTGCAGGTTTAGCCGACAAT	bw: ATCCGGTCCCGCTCATTTT
AChRγ	fw: AACGAGACTCGGATGTGGTC	bw: GTCGCACCACTGCATCTCTA
AChRα	fw: CGTCTGGTGGCAAAGCT	bw: CCGCTCTCCATGAAGTT
UCP1	fw: CGACTCAGTCCAAGAGTACTTCTCTTC	bw: GCCGGCTGAGATCTTGTTTC
UCP2	fw: TCCCCTGTTGATGTGGTCAA	bw: CAGTGACCTGCGCTGTGGTA
PolR2a	fw: AATCCGCATCATGAACAGTG	bw: CAGCATGTTGGACTCAATGC
TBP	fw: TGCTGTTGGTGATTGTTGGT	bw: CTGGCTTGTGTGGGAAAGAT

Antibodies

HIF-1α and Hydroxy-HIF-1α (Pro564) from Cell Signaling were used for western blot.

Figure S1

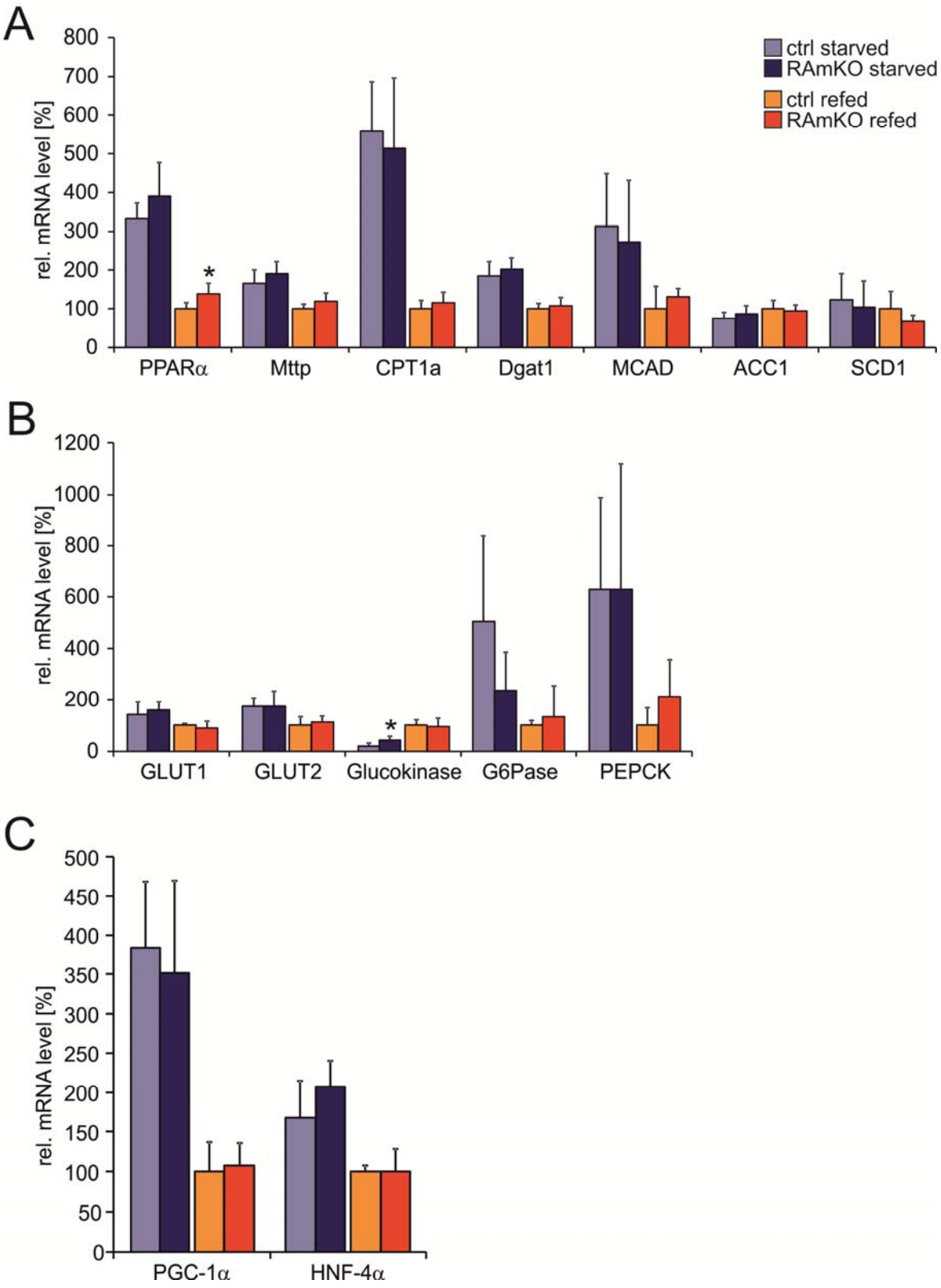
A
rel. mRNA level [%]
800
700
600
500
400
300
200
100
0
ctrl starved
RAmKO starved
ctrl refed
RAmKO refed
*
PPARα
Mttp
CPT1a
Dgat1
MCAD
ACC1
SCD1
B
rel. mRNA level [%]
1200
1000
800
600
400
200
0
*
GLUT1
GLUT2
Glucokinase
G6Pase
PEPCK
C
rel. mRNA level [%]
500
450
400
350
300
250
200
150
100
50
0
PGC-1α
HNF-4α

Figure S1.

(A) Relative mRNA levels of the indicated genes controlling fatty acid (FA) metabolism in liver of 12-week-old mice determined by qRT-PCR. FA metabolism is not changed in the liver of RAmKO mice. The following transcripts were analyzed: peroxisome proliferator-activated receptor α (PPARα), microsomal triglyceride transfer protein (Mttp), carnitine palmitoyltransferase I (CPT1a), diglyceride acyltransferase 1 (Dgat1), medium-chain acyl-CoA dehydrogenase (MCAD), acetyl-CoA carboxylase 1 (ACC1), stearoyl-CoA desaturase-1 (SCD1) (n=4-6).

(B) Relative mRNA levels of the indicated genes controlling glucose metabolism in liver of 12-week-old mice as determined by qRT-PCR. Transcription of glycolytic genes is not changed in the liver of RAmKO mice. The following transcripts were analyzed: glucose transporter 1 and 2 (GLUT 1, 2), glucokinase, glucose-6-phosphatase (G6Pase), phosphoenolpyruvate carboxykinase (PEPCK) (n=4-6).

(C) Relative mRNA levels of the main regulator of mitochondrial biogenesis, PPARγ coactivator-1α (PGC-1α), and a liver specific regulator of lipid transport and glucose metabolism, hepatocyte nuclear factor 4α (HNF-4α), in liver of 12-week-old mice as determined by qRT-PCR (n=4-6).

All mice for the liver analysis were starved overnight and half of them were refed for 4 hrs. All values represent mean ± SD. p values are *$p < 0.05$, **$p < 0.01$, ***$p < 0.001$.

Figure S2

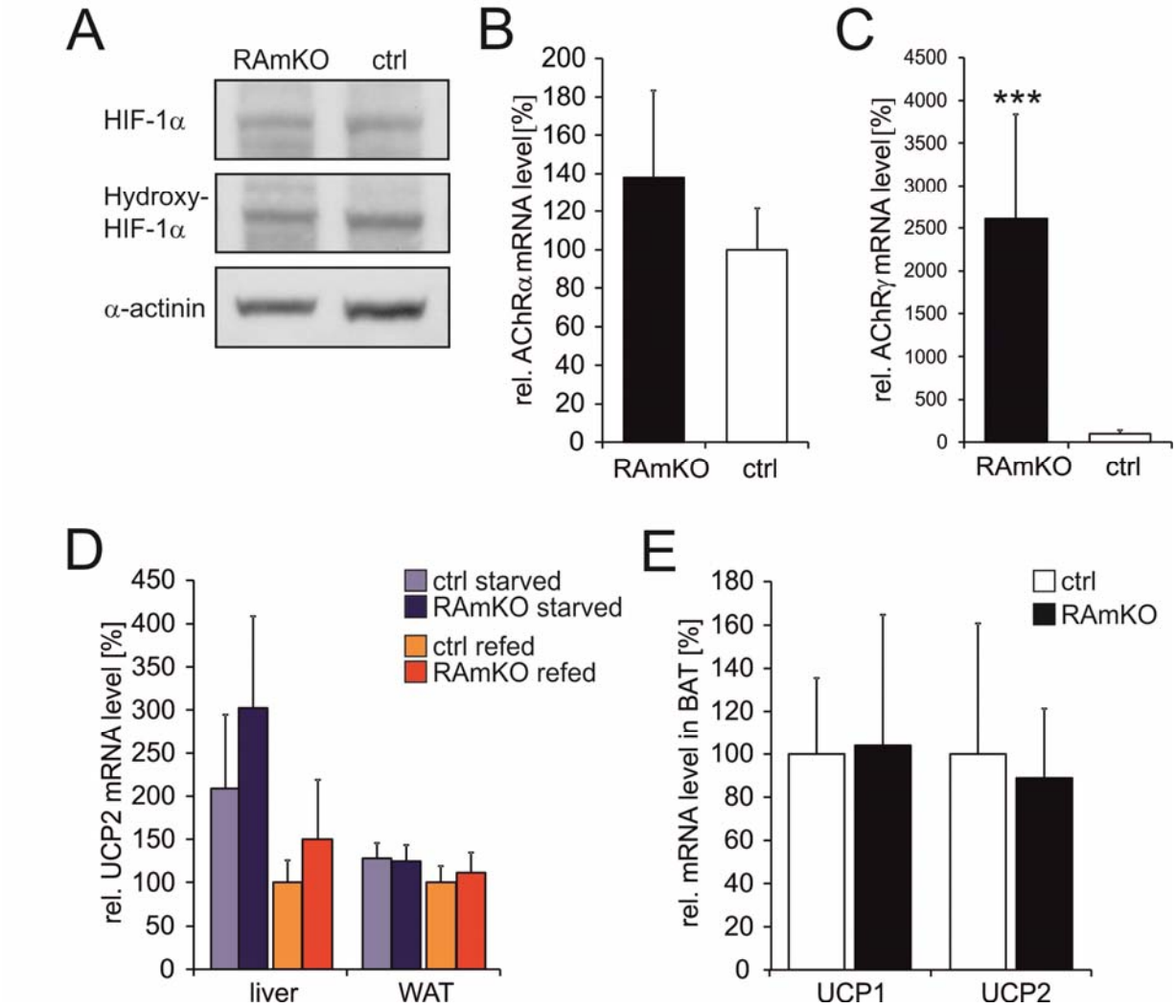

Figure S2.

(A) Representative western blot of soleus muscle lysates from 12-week-old mice using antibodies directed against the proteins indicated. The levels of hypoxia-inducible factor-1α (HIF-1α) and its hydroxylated form Hydroxy-HIF-1α are unchanged in RAmKO muscles. Equal amount of protein was loaded in each lane. An antibody against α-actinin was used as loading control.

(B, C) Relative mRNA levels of acetylcholine receptor α and γ (AChRα, γ) in soleus muscle of 12-weeks-old mice determined by qRT-PCR (n=3-4).

(D) Relative mRNA levels of UCP2 in liver and white adipose tissue (WAT) of 12-weeks-old mice determined by qRT-PCR. Mice were starved overnight and half of them were refed for 4 hrs (liver: n=7-9, WAT: n=2-4).

(E) Relative mRNA levels of UCP1 and 2 in brown adipose tissue (BAT) of 12-weeks-old mice determined by qRT-PCR (n=4-5).

All values represent mean ± SD. p values are *p < 0.05, **p < 0.01, ***p < 0.001.

Table S1

	control	RAmKO
body weight (g)	37.7 ± 3.7	19.3 ± 3.8*
Tibialis anterior (mg)	41.2 ± 1.6	30.6 ± 2.7*
epididymal fat pad (mg)	2544.5 ± 439.7	605.3 ± 458.9*
heart (mg)	104.1 ± 23.9	89.5 ± 6.0
liver (mg)	1303.6 ± 162.9	828.8 ± 94.1

Table S1.

Body weight and weight of different organs of ctrl and RAmKO mice after 100 days on HFD (n=3-5).

All values represent mean ± SD. p values are *p < 0.05, **p < 0.01, ***p < 0.001.

Table S2

	control	RAmKO
HDAC4	100 ± 44	299 ± 96**
HDAC5	100 ± 56	325 ± 159*
UCP2	100 ± 28	715 ± 126***
UCP3	100 ± 26	691 ± 144***

Table S2.

Quantification of Western blot analysis of soleus muscle lysates from 12-week-old mice for the proteins indicated. Numbers given represent average grey value ± SD after subtraction of the background. p values are *p < 0.05, **p < 0.01, ***p < 0.001.

Additional Findings

Although RAmKO mice have better metabolic parameters, such as a resistance to diet-induced obesity, they still die at an age of 17-27 weeks. There are several possibilities for the cause of this early death. RAmKO mice suffer from progressive muscle atrophy in all muscles including the diaphragm (Bentzinger et al., 2008). Atrophy of the diaphragm and the intercostal muscles could eventually lead to insufficient respiration and therefore cause premature death. Nevertheless, other reasons like kidney failure cannot be excluded. In fact, a very common complication in patients suffering from metabolic myopathies, like McArdle's disease, is kidney failure. In damaged skeletal muscle specific proteins, like creatine kinase, can enter into the bloodstream via the disrupted muscle membrane (Warren et al., 2002). The kidneys normally clear the blood from excessive proteins, but too high levels can lead to renal failure. To elucidate the cause of death we therefore did extensive blood analysis of the RAmKO mice.

RAmKO mice die of respiratory failure caused by progressive muscle atrophy

Analysis of RAmKO mice showed that 9-week-old mice have unchanged blood pH, however after 20 weeks the pH is significantly lowered (Table 1). A possible explanation is metabolic acidosis which is caused by kidney failure. As mentioned above, kidney failure in RAmKO mice would eventually be caused by to high creatine kinase levels in the blood due to muscle damage. In general, renal acidosis is associated with an accumulation of creatinine in the blood. Therefore, we checked both creatine kinase and creatinine levels in the blood of RAmKO mice (Table 1). Both parameters were unchanged, therefore we can exclude that the RAmKO mice suffer from inefficient kidney function. Interestingly, the observation that the incorporation of the Evans blue dye into muscle fibers of RAmKO mice is not increased as in other muscle dystrophies confirms that the muscle damage in RAmKO mice is not as severe as in other myopathies (Bentzinger et al., 2008).

A second type of acidosis is the so-called respiratory acidosis, caused by a build-up of carbon dioxide in the blood due to hypoventilation. Indeed, 20-week-old RAmKO mice show a significant increase of the carbon dioxide in the blood. The finding is accompanied by lower blood oxygen levels at the same age (Table 1), suggesting insufficient respiration. The fact that also for the blood gases we only see significant changes in the older mice highlights that the acidosis is coupled to the progressive muscle atrophy observed in the RAmKO mice.
In conclusion, old RAmKO mice suffer from hypoxia caused by muscle atrophy. The progression of the atrophy leads to impaired respiration and an early death.

Methods and Materials

Blood was taken from the tail vein and pH and blood gases were determined by the i-STAT system (Abbott) (n=6-7). The analysis of creatinine and creatine kinase clearance from the blood was done by the Universitätsspital Basel (n=4-6).

	9-week-old		20-weeks-old	
	control	RAmKO	control	RAmKO
pH	7.51 ±0.06	7.56 ±0.07	7.55 ±0.07	7.45 ±0.05*
pO2 [mm Hg]	82.8 ±16.3	97.3 ±17.1	90.7 ±7.2	68.7 ±5.6***
pCO2 [mm Hg]	18.5 ±5.8	16.4 ±4.0	18.5 ±2.3	32.8 ±8.2**
creatinine [umol/L]	-	-	9.5 ±1.0	7.3 ±3.6
creatine kinase [U/L]	-	-	102.3 ±60.7	93.5 ±19.8

Table 1. Blood analysis of RAmKO and control mice at different ages. Values represent mean ± SD. p values are *p < 0.05, **p < 0.01, ***p < 0.001.

CONCLUDING REMARKS

Loss of muscle mass and the regulation of whole body metabolism by the muscle are major components of several diseases including cancer, metabolic diseases and aging. Thus, it is of fundamental importance to improve the understanding of the molecular mechanisms and the signaling pathways that control muscle size and function but also the metabolic pathways regulating skeletal muscle physiology. This work demonstrates that mTORC1 controls the central metabolic pathways in skeletal muscle. Inactivation of muscle mTORC1 leads to a lethal myopathy, reduction of mitochondrial function and changes in glucose metabolism.

In this study we attempted to dissect the role of the different pathways that are influenced by mTORC1 in skeletal muscle. By assembling in a complex with YY1 and PGC-1α mTORC1 regulates mitochondrial number and activity. We could confirm that the changes in the oxidative capacity caused by mTORC1 inactivation can be rescued by the increase of PGC-1α levels (Publication 1). Moreover, the reduced mitochondrial activity also leads to a downregulation of FA metabolism genes and β-oxidation (Publication 2). Interestingly, the myopathy seems unaffected when PGC-1α levels are restored. In addition, PGC-1α seems not to play a role in the dramatic increase in glycogen content observed after mTORC1 inactivation in muscle. More likely, the increased glycogen content is regulated through the hyperactivation of PKB/Akt due to the loss of the inhibitory feedback loop from S6K on IRS-1. Other parts of glucose metabolism, namely glucose uptake and glycolysis, are independent of PKB/Akt activation in mTORC1-deficient muscle. The expression of these glycolytic genes are probably reduced due to the upregulation of HDAC4 and 5 and result in a mild effect on glucose tolerance (Publication 2 and Bentzinger et al., 2008, see appendix).

Further striking is the fact that we do not observe a classical fiber-type switch in the muscles of RAmKO mice. mTORC1 inactivation leads to structural changes in the muscle fibers such as an

upregulation of slow myosin heavy chain and other proteins typical for slow-twitch (type I) fibers (Bentzinger et al., 2008, see appendix). Additionally, the contractile properties show a shift towards slow twitch fiber type, as time to peak and relaxation time of the twitch are increased (Bentzinger et al., 2008, see appendix). From a metabolical point of view, the properties of mTORC1-inactivated muscle fibers look very different. The reduction of glycolytic proteins would fit to the fiber-type shift towards slow twitch muscles, but the RAmKO mice also show an increase in glycogen storage and a reduction of mitochondria and the oxidative capacity, arguing that the shift would go in the opposite direction, namely towards fast-twitch (type II) muscle fibers. Hence, we can conclude that mTORC1 regulates several fiber type-specific structural and metabolic properties from muscle fibers, but that there is no shift in substrate utilization. In addition, our results imply that the different fiber-type properties are partially regulated independently from each other.

With this work we show that skeletal muscle mTORC1 plays a crucial role in whole body homeostasis and energy expenditure. When mTORC1 activity is reduced in muscle, the low nutrient utilization, coupled to increased energy demand, lead to beneficial systemic effects and to a resistance to diet-induced obesity.

REFERENCES

Azzu, V., and Brand, M.D. (2010). The on-off switches of the mitochondrial uncoupling proteins. Trends Biochem Sci *35*, 298-307.

Bentzinger, C.F., Romanino, K., Cloetta, D., Lin, S., Mascarenhas, J.B., Oliveri, F., Xia, J., Casanova, E., Costa, C.F., Brink, M.*, et al.* (2008). Skeletal muscle-specific ablation of raptor, but not of rictor, causes metabolic changes and results in muscle dystrophy. Cell metabolism *8*, 411-424.

Blattler, S.M., Cunningham, J.T., Verdeguer, F., Chim, H., Haas, W., Liu, H., Romanino, K., Ruegg, M.A., Gygi, S.P., Shi, Y.*, et al.* (2012a). Yin Yang 1 deficiency in skeletal muscle protects against rapamycin-induced diabetic-like symptoms through activation of insulin/IGF signaling. Cell metabolism *15*, 505-517.

Blattler, S.M., Verdeguer, F., Liesa, M., Cunningham, J.T., Vogel, R.O., Chim, H., Liu, H., Romanino, K., Shirihai, O.S., Vazquez, F.*, et al.* (2012b). Defective mitochondrial morphology and bioenergetic function in mice lacking the transcription factor YY1 in skeletal muscle. Molecular and cellular biology.

Brand, M.D., and Esteves, T.C. (2005). Physiological functions of the mitochondrial uncoupling proteins UCP2 and UCP3. Cell metabolism *2*, 85-93.

Canto, C., Gerhart-Hines, Z., Feige, J.N., Lagouge, M., Noriega, L., Milne, J.C., Elliott, P.J., Puigserver, P., and Auwerx, J. (2009). AMPK regulates energy expenditure by modulating NAD+ metabolism and SIRT1 activity. Nature *458*, 1056-1060.

Clapham, J.C., Arch, J.R., Chapman, H., Haynes, A., Lister, C., Moore, G.B., Piercy, V., Carter, S.A., Lehner, I., Smith, S.A.*, et al.* (2000). Mice overexpressing human uncoupling protein-3 in skeletal muscle are hyperphagic and lean. Nature *406*, 415-418.

Cohen, T.J., Waddell, D.S., Barrientos, T., Lu, Z., Feng, G., Cox, G.A., Bodine, S.C., and Yao, T.P. (2007). The histone deacetylase HDAC4 connects neural activity to muscle transcriptional reprogramming. The Journal of biological chemistry *282*, 33752-33759.

Cunningham, J.T., Rodgers, J.T., Arlow, D.H., Vazquez, F., Mootha, V.K., and Puigserver, P. (2007). mTOR controls mitochondrial oxidative function through a YY1-PGC-1alpha transcriptional complex. Nature *450*, 736-740.

Duvel, K., Yecies, J.L., Menon, S., Raman, P., Lipovsky, A.I., Souza, A.L., Triantafellow, E., Ma, Q., Gorski, R., Cleaver, S.*, et al.* (2010). Activation of a metabolic gene regulatory network downstream of mTOR complex 1. Mol Cell *39*, 171-183.

Fernandez-Marcos, P.J., and Auwerx, J. (2011). Regulation of PGC-1alpha, a nodal regulator of mitochondrial biogenesis. Am J Clin Nutr *93*, 884S-890.

Fraenkel, M., Ketzinel-Gilad, M., Ariav, Y., Pappo, O., Karaca, M., Castel, J., Berthault, M.F., Magnan, C., Cerasi, E., Kaiser, N.*, et al.* (2008). mTOR inhibition by rapamycin prevents beta-cell adaptation to hyperglycemia and exacerbates the metabolic state in type 2 diabetes. Diabetes *57*, 945-957.

Gangloff, Y.G., Mueller, M., Dann, S.G., Svoboda, P., Sticker, M., Spetz, J.F., Um, S.H., Brown, E.J., Cereghini, S., Thomas, G.*, et al.* (2004). Disruption of the mouse mTOR gene leads to early postimplantation lethality and prohibits embryonic stem cell development. Molecular and cellular biology *24*, 9508-9516.

Garcia-Martinez, J.M., and Alessi, D.R. (2008). mTOR complex 2 (mTORC2) controls hydrophobic motif phosphorylation and activation of serum- and glucocorticoid-induced protein kinase 1 (SGK1). Biochem J *416*, 375-385.

Gerhart-Hines, Z., Rodgers, J.T., Bare, O., Lerin, C., Kim, S.H., Mostoslavsky, R., Alt, F.W., Wu, Z., and Puigserver, P. (2007). Metabolic control of muscle mitochondrial function and fatty acid oxidation through SIRT1/PGC-1alpha. Embo J *26*, 1913-1923.

Guertin, D.A., Stevens, D.M., Thoreen, C.C., Burds, A.A., Kalaany, N.Y., Moffat, J., Brown, M., Fitzgerald, K.J., and Sabatini, D.M. (2006). Ablation in mice of the mTORC components raptor, rictor, or mLST8 reveals that mTORC2 is required for signaling to Akt-FOXO and PKCalpha, but not S6K1. Dev Cell *11*, 859-871.

Handschin, C., and Spiegelman, B.M. (2006). Peroxisome proliferator-activated receptor gamma coactivator 1 coactivators, energy homeostasis, and metabolism. Endocr Rev *27*, 728-735.

Harper, M.E., and Himms-Hagen, J. (2001). Mitochondrial efficiency: lessons learned from transgenic mice. Biochim Biophys Acta *1504*, 159-172.

Harrington, L.S., Findlay, G.M., Gray, A., Tolkacheva, T., Wigfield, S., Rebholz, H., Barnett, J., Leslie, N.R., Cheng, S., Shepherd, P.R.*, et al.* (2004). The TSC1-2 tumor suppressor controls insulin-PI3K signaling via regulation of IRS proteins. The Journal of cell biology *166*, 213-223.

Hosokawa, N., Hara, T., Kaizuka, T., Kishi, C., Takamura, A., Miura, Y., Iemura, S., Natsume, T., Takehana, K., Yamada, N.*, et al.* (2009). Nutrient-dependent mTORC1 association with the ULK1-Atg13-FIP200 complex required for autophagy. Mol Biol Cell *20*, 1981-1991.

Houde, V.P., Brule, S., Festuccia, W.T., Blanchard, P.G., Bellmann, K., Deshaies, Y., and Marette, A. (2010). Chronic rapamycin treatment causes glucose intolerance and hyperlipidemia by upregulating hepatic gluconeogenesis and impairing lipid deposition in adipose tissue. Diabetes *59*, 1338-1348.

Inoki, K., Li, Y., Xu, T., and Guan, K.L. (2003). Rheb GTPase is a direct target of TSC2 GAP activity and regulates mTOR signaling. Genes & development *17*, 1829-1834.

Izumiya, Y., Hopkins, T., Morris, C., Sato, K., Zeng, L., Viereck, J., Hamilton, J.A., Ouchi, N., LeBrasseur, N.K., and Walsh, K. (2008). Fast/Glycolytic muscle fiber growth reduces fat mass and improves metabolic parameters in obese mice. Cell metabolism *7*, 159-172.

Jacinto, E., Facchinetti, V., Liu, D., Soto, N., Wei, S., Jung, S.Y., Huang, Q., Qin, J., and Su, B. (2006). SIN1/MIP1 maintains rictor-mTOR complex integrity and regulates Akt phosphorylation and substrate specificity. Cell *127*, 125-137.

Jager, S., Handschin, C., St-Pierre, J., and Spiegelman, B.M. (2007). AMP-activated protein kinase (AMPK) action in skeletal muscle via direct phosphorylation of PGC-1alpha. Proceedings of the National Academy of Sciences of the United States of America *104*, 12017-12022.

Khamzina, L., Veilleux, A., Bergeron, S., and Marette, A. (2005). Increased activation of the mammalian target of rapamycin pathway in liver and skeletal muscle of obese rats: possible involvement in obesity-linked insulin resistance. Endocrinology *146*, 1473-1481.

Kim, J., Kundu, M., Viollet, B., and Guan, K.L. (2011). AMPK and mTOR regulate autophagy through direct phosphorylation of Ulk1. Nat Cell Biol *13*, 132-141.

Lamming, D.W., Ye, L., Katajisto, P., Goncalves, M.D., Saitoh, M., Stevens, D.M., Davis, J.G., Salmon, A.B., Richardson, A., Ahima, R.S.*, et al.* (2012). Rapamycin-induced insulin resistance is mediated by mTORC2 loss and uncoupled from longevity. Science *335*, 1638-1643.

Laplante, M., and Sabatini, D.M. (2012). mTOR signaling in growth control and disease. Cell *149*, 274-293.

Li, X., Monks, B., Ge, Q., and Birnbaum, M.J. (2007). Akt/PKB regulates hepatic metabolism by directly inhibiting PGC-1alpha transcription coactivator. Nature *447*, 1012-1016.

Lin, J., Handschin, C., and Spiegelman, B.M. (2005). Metabolic control through the PGC-1 family of transcription coactivators. Cell metabolism *1*, 361-370.

Lin, J., Wu, H., Tarr, P.T., Zhang, C.Y., Wu, Z., Boss, O., Michael, L.F., Puigserver, P., Isotani, E., Olson, E.N.*, et al.* (2002). Transcriptional co-activator PGC-1 alpha drives the formation of slow-twitch muscle fibres. Nature *418*, 797-801.

Long, X., Lin, Y., Ortiz-Vega, S., Yonezawa, K., and Avruch, J. (2005). Rheb binds and regulates the mTOR kinase. Curr Biol *15*, 702-713.

Ma, X.M., and Blenis, J. (2009). Molecular mechanisms of mTOR-mediated translational control. Nat Rev Mol Cell Biol *10*, 307-318.

Martin, D.E., and Hall, M.N. (2005). The expanding TOR signaling network. Curr Opin Cell Biol *17*, 158-166.

McGee, S.L., van Denderen, B.J., Howlett, K.F., Mollica, J., Schertzer, J.D., Kemp, B.E., and Hargreaves, M. (2008). AMP-activated protein kinase regulates GLUT4 transcription by phosphorylating histone deacetylase 5. Diabetes *57*, 860-867.

Moresi, V., Williams, A.H., Meadows, E., Flynn, J.M., Potthoff, M.J., McAnally, J., Shelton, J.M., Backs, J., Klein, W.H., Richardson, J.A.*, et al.* (2010). Myogenin and class II HDACs control neurogenic muscle atrophy by inducing E3 ubiquitin ligases. Cell *143*, 35-45.

Murakami, M., Ichisaka, T., Maeda, M., Oshiro, N., Hara, K., Edenhofer, F., Kiyama, H., Yonezawa, K., and Yamanaka, S. (2004). mTOR is essential for growth and proliferation in early mouse embryos and embryonic stem cells. Molecular and cellular biology *24*, 6710-6718.

Peterson, T.R., Laplante, M., Thoreen, C.C., Sancak, Y., Kang, S.A., Kuehl, W.M., Gray, N.S., and Sabatini, D.M. (2009). DEPTOR is an mTOR inhibitor frequently overexpressed in multiple myeloma cells and required for their survival. Cell *137*, 873-886.

Peterson, T.R., Sengupta, S.S., Harris, T.E., Carmack, A.E., Kang, S.A., Balderas, E., Guertin, D.A., Madden, K.L., Carpenter, A.E., Finck, B.N.*, et al.* (2011). mTOR complex 1 regulates lipin 1 localization to control the SREBP pathway. Cell *146*, 408-420.

Polak, P., Cybulski, N., Feige, J.N., Auwerx, J., Ruegg, M.A., and Hall, M.N. (2008). Adipose-specific knockout of raptor results in lean mice with enhanced mitochondrial respiration. Cell metabolism *8*, 399-410.

Polak, P., and Hall, M.N. (2009). mTOR and the control of whole body metabolism. Curr Opin Cell Biol *21*, 209-218.

Puigserver, P., Rhee, J., Lin, J., Wu, Z., Yoon, J.C., Zhang, C.Y., Krauss, S., Mootha, V.K., Lowell, B.B., and Spiegelman, B.M. (2001). Cytokine stimulation of energy expenditure through p38 MAP kinase activation of PPARgamma coactivator-1. Mol Cell *8*, 971-982.

Puigserver, P., Wu, Z., Park, C.W., Graves, R., Wright, M., and Spiegelman, B.M. (1998). A cold-inducible coactivator of nuclear receptors linked to adaptive thermogenesis. Cell *92*, 829-839.

Risson, V., Mazelin, L., Roceri, M., Sanchez, H., Moncollin, V., Corneloup, C., Richard-Bulteau, H., Vignaud, A., Baas, D., Defour, A.*, et al.* (2009). Muscle inactivation of mTOR causes metabolic and dystrophin defects leading to severe myopathy. The Journal of cell biology *187*, 859-874.

Romanino, K., Mazelin, L., Albert, V., Conjard-Duplany, A., Lin, S., Bentzinger, C.F., Handschin, C., Puigserver, P., Zorzato, F., Schaeffer, L.*, et al.* (2011). Myopathy caused by mammalian target of rapamycin complex 1 (mTORC1) inactivation is not reversed by restoring mitochondrial function. Proceedings of the National Academy of Sciences of the United States of America *108*, 20808-20813.

Sancak, Y., Peterson, T.R., Shaul, Y.D., Lindquist, R.A., Thoreen, C.C., Bar-Peled, L., and Sabatini, D.M. (2008). The Rag GTPases bind raptor and mediate amino acid signaling to mTORC1. Science *320*, 1496-1501.

Sancak, Y., Thoreen, C.C., Peterson, T.R., Lindquist, R.A., Kang, S.A., Spooner, E., Carr, S.A., and Sabatini, D.M. (2007). PRAS40 is an insulin-regulated inhibitor of the mTORC1 protein kinase. Mol Cell *25*, 903-915.

Sarbassov, D.D., Ali, S.M., Kim, D.H., Guertin, D.A., Latek, R.R., Erdjument-Bromage, H., Tempst, P., and Sabatini, D.M. (2004). Rictor, a novel binding partner of mTOR, defines a rapamycin-insensitive and raptor-independent pathway that regulates the cytoskeleton. Curr Biol *14*, 1296-1302.

Sarbassov, D.D., Ali, S.M., Sengupta, S., Sheen, J.H., Hsu, P.P., Bagley, A.F., Markhard, A.L., and Sabatini, D.M. (2006). Prolonged rapamycin treatment inhibits mTORC2 assembly and Akt/PKB. Mol Cell *22*, 159-168.

Sarbassov, D.D., Guertin, D.A., Ali, S.M., and Sabatini, D.M. (2005). Phosphorylation and regulation of Akt/PKB by the rictor-mTOR complex. Science *307*, 1098-1101.

Schieke, S.M., Phillips, D., McCoy, J.P., Jr., Aponte, A.M., Shen, R.F., Balaban, R.S., and Finkel, T. (2006). The mammalian target of rapamycin (mTOR) pathway regulates mitochondrial oxygen consumption and oxidative capacity. The Journal of biological chemistry *281*, 27643-27652.

Schwander, M., Leu, M., Stumm, M., Dorchies, O.M., Ruegg, U.T., Schittny, J., and Muller, U. (2003). Beta1 integrins regulate myoblast fusion and sarcomere assembly. Dev Cell *4*, 673-685.

Sehgal, S.N., Baker, H., and Vezina, C. (1975). Rapamycin (AY-22,989), a new antifungal antibiotic. II. Fermentation, isolation and characterization. J Antibiot (Tokyo) *28*, 727-732.

Selman, C., Tullet, J.M., Wieser, D., Irvine, E., Lingard, S.J., Choudhury, A.I., Claret, M., Al-Qassab, H., Carmignac, D., Ramadani, F.*, et al.* (2009). Ribosomal protein S6 kinase 1 signaling regulates mammalian life span. Science *326*, 140-144.

Shiota, C., Woo, J.T., Lindner, J., Shelton, K.D., and Magnuson, M.A. (2006). Multiallelic disruption of the rictor gene in mice reveals that mTOR complex 2 is essential for fetal growth and viability. Dev Cell *11*, 583-589.

Tang, H., and Goldman, D. (2006). Activity-dependent gene regulation in skeletal muscle is mediated by a histone deacetylase (HDAC)-Dach2-myogenin signal transduction cascade. Proceedings of the National Academy of Sciences of the United States of America *103*, 16977-16982.

Tang, H., Macpherson, P., Marvin, M., Meadows, E., Klein, W.H., Yang, X.J., and Goldman, D. (2009). A histone deacetylase 4/myogenin positive feedback loop coordinates denervation-dependent gene induction and suppression. Mol Biol Cell *20*, 1120-1131.

Thedieck, K., Polak, P., Kim, M.L., Molle, K.D., Cohen, A., Jeno, P., Arrieumerlou, C., and Hall, M.N. (2007). PRAS40 and PRR5-like protein are new mTOR interactors that regulate apoptosis. PLoS One *2*, e1217.

Tremblay, F., Gagnon, A., Veilleux, A., Sorisky, A., and Marette, A. (2005). Activation of the mammalian target of rapamycin pathway acutely inhibits insulin signaling to Akt and glucose transport in 3T3-L1 and human adipocytes. Endocrinology *146*, 1328-1337.

Um, S.H., D'Alessio, D., and Thomas, G. (2006). Nutrient overload, insulin resistance, and ribosomal protein S6 kinase 1, S6K1. Cell metabolism *3*, 393-402.

Um, S.H., Frigerio, F., Watanabe, M., Picard, F., Joaquin, M., Sticker, M., Fumagalli, S., Allegrini, P.R., Kozma, S.C., Auwerx, J., *et al.* (2004). Absence of S6K1 protects against age- and diet-induced obesity while enhancing insulin sensitivity. Nature *431*, 200-205.

Vezina, C., Kudelski, A., and Sehgal, S.N. (1975). Rapamycin (AY-22,989), a new antifungal antibiotic. I. Taxonomy of the producing streptomycete and isolation of the active principle. J Antibiot (Tokyo) *28*, 721-726.

Warren, J.D., Blumbergs, P.C., and Thompson, P.D. (2002). Rhabdomyolysis: a review. Muscle Nerve *25*, 332-347.

Wullschleger, S., Loewith, R., and Hall, M.N. (2006). TOR signaling in growth and metabolism. Cell *124*, 471-484.

Cell Metabolism
Article

Skeletal Muscle-Specific Ablation of *raptor*, but Not of *rictor*, Causes Metabolic Changes and Results in Muscle Dystrophy

C. Florian Bentzinger,[1] Klaas Romanino,[1] Dimitri Cloëtta,[1] Shuo Lin,[1] Joseph B. Mascarenhas,[1] Filippo Oliveri,[1] Jinyu Xia,[2] Emilio Casanova,[3] Céline F. Costa,[1] Marijke Brink,[3] Francesco Zorzato,[2] Michael N. Hall,[1] and Markus A. Rüegg[1,*]
[1]Biozentrum, University of Basel, CH-4056 Basel, Switzerland
[2]Departments of Anesthesia and Biomedicine, Basel University Hospital, CH-4031 Basel, Switzerland
[3]Institute of Physiology, Department of Biomedicine, University of Basel, CH-4056, Basel, Switzerland
*Correspondence: markus-a.ruegg@unibas.ch
DOI 10.1016/j.cmet.2008.10.002

SUMMARY

Mammalian target of rapamycin (mTOR) is a central controller of cell growth. mTOR assembles into two distinct multiprotein complexes called mTOR complex 1 (mTORC1) and mTORC2. Here we show that the mTORC1 component raptor is critical for muscle function and prolonged survival. In contrast, muscles lacking the mTORC2 component rictor are indistinguishable from wild-type controls. Raptor-deficient muscles become progressively dystrophic, are impaired in their oxidative capacity, and contain increased glycogen stores, but they express structural components indicative of oxidative muscle fibers. Biochemical analysis indicates that these changes are probably due to loss of activation of direct downstream targets of mTORC1, downregulation of genes involved in mitochondrial biogenesis, including PGC1α, and hyperactivation of PKB/Akt. Finally, we show that activation of PKB/Akt does not require mTORC2. Together, these results demonstrate that muscle mTORC1 has an unexpected role in the regulation of the metabolic properties and that its function is essential for life.

INTRODUCTION

Growth of an organ during development and during adaptation in the adult can be controlled by alterations in either the number or the size of cells. The two mechanisms are fundamentally different and require distinct regulation. Rapamycin is a cell growth inhibitor used to treat a number of clinical indications including graft rejection and cancer (Tsang et al., 2007). The molecular target of rapamycin is a Ser/Thr kinase, called TOR in yeast (Heitman et al., 1991) or mTOR in mammals. The evolutionarily conserved TOR pathway controls many cellular processes, including protein synthesis, ribosome biogenesis, nutrient transport, and autophagy (reviewed in Wullschleger et al., 2006). mTOR assembles into two distinct multiprotein complexes, termed mTORC1 and mTORC2 (Jacinto et al., 2004; Sarbassov et al., 2004). mTORC1 consists of raptor (*r*egulatory *a*ssociated *p*rotein of m*TOR*), mLST8, PRAS40, and mTOR (Wullschleger et al., 2006) and is sensitive to rapamycin. mTORC2 consists of rictor (*r*apamycin *i*nsensitive *c*ompanion of m*TOR*), mSIN1, mLST8, and mTOR (Jacinto et al., 2004; Sarbassov et al., 2004).

Changes in the size of adult muscle, in response to external stimuli, are mainly due to the growth of individual muscle fibers and not an increase in fiber number (Glass, 2005). As mTOR controls cell growth, it has also been implicated in the control of muscle mass. For example, rapamycin inhibits recovery of skeletal muscle from atrophy (Bodine et al., 2001). Moreover, activation of the mTORC1-upstream component PKB/Akt induces muscle hypertrophy (Bodine et al., 2001; Pallafacchina et al., 2002; Izumiya et al., 2008), and this increase is rapamycin sensitive (Izumiya et al., 2008). Conversely, muscle fibers of mice deficient for the mTOR downstream target S6 kinase 1 (S6K1) are atrophic (Ohanna et al., 2005). In contrast, little is known of the function of rapamycin-insensitive mTORC2, whose primary readouts are thought to be the organization of the actin cytoskeleton. Moreover, mTORC2 has been shown to be the kinase that phosphorylates PKB/Akt on Ser473 (Sarbassov et al., 2005).

To circumvent the early embryonic lethality of mice deficient for raptor or rictor (Guertin et al., 2006; Shiota et al., 2006), we generated mice with floxed *raptor* or *rictor* alleles. Here we describe the phenotype of mice that lack raptor (i.e., mTORC1), rictor (i.e., mTORC2), or both proteins specifically in skeletal muscle. We find that deletion of mTORC2 does not cause an overt muscle phenotype. In contrast, mTORC1-deficient muscles manifest signs of atrophy and become progressively dystrophic. Moreover, muscles behave metabolically like fast-twitch, glycolytic skeletal muscle but exhibit structural features and contraction properties indicative of slow-twitch, oxidative muscle fibers. Biochemical analysis indicates that this phenotype can be accounted for by the absence of phosphorylation of the immediate mTORC1 downstream targets S6K/S6 and 4EBP1, the downregulation of PGC1α, and hyperphosphorylation of PKB/Akt. Finally, deficiency of both raptor and rictor results in a phenotype indistinguishable from that of muscles lacking only raptor. Importantly, PKB/Akt is still hyperphosphorylated under these conditions, suggesting that mTORC2 is not the only kinase able to phosphorylate PKB/Akt on Ser473.

RESULTS

Skeletal Muscle-Specific Ablation of *raptor* and *rictor*

To examine the function of raptor and rictor in skeletal muscle we used the Cre-loxP recombination system. To this end, we introduced loxP sites into the *raptor* locus and the *rictor* locus (Figure 1A). In

Cell Metabolism
Role of mTORC1 and mTORC2 in Skeletal Muscle

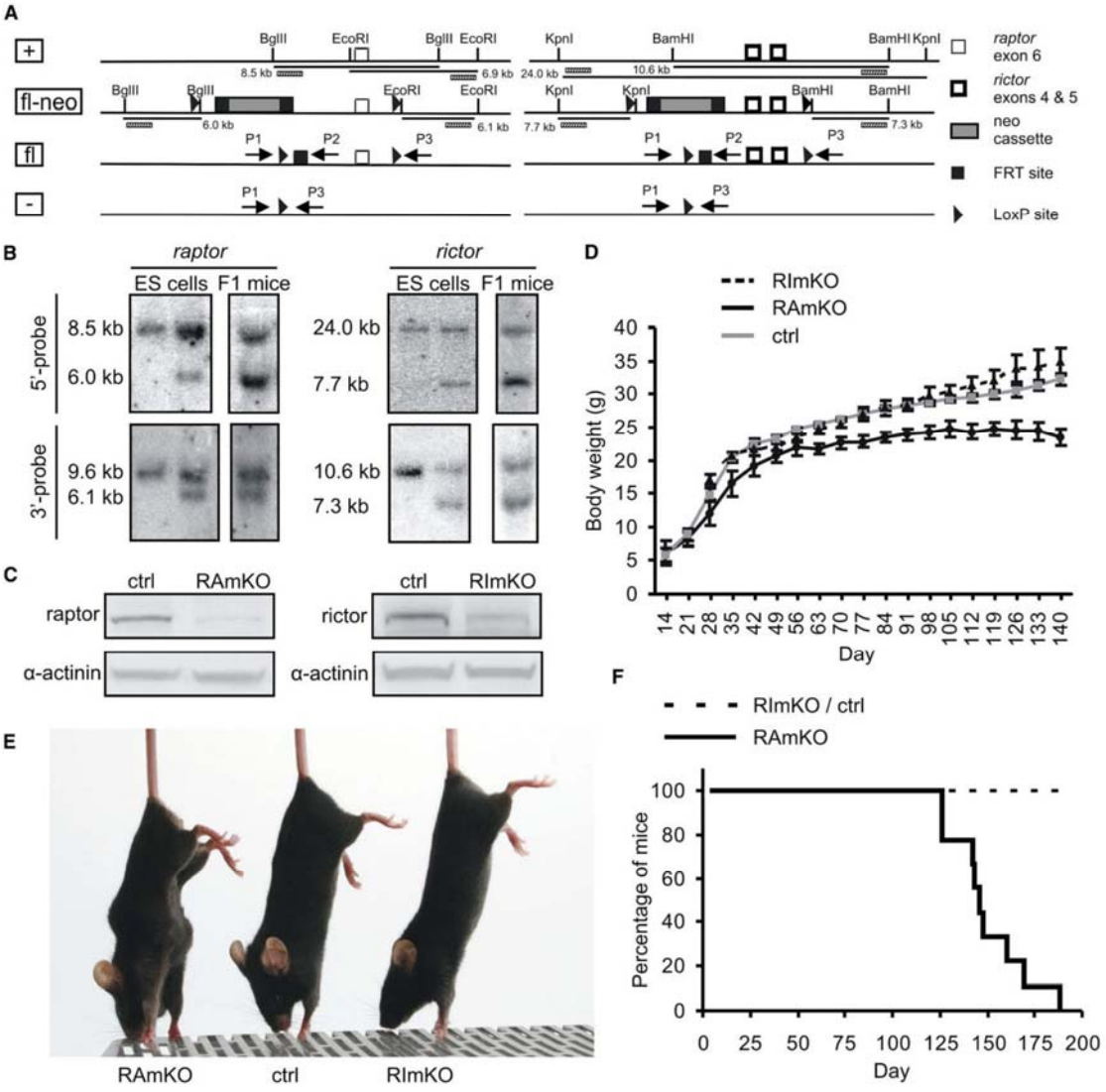

Figure 1. Targeting Strategy and Initial Characterization of RAmKO and RImKO Mice

(A) Schematic presentation of wild-type and targeted alleles of *raptor* (left panel) and *rictor* (right panel) before and after recombination. Localization and size of DNA fragments generated by particular restriction digests are indicated. Probes used for Southern blot analysis are shown by hatched bars. PCR primers for genotyping are indicated by arrows. +: wild-type allele; fl-neo: targeted allele; fl: alleles after recombination by Flp; -: alleles after recombination by Cre.

(B) Southern blot analysis of genomic DNA from ES cells and F1 progeny of resulting chimeras. Correct targeting of the 5′ end is indicated by the presence of a 6.0 kb band in the *raptor* locus and a 7.3 kb band in the *rictor* locus. Correct targeting at the 3′ end is indicated by a 6.1 kb band and a 7.3 kb band. In each blot of ES cells, wild-type is to the left.

(C) Western blot analysis of protein extracts from skeletal muscle of RAmKO and RImKO mice. Controls correspond to muscle extracts from mice that carry the floxed alleles but are negative for *HSA-Cre*. Equal protein loading is confirmed by blotting for α-actinin.

(D) Growth curve of RAmKO, RImKO, and control mice. Mice of each genotype were weighed every week. A significant difference between RAmKO and control mice ($p < 0.05$) was observed after the age of 63 days. Individual data points represent means ± SEM (n = 5 for RAmKO; n = 3 for RImKO; n = 10 for controls).

(E) Photograph of 140-day-old RAmKO, control (ctrl), and RImKO mice.

(F) Survival curve of RAmKO, RImKO, and control mice.

Cell Metabolism
Role of mTORC1 and mTORC2 in Skeletal Muscle

Table 1. Analysis of Particular Tissues in Control and RAmKO Mice

	90 day		140 day	
	ctrl	RAmKO	ctrl	RAmKO
Tibia length (cm)	2.0 ± 0.1	2.0 ± 0.1	2.0 ± 0.1	2.1 ± 0.1
Lower hindleg (mg)	449.2 ± 19.3	344.0 ± 11.4***	428.0 ± 28.0	331.6 ± 41.3**
Triceps brachii (mg)	98.3 ± 11.3	67.0 ± 10.4***	89.5 ± 14.0	68.8 ± 13.8*
Soleus (mg)	9.7 ± 0.8	7.4 ± 0.6***	9.2 ± 0.8	7.1 ± 1.2*
EDL (mg)	12.7 ± 0.8	10.3 ± 0.7***	12.0 ± 0.7	9.4 ± 1.4*
Tibialis anterior (mg)	58.3 ± 2.7	40.8 ± 2.3***	55.6 ± 1.8	39.0 ± 1.3***
Epididymal fat pad (mg)	566.4 ± 214.9	438.9 ± 93.1	616.0 ± 194.8	242.5 ± 118.7**
Heart (mg)	85.12 ± 6.6	68.1 ± 4.1*	88.5 ± 2.1	72.1 ± 4.4**
Liver (mg)	1350.9 ± 185.0	1187.5 ± 161.0	1232.0 ± 187.5	1055.0 ± 269.1

Weight or length was measured for different muscles, bones, and other organs in 90- and 140-day-old mice. p values determined by Student's t test are indicated by asterisks (n = 4 mice). Values represent means ± SD. *p < 0.05, **p < 0.01, ***p < 0.001.

both cases, Cre-mediated recombination causes a frame shift and early stop of translation. In addition, Flp recognition target (FRT) sites were inserted that flanked a neomycin resistance cassette for the selection of targeted embryonic stem (ES) cells. This cassette was removed using Flp deleter mice (Figure 1A; Rodriguez et al., 2000). Southern blot analysis confirmed successful targeting in ES cells and germline transmission of resulting chimeras (Figure 1B). Mice homozygous for the floxed allele (*raptor*$^{fl/fl}$ or *rictor*$^{fl/fl}$) were mated with heterozygous floxed mice that also expressed Cre recombinase under the control of the muscle-specific human skeletal actin (HSA) promoter (Schwander et al., 2003). Mice positive for the *HSA-Cre* transgene that also carried two floxed alleles were then analyzed. For simplicity, we refer to *HSA-Cre*; *raptor*$^{fl/fl}$ as RAmKO (for *r*aptor *m*uscle *k*nockout) and to *HSA-Cre*; *rictor*$^{fl/fl}$ as RImKO (for *ri*ctor *m*uscle *k*nockout) mice. Successful recombination of *raptor* or *rictor* was confirmed by PCR on genomic DNA isolated from tibialis muscle (Figure S1A available online). Western blot analysis of RAmKO and RImKO skeletal muscle revealed a strong reduction of the respective proteins (Figures 1C and S1B; Table S1). Residual expression of these proteins in knockout muscle is not due to leaky recombination of the targeted allele as *raptor*$^{fl/fl}$ or *rictor*$^{fl/fl}$ mice crossed to other Cre-expressing mice led to a complete loss of the respective protein in the targeted tissue (Figure S1B; Polak et al., 2008; M.N. Hall, personal communication). Thus, the low levels of raptor and rictor protein that were detected in the RAmKO and RImKO muscles are ascribable to the expression of raptor or rictor in nontargeted cells, such as fibroblasts, satellite cells, Schwann cells, and peripheral nerves, which are also contained in skeletal muscle.

Neither RAmKO nor RImKO mice showed an overt phenotype in the first weeks of life. Starting at the age of approximately 5 weeks, RAmKO mice could be distinguished from their littermates by their lower body weight. The difference became significant after day 63, and the mice remained lighter throughout life (Figure 1D). In contrast, the body weight of RImKO mice did not differ significantly from controls, although at higher age RImKO mice were slightly heavier (Figure 1D). For both RAmKO and RImKO mice, the food consumption was comparable to controls (Figure S1C and data not shown). RAmKO mice developed a pronounced kyphosis starting at the age of approximately 2 months and became markedly lean (Figures 1E and S1D). In contrast, RImKO mice appeared normal. Finally, RAmKO mice began to die at the age of 110 days, and none survived for more than 190 days (Figure 1F). RImKO mice did not die prematurely (the oldest RImKO mice now being more than 2 years old).

To examine whether the difference in weight gain was based on reduced muscle mass in RAmKO mice, we weighed different muscles and several other organs at day 90 (i.e., before the mice showed a severe phenotype) and at day 140. As shown in Table 1, all the muscles measured were significantly lighter in 90- and 140-day-old RAmKO mice compared to controls. As RAmKO mice appeared lean (Figure 1E) and only little or no fat was detected in older mice (Figure S1D), we also weighed the epididymal fat pads. Indeed, RAmKO mice contained significantly less adipose tissue at the age of 140 days (Table 1). The loss of adipose tissue does not seem to be due to changes in mitochondrial uncoupling properties as the body temperature of RAmKO mice was not different from those of control littermates (Figure S1E). The weight of the liver was indistinguishable from controls whereas hearts were again lighter (Table 1). The left ventricle mass of the heart, however, correlated with the difference in body weight (Figure S1F), indicating that the difference in heart weight is probably due to allometric scaling (Popovic et al., 2005). Moreover, the ejection fraction determined by echocardiography was indistinguishable from littermate controls (data not shown). Finally, we could not detect any recombination events in the hearts of RAmKO mice (Figure S1A). Our data therefore show that raptor deficiency in skeletal muscle causes a progressive, disproportional loss of skeletal muscle and fat.

Deficiency of mTORC1 but Not mTORC2 Causes Muscle Dystrophy

Kyphosis and early death are often signs of muscle dystrophy (Laws and Hoey, 2004). We therefore examined different skeletal muscles of RAmKO and RImKO mice using hematoxylin and eosin (H&E) staining. No change in the overall architecture of soleus and extensor digitorum longus (EDL) muscles was found in RImKO mice (Figure 2A). Muscles from RAmKO mice showed

Cell Metabolism
Role of mTORC1 and mTORC2 in Skeletal Muscle

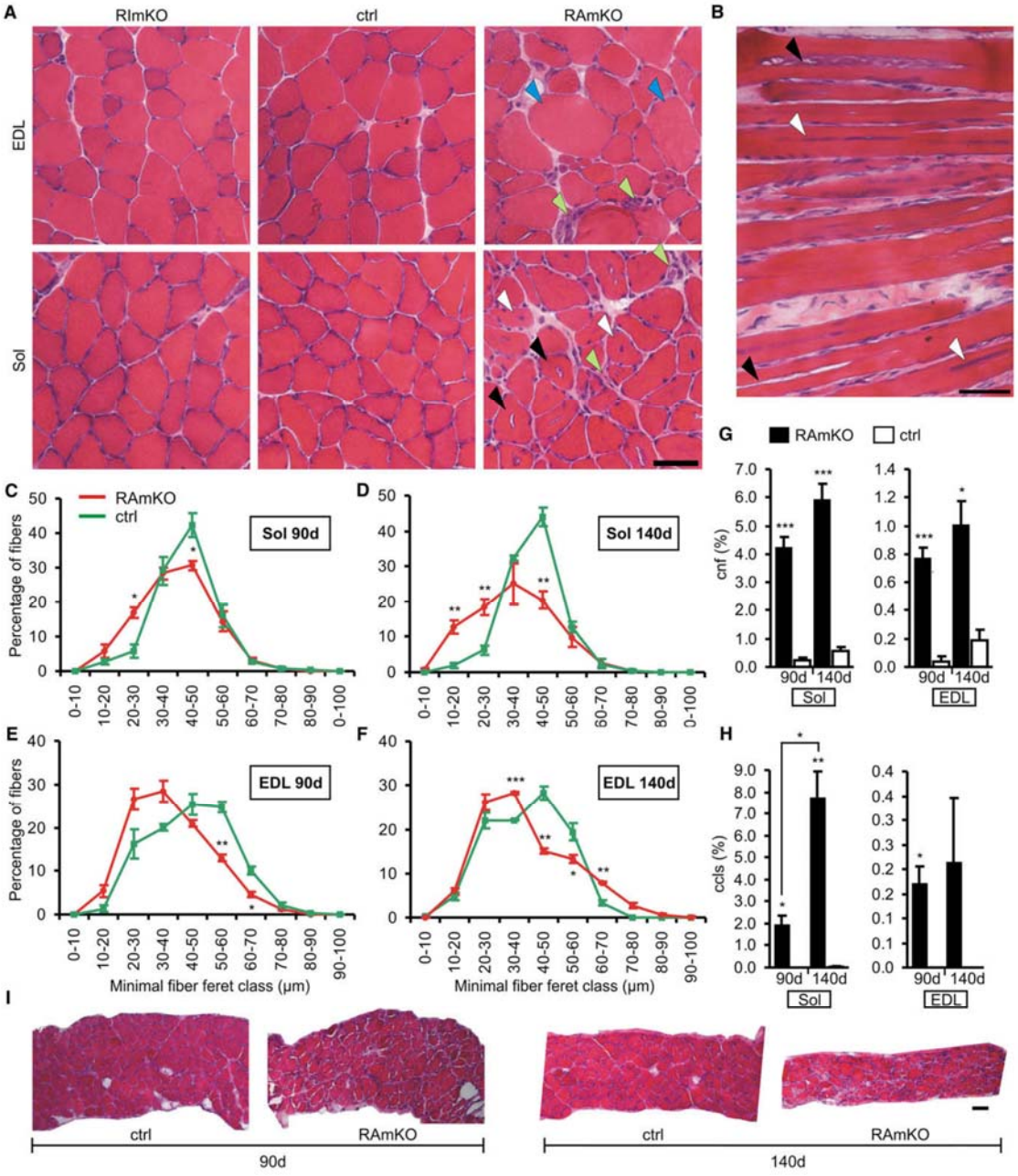

Figure 2. Muscles of RAmKO Mice Show Signs of a Progressive Dystrophy

(A) Hematoxylin and eosin (H&E) staining of muscle cross-sections from the EDL and soleus (Sol) muscle of 140-day-old mice. In EDL muscle of RAmKO mice, some large (blue arrowheads) but also small fibers are present. Centralized nuclei (white arrowheads) and central core-like structures (black arrowheads) can be found in soleus muscle of RAmKO mice. Both muscles contain many mononuclear cells (green arrowheads).

(B) Longitudinal section of soleus muscle of a 140-day-old RAmKO mouse. Besides centrally aligned nuclei (white arrowheads), central core-like structures (black arrowheads), which expand longitudinally in muscle fibers, are visible.

(C–F) Fiber size distribution in the soleus muscle of 90-day- (C) and 140-day-old (D) and in the EDL muscle of 90-day- (E) and 140-day-old (F) RAmKO and control mice.

Cell Metabolism
Role of mTORC1 and mTORC2 in Skeletal Muscle

signs of a dystrophy, such as mononuclear cells (green arrowheads) and a high number of small and large muscle fibers (blue arrowheads). In soleus muscle and to a lower extent in EDL, we also found muscle fibers with centralized nuclei (white arrowheads), indicative of ongoing de- and regeneration, and structures reminiscent of central cores (black arrowheads in Figures 2A and 2B). Quantification showed that the fiber size distribution was strongly altered in both soleus and EDL muscle (Figures 2C–2F). In addition, the number of centralized myonuclei (Figure 2G) and the relative percentage of muscle fibers with the central core-like structures (Figure 2H) were higher in RAmKO mice compared to controls. Dystrophic hallmarks seemed more pronounced in soleus than in EDL muscle. Interestingly, the severity of the dystrophy correlated with the high endogenous expression of raptor, rictor, mTOR, or PKB/Akt in wild-type soleus muscle (Figure S2A). Muscles of RAmKO mice also showed increased immunoreactivity for tenascin-c and f4/80 (Figure S2B), which mark fibrotic tissue (Ringelmann et al., 1999) and infiltrating macrophages (Austyn and Gordon, 1981), respectively. However, other dystrophic hallmarks including increased uptake of Evans blue into muscle fibers and increased levels of creatine kinase in the blood could not be detected (Figure S2C and data not shown). Similarly, the number of muscle fibers was not changed in soleus muscle of RAmKO mice compared to controls (Figure S2D). Neuromuscular junctions of RAmKO mice were indistinguishable from those in control mice (Figure S2E). Probably due to ongoing de- and regeneration, many extrasynaptic acetylcholine receptor (AChR) clusters could be detected in the diaphragm of RAmKO mice (Figure S2F). Based on the extensive muscle wasting and the high degree of fibrosis, the dystrophy was particularly severe in the diaphragm of older mice (Figure 2I), suggesting that respiratory failure might be the cause of premature death. In contrast to RAmKO mice, muscles of RImKO mice did not show any alterations in fiber size (Figure S3A) and in the cytoskeletal organization as indicated by the sarcomeric arrangement of α-actinin (Figure S3B). In summary, our data show that ablation of *raptor* and thus of mTORC1, but not of *rictor*, results in a progressive muscle dystrophy.

Skeletal Muscles of RAmKO Mice Show Alterations in Their Metabolic and Structural Properties

One of the first observations we made during the course of this work was that muscles of RAmKO mice appeared paler than those of RImKO or control mice. This difference was particularly striking for the soleus muscle (Figure 3A, arrowhead) and was not based on decreased vascularization, as revealed by staining for laminin-α5 (data not shown), which is expressed in blood vessels (Sorokin et al., 1997). To test for changes in mitochondrial function, we used an NADH-tetrazolium (NADH-TR) staining. Indeed, the activity of oxidative enzymes appeared lower in both EDL and soleus muscles of RAmKO mice (Figure 3B). Fibers with central core-like structures, which were completely devoid of NADH-TR reactivity, could be found in RAmKO soleus muscle (black arrowheads). Such a lack of NADH staining is a diagnostic feature of central core disease (Sewry et al., 2002). To further test whether the changes in NADH-TR reactivity involved mitochondria, we also examined longitudinal sections of soleus muscle by electron microscopy. Muscle of RAmKO mice was distinguishable from control muscle by a substantial loss of intermyofibrillar mitochondria, which are normally localized perpendicular to the Z disks (arrows in upper panel, Figure 3C). Only few intermyofibrillar mitochondria remained (arrow lower panel, Figure 3C). Moreover, mitochondria localized in the subsarcolemmal space seemed more densely packed and swollen in RAmKO mice (Figure S4A). As a decrease in oxidative properties is often accompanied by a compensatory increase in glycolytic activity, we performed a periodic acid-Schiff (PAS) staining. Indeed, the glycogen content was increased in both EDL and soleus muscle (Figure 3D). The increase was more pronounced in the fast-twitch EDL muscle. The glycogen content in the *gastrocnemius* muscle, which consists of a mixed population of fast- and slow-twitch fibers, was more than five times higher than in control mice (control: 21 ± 7 μmol glucose/g tissue; RAmKO: 108 ± 22 μmol glucose/g tissue; mean ± SEM; n = 4 mice). The change in oxidative capacity and glycogen content in skeletal muscle also affected overall metabolism as glucose uptake from the blood was significantly slower in RAmKO mice compared to littermate controls (Figure 3E).

High content of glycogen is indicative of fast-twitch (type II) muscle fibers. To test whether muscles in RAmKO mice also changed their structural properties, we stained EDL and soleus muscle for the slow myosin heavy chain (slMHC), a marker of slow-twitch fibers. Surprisingly, EDL and soleus muscles of 140-day-old RAmKO mice contained even more slMHC-positive muscle fibers (Figure 3F, green) than controls, and the increase of slMHC was regionalized in individual muscles (Figure S4B). In both muscles, the number of slMHC-positive fibers was approximately two to three times higher than in controls (Figures 3G and 3H). In soleus muscle of RAmKO mice, almost 100% of the fibers were positive for slMHC (Figure 3H), and this increase was also seen by western blot analysis (Figure 3I; Table S1). Moreover, other components characteristic for slow-twitch muscle, such as the slow isoform of troponinT (slTnT) and of troponinI (slTnI), were also increased in soleus muscle of RAmKO mice (Figures 3I and 3J; Table S1). Thus, deletion of mTORC1 in skeletal muscle fibers causes a shift of their metabolic properties from oxidative to glycolytic. However, this change in the metabolic characteristics of muscles is opposite to their structural properties.

Functional Characterization of Muscles in RAmKO Mice

To address whether the observed changes in metabolic and structural characteristics had consequences on the overall performance of muscle, we allowed 90-day-old mice to exercise using voluntary wheel running. The representative activity chart of a single mouse shows that running sessions of RAmKO mice were shorter and less frequent than those of controls

(G) Mean percentage of muscle fibers with centralized nuclei (cnf) in the soleus and EDL muscle of RAmKO and control mice.
(H) Percentage of muscle fibers containing central core-like structures (ccls) in soleus and EDL muscle of RAmKO and control mice.
(I) H&E staining of cross-sections of the diaphragms of 90-day- and 140-day-old RAmKO and control mice.
Individual data points and bars (C–H) represent means ± SEM (n = 4 mice). Scale bars (A, B, and I) = 50 μm. p values are ***p < 0.001; **p < 0.01; *p < 0.05.

Cell Metabolism
Role of mTORC1 and mTORC2 in Skeletal Muscle

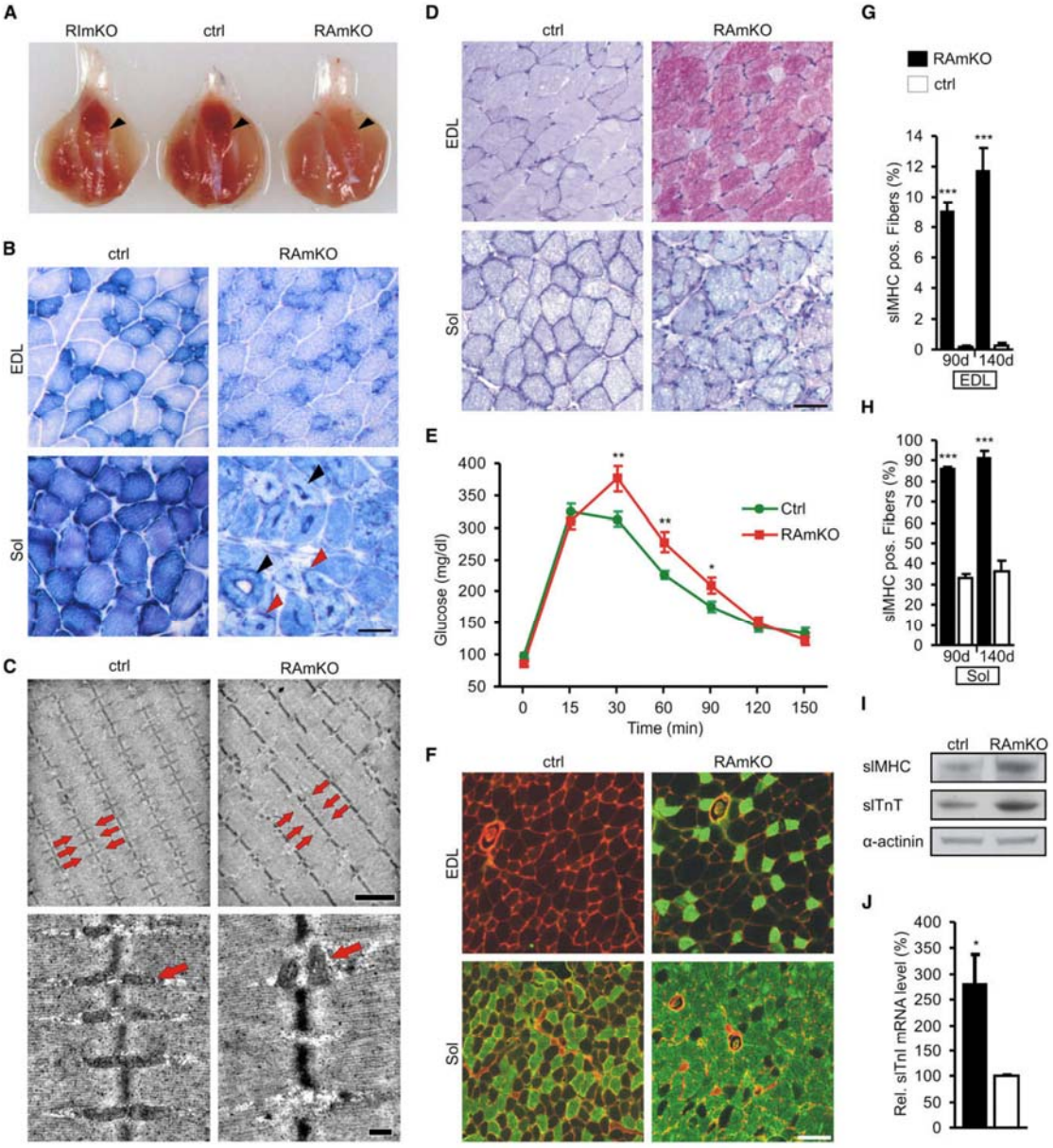

Figure 3. Metabolic and Structural Properties Diverge in Skeletal Muscle of RAmKO Mice

(A) Preparation of the entire hindleg isolated from 90-day-old mice of the genotypes indicated. Note that soleus muscle (arrowheads) is pale in RAmKO mice compared to RImKO and control mice.

(B) Activity of oxidative enzymes examined by NADH-tetrazolium staining (blue precipitate) in EDL and soleus muscle of 140-day-old mice. Central core-like structures devoid of NADH staining (black arrowheads) and increased subsarcolemmal reactivity (red arrowheads) were detected in some RAmKO soleus fibers.

(C) Electron micrographs of longitudinal sections of soleus muscle from 140-day-old mice. Most intermyofibrillar mitochondria in RAmKO muscle are lost from their specific position next to Z disks (red arrows, upper panel). Remaining mitochondria in RAmKO mice show high morphologic variability (red arrow, lower panel).

(D) Periodic acid-Schiff (PAS) staining of cross-sections from 140-day-old mice. The reaction product (magenta color) is indicative of the amount of glycogen in the tissue.

Cell Metabolism
Role of mTORC1 and mTORC2 in Skeletal Muscle

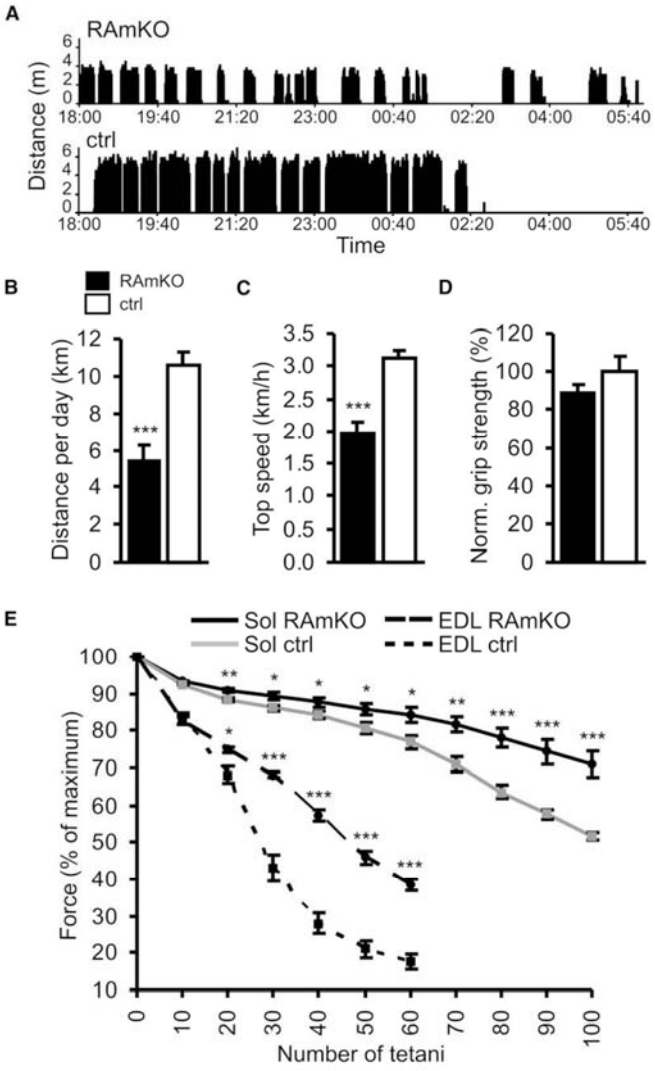

Figure 4. Exercise Performance and Muscle Physiology

(A) Representative activity chart with bins of 10 s from a single 95-day-old RAmKO mouse or a control mouse. Charts were measured from 6 pm to 6 am (dark cycle).

(B) Average distance run per day determined during one week (starting at the age of 90 days, n = 4 for RAmKO and n = 9 for controls).

(C) Average of the top 10% speed measured over one week (starting at the age of 90 days, n = 4 for RAmKO and n = 9 for controls).

(D) Grip strength of 90-day-old RAmKO and control mice. Average time mice were able to hold on a horizontal grid was normalized to body weight. Values of control mice were set to 100% (n = 3).

(E) Force capacity resistance of EDL or soleus muscle isolated from 140-day-old mice was measured during muscle fatigue induced by intermittent tetanic stimulation. Trains of 150 Hz tetani of 350 ms duration were given at 3.6 s intervals (n = 3 for RAmKO and n = 4 for control mice).

Individual data points and bars (B–E) represent means ± SEM. p values are ***p < 0.001; **p < 0.01; *p < 0.05.

(Figure 4A). When averaged over one week, the total distance run per day by RAmKO mice was ~60% of that of control mice (Figure 4B), and the top running speed was significantly lower (Figure 4C). In contrast to the aerobic wheel running task, RAmKO mice performed as well as control animals in a grip strength test on a horizontal grid (Figure 4D). To examine the contraction properties of muscles, force measurements were performed on isolated EDL and soleus muscles. In line with the observed increase of fibers expressing structural proteins characteristic of slow-twitch muscle, time to peak, half time to peak, and relaxation time of the twitch were all increased (Table 2). This difference to control mice did not reach significance in EDL muscle but was highly significant in soleus muscle (Table 2). Twitch force and maximal tetanic absolute force for both muscles were, however, significantly lower in RAmKO mice. The decrease of absolute force capacity reflects the decrease of muscle mass (Table 1) since there is no difference of the maximal tetanic force when normalized to the muscle cross-sectional area (Table 2). An intermittent maximal tetanic stimulation protocol revealed that both EDL and soleus muscles from RAmKO mice were more resistant to fatigue (Figure 4E). These data indicate that raptor-deficient muscle fibers have a reduced aerobic capacity (voluntary wheel running) like fast-twitch, glycolytic muscle fibers but exert contraction properties (isolated muscles) of slow-twitch, oxidative muscle fibers.

Inactivation of *raptor* or *rictor* Affects Activation of PKB/Akt

In search of a mechanistic explanation for the phenotypes, we examined soleus muscle of RAmKO and RImKO mice

(E) Glucose tolerance test with 65-day-old mice (n = 8 for RAmKO and n = 11 for control mice).
(F) Immunostaining for slow myosin heavy chain (sIMHC; green) and the laminin γ1 chain (red) of cross-section from 140-day-old mice.
(G and H) Quantification of sIMHC-positive muscle fibers in soleus and EDL muscle from 90- and 140-day-old mice (n = 4).
(I) Western blot analysis for sIMHC and slow troponin T (sITnT) using soleus muscle of 90-day-old mice. α-actinin is shown as a loading control.
(J) Relative mRNA levels of the slow skeletal muscle troponin I isoform (sITnI) in the soleus of 90-day-old mice as determined by qRT-PCR (n = 3).
Individual data points and bars (E, G, H, and J) represent means ± SEM. Scale bars = 50 μm (B and D), 2 μm (upper pictures, C), 250 nm (lower pictures, C), and 125 μm (F). p values are ***p < 0.001; **p < 0.01; *p < 0.05.

Table 2. Analysis of the Contractile Properties of EDL and Soleus Muscles of Control and RAmKO Mice

	EDL		Sol	
	ctrl	RAmKO	ctrl	RAmKO
Twitch				
Time to peak (ms)	10.1 ± 0.9	11.1 ± 1.2	20.3 ± 4.2	39.7 ± 2.4***
Half time to peak (ms)	3.0 ± 0.4	3.5 ± 0.5	5.6 ± 0.6	11.6 ± 1.1***
Half relaxation time (ms)	15.5 ± 2.2	16.8 ± 3.3	30.8 ± 8.7	63.0 ± 5.1***
Absolute force (mN)	54.0 ± 13.2	45.0 ± 9.7	30.0 ± 5.6	21.0 ± 8.1*
Tetanus				
Half contraction time (ms)	16.6 ± 2.0	14.4 ± 1.1*	27.5 ± 5.4	41.0 ± 5.4***
Half relaxation time (ms)	22.1 ± 1.3	24.1 ± 1.6*	55.2 ± 3.9	124.4 ± 13.2***
Absolute force (mN)	311 ± 57.6	224 ± 38.1**	205 ± 20.8	164.0 ± 42.83
Specific force (mN/mm^2)	380.2 ± 57.2	328.3 ± 62.7	311.6 ± 56.3	264 ± 66.9

Data were recorded from EDL and soleus muscles of 140-day-old mice. p values determined by Student's t test are indicated by asterisks (n = 3 for RAmKO and n = 4 for control mice). Values represent mean ± SD.

biochemically. In each experiment, at least three different mice were compared with three littermate controls. Deletion of *raptor* or *rictor* did not significantly affect the levels of mTOR (Figure 5A; Table S1). The levels of rictor were not lowered in RAmKO mice, and there was a slight decrease of raptor in RImKO mice (Figure 5A; Table S1). The amount of S6K, S6, and 4EBP1, which are the main targets of mTORC1, was not changed in RAmKO mice. However, phosphorylation of S6 and 4EBP1 was strongly decreased (Figure 5A; Table S1). In RImKO mice, mTORC1 targets were not changed, but the level and activation state of PKB/Akt and PKCα, which are both well-characterized substrates of mTORC2 (Sarbassov et al., 2004, 2005), were lower. More importantly, phosphorylation of PKB/Akt on residues Thr308 and Ser473 was strongly increased in RAmKO mice (Figure 5A; Table S1). Furthermore, the total amount of FoxO1 and FoxO3a was increased in RAmKO mice concomitant with an increase in phosphorylation of FoxO1 on Thr24 (Figure 5A; Table S1). In contrast, phosphorylation of FoxO1 on Ser316 and of FoxO3a on Thr32 was not increased.

Activation of S6K by mTORC1 causes feedback inhibition of the insulin/IGF1 pathway by affecting the levels and the phosphorylation of IRS-1 (Um et al., 2004; Harrington et al., 2004). Consistent with this notion, deficiency of mTORC1 and thus absence of S6K/S6 activation abrogated this inhibitory feedback and strongly increased IRS-1 levels in muscles of RAmKO mice (Figure 5B; Table S1). Concomitant with the high protein levels, IRS phosphorylation on Ser636 and Ser639 was increased. On the other hand, there was no significant change in either the levels or the phosphorylation of the mitogen-activated protein kinases Erk1 and Erk2 (Figure 5B; Table S1). Thus, activation of PKB/Akt is probably due to the failure of raptor-deficient muscle fibers to activate S6K and thus due to the absence of the inhibitory feedback onto IRS. The release of this feedback in muscle may require prolonged inactivation of mTORC1 as phosphorylation of PKB/Akt was not increased after 8 hr treatment of cultured C2C12 myotubes with rapamycin and was only slightly elevated after 16 hr (Figure S5C).

Next, we asked whether part of the phenotype of RAmKO mice could be based on this hyperphosphorylation of PKB/Akt. To determine whether PKB/Akt was indeed activated within muscle fibers and not in non-muscle tissue of RAmKO mice, we stained cross-sections of soleus muscle with antibodies specific for PKB/Akt phosphorylated on Ser473 (P-PKB/Akt^{S473}). Indeed, many of the muscle fibers were strongly positive for P-PKB/Akt^{S473} (Figure S5A). Akt/PKB has been shown to regulate expression of atrogenes, called *atrogin-1/MAFbx* and *MuRF-1*, via the FoxOs (Sandri et al., 2004; Stitt et al., 2004). As expected, mRNA levels for both atrogenes were significantly lower in RAmKO mice than in controls (Figure 5C). A further target of PKB/Akt is glycogen synthase kinase3β (GSK3β), which in turn inhibits glycogen synthase (Sakamoto and Goodyear, 2002). Whereas the amount of GSK3β was unaffected, phosphorylation of Ser9 was significantly increased (Figure 5C; Table S1). Moreover, glycogen phosphorylase, which is the enzyme that generates free glucose from glycogen, was downregulated (Figure 5C; Table S1). Thus, hyperphosphorylation of PKB/Akt in conjunction with downregulation of glycogen phosphorylase is probably the basis for the increased levels of glycogen observed in RAmKO mice.

In an attempt to identify the pathway that might underlie the increased number of muscle fibers expressing slMHC, we found a slight increase in the levels of calcineurin and a highly significant increase in myocyte-enhancer factor 2A (Mef2A; Figure 5C; Table S1). A slight, but not significant increase in Mef2D was also observed. The increase in Mef2A is not a consequence of the ongoing de- and regeneration in soleus muscle as Mef2A was also increased in the least affected EDL muscle (Figure S5B). In contrast to skeletal muscle in vivo, Mef2A and slMHC were not increased in cultured C2C12 myotubes upon prolonged treatment with rapamycin (Figure S5C).

Genes Involved in Mitochondrial Biogenesis Are Downregulated in RAmKO Mice

One of the most striking features of RAmKO skeletal muscle is its lower oxidative capacity that is probably due to ultrastructural changes and loss of mitochondria. Thus, we also tested whether genes involved in mitochondrial biogenesis were affected by the deletion of *raptor*. Recent evidence indicates a function of mTORC1 in the regulation of mitochondrial function via PGC1α (Cunningham et al., 2007). Consistent with these findings, transcript levels for PGC1α and for its target gene *myoglobin* were significantly reduced in RAmKO muscle (Figure 5E). Moreover, the protein levels of the PGC1α coactivator PPARγ and the mitochondrial marker cytochrome *c* oxidase IV (COX IV) were significantly decreased in RAmKO mice (Figure 5F; Table S1). These results are consistent with the low oxidative capacity of muscle from RAmKO mice, and they support the notion that this is due to loss of PGC1α.

Cell Metabolism
Role of mTORC1 and mTORC2 in Skeletal Muscle

Activation of PKB/Akt Is Independent of mTORC2

To test whether the hyperactivated state of PKB/Akt in RAmKO mice can be prevented by additional deletion of *rictor*, we generated double floxed mice and mated those with *HSA-Cre* mice. The resulting mice, called DmKO, lacked both raptor and rictor in skeletal muscle (Figure 5G; Table S1). Their overall phenotype was indistinguishable from RAmKO mice (data not shown). Like in RAmKO mice, skeletal muscle of DmKO mice contained high levels of glycogen and was less oxidative (Figure 5H). Levels of mTOR were significantly lower in DmKO mice than in either of the single knockouts (Figure 5G; Table S1). As mTORC2 was shown to phosphorylate PKB/Akt on Ser473 (Sarbassov et al., 2005), we also tested the activation state of PKB/Akt in DmKO muscle. As shown in Figure 5G and in Table S1, PKB/Akt was still hyperphosphorylated on Thr308 and Ser473 in DmKO mice. Again, phosphorylation of PBK/Akt occurred only in muscle fibers and not in non-muscle tissue (Figure 5J). In summary, these results indicate that mTORC2 is not the only kinase that phosphorylates PKB/Akt on Ser473.

DISCUSSION

Our work dissects the role of raptor and rictor (i.e., mTORC1 and mTORC2, respectively) in skeletal muscle. The *HSA-Cre* mice used for our experiments start to express Cre at the earliest stages of skeletal muscle development when the first myotubes are formed. In fully developed muscle, Cre is exclusively expressed in skeletal muscle fibers but not in non-muscle cells, such as Schwann cells, fibroblasts, or satellite cells (Schwander et al., 2003). Neither RAmKO nor RImKO mice showed any abnormalities at birth, indicating that mTORC1 and mTORC2 are not essential for muscle development. Whereas no overt phenotype was detected in RImKO mice throughout adulthood, which is consistent with another report (Kumar et al., 2008), RAmKO mice developed a progressive dystrophy and ultimately died around the age of 5 months. Interestingly, DmKO mice showed very similar pathological changes as RAmKO mice, indicating that mTOR function in skeletal muscle requires only mTORC1.

The dystrophy in RAmKO mice did not affect all muscles to the same extent. For example, diaphragm and soleus muscles were severely affected while EDL showed many fewer changes. Prominent features of the dystrophy were elevated numbers of muscle fibers with centralized nuclei and the presence of central core-like structures. Central cores are hallmarks of "central core diseases," which are inherited neuromuscular disorders with a myopathic syndrome. The most frequent causes of this group of diseases are mutations in the ryanodine receptor, which is the main protein responsible for calcium homeostasis in muscle (reviewed in Treves et al., 2008). Thus, the similarity of the pathology in RAmKO to this class of disease suggests that mishandling of intracellular calcium may underlie the disease. The low levels of PGC1α may additionally contribute to the dystrophic phenotype of RAmKO mice as conditional ablation of *PGC1α* in skeletal muscle results in a myopathic phenotype (Handschin et al., 2007). Finally, several metabolic diseases that cause accumulation of glycogen in skeletal muscle, such as Pompe's and McArdle's diseases, affect skeletal muscle function. The most severely affected patients may even die because of respiratory distress (Winkel et al., 2005). In summary, RAmKO mice show changes in muscle homeostasis that together may lead to the progressive muscle dystrophy.

Raptor Is Required for High Oxidative Capacity of Skeletal Muscle

We found that the severity of the muscle dystrophy correlated with the relative levels of raptor, rictor, mTOR, and PKB/Akt in particular muscles. Interestingly, the most affected muscles, such as soleus or diaphragm, are also those that are insulin sensitive (Song et al., 1999) and contain a high number of slow-twitch, oxidative fibers. Biochemical and morphological analysis showed that soleus muscle expressed little of the oxygen carrier myoglobin and of COX IV and contained fewer and misshaped mitochondria. A direct role of mTOR and raptor for the function of mitochondria has recently been suggested using cultured Jurkat cells (Schieke et al., 2006). Moreover, mTOR has been shown to form a complex with PGC1α (Cunningham et al., 2007), which together with its cofactor PPARγ is a key regulator of mitochondrial biogenesis and function. Consistent with a regulatory function of mTORC1 for mitochondria, mRNA levels for PGC1α and protein levels of PPARγ were decreased in RAmKO mice. Furthermore, mRNA and protein levels of target genes for PGC1α/PPARγ, such as myoglobin (Lin et al., 2002) and glycogen phosphorylase (Wende et al., 2007), were also reduced in RAmKO mice. Also, very similar to the phenotype of RAmKO mice, a reduced intermyofibrillar mitochondrial content in slow-twitch muscles has been reported in PGC1α knockout mice (Leone et al., 2005). In summary, our data indicate that mTORC1 is essential for the function of mitochondria in skeletal muscle, and they link mTORC1 to the regulation of PGC1α in vivo.

Segregation of Metabolic and Structural Properties in Skeletal Muscle of RAmKO Mice

Despite the loss of oxidative capacity and the downregulation of PGC1α, expression of slow structural proteins (sISP; Figure 5K) was increased in RAmKO mice. Analysis of the mechanical properties in EDL and soleus muscle further confirmed that both muscles adapt characteristics indicative of slow-twitch fibers. These results suggest that RAmKO mice induce a structural program for slow-twitch fibers. As muscle-specific inactivation of *PGC1α* causes a fiber-type switch to fast-contracting muscle fibers (Handschin et al., 2007) and transgenic overexpression causes an increase in oxidative muscle (Lin et al., 2002), we also tested whether any other pathways that affect muscle differentiation were altered in the RAmKO mice. Besides PGC1α, the best characterized factors involved in fiber-type determination are calcineurin/NFAT and the Mef2 transcription factors (Bassel-Duby and Olson, 2006). Of those candidate genes, the levels of calcineurin and in particular of Mef2A and Mef2D were increased in RAmKO mice. Thus, facilitated Mef2-mediated transcription may be the basis for the increased levels of sISP despite the low levels of PGC1α. Opposite regulation of PGC1α and Mef2A has also been seen in cultured cells when treated with rapamycin (Cunningham et al., 2007). Mef2 has also been shown to be dominant in the regulation of muscle fiber type as transgenic overexpression of a constitutively active form of Mef2 is sufficient to increase the number of slow muscle fibers (Potthoff et al., 2007). Mef2 is generally thought to be controlled

Cell Metabolism
Role of mTORC1 and mTORC2 in Skeletal Muscle

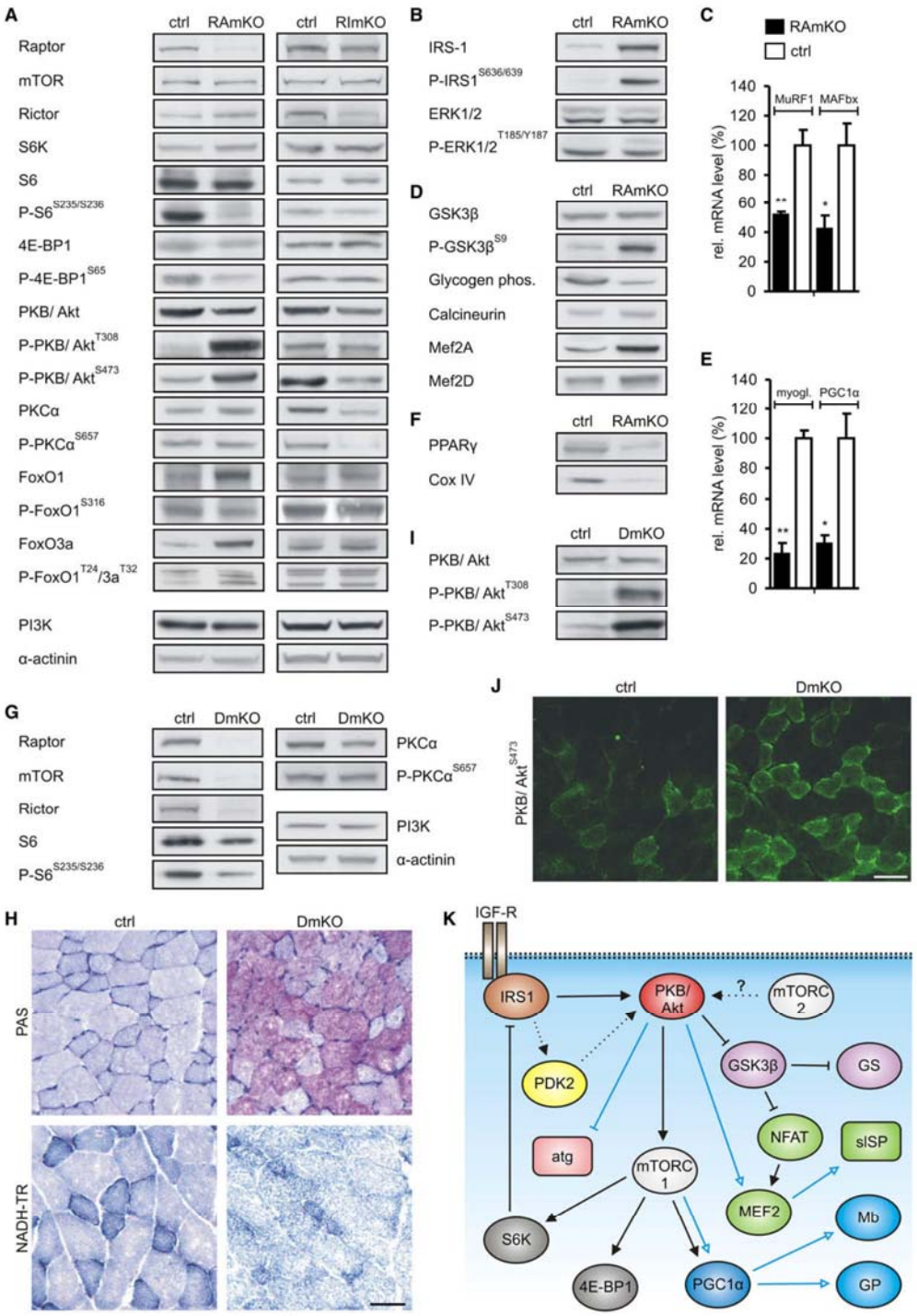

Cell Metabolism
Role of mTORC1 and mTORC2 in Skeletal Muscle

by calcium-activated processes acting via calcineurin and CaM kinase IV (Wu et al., 2000). In this context it is interesting to note that the increase of the half-relaxation time in RAmKO muscles may result from a lower removal rate of calcium from the myoplasm by the sarcoplasmic reticulum (Gollnick et al., 1991). This prolonged presence of intracellular calcium during contractile activity might contribute to the activation of calcium-dependent signaling pathways and thus to the upregulation of slSP (Figure 5K). On the other hand, it is possible that Mef2 expression is increased because of hyperactivation of PKB/Akt (Wiedmann et al., 2005). Consistent with this notion, failure to induce a pronounced phosphorylation of PKB/Akt in cultured C2C12 myotubes by treatment with rapamycin coincided with unchanged levels of Mef2A and slMHC (Figure S5C).

Raptor Deficiency Affects Protein Synthesis Directly and PKB/Akt Activation Indirectly

Ablation of mTORC1 in skeletal muscles prevented phosphorylation of S6K/S6 and 4EBP1. This branch of the mTOR signaling pathway is characterized best and has been shown to directly control protein synthesis. Impaired efficacy of protein synthesis in postnatal muscle might also be the reason for the muscles being lighter in RAmKO mice. This effect may also contribute to the shift in fiber size distribution toward smaller values. Our data thus implicate mTORC1 in the maintenance of mass even in fully innervated muscle. Therefore, they extend previous results in which mTOR inhibition by rapamycin was shown to prevent compensatory hypertrophy and recovery from atrophy but not to cause atrophy (Bodine et al., 2001). Our results are also consistent with the findings that skeletal muscles of S6K1-deficient mice are atrophic (Ohanna et al., 2005). The difference in weight of the RAmKO mice became significant only after the age of approximately 2 months, suggesting that the absence of raptor might be compensated for during early periods of muscle growth. One compensatory mechanism could be PKB/Akt-mediated phosphorylation of GSK3β as inhibition of GSK3β has been shown to cause hypertrophy in cultured C2C12 myotubes (Rommel et al., 2001). We also provide evidence that the lack of S6K activation in RAmKO mice is responsible for the hyperphosphorylation of PKB/Akt on Thr308 and Ser473 as levels of IRS-1 were highly increased. Activation of S6K has been shown to decrease the levels of IRS-1 (reviewed in Manning, 2004). Interestingly, the same hyperactivation of PKB/Akt is seen in mice with an adipocyte-specific ablation of *raptor* (Polak et al., 2008).

Raptor-Deficient Skeletal Muscles Are Small, despite High Energy Consumption

Whereas changes in mitochondrial content and function might be based on a direct influence of mTORC1 (Figure 5K), other aspects such as the loss of adipose tissue are probably a consequence of the hyperactivation of PKB/Akt. Muscle-specific overexpression of a constitutively active form of PKB/Akt causes pronounced hypertrophy (Izumiya et al., 2008). Concomitantly with the hypertrophy, mice are lean and do not become obese on a high-fat diet (Izumiya et al., 2008). In the RAmKO mice, PKB/Akt was hyperactive resulting in mice that had much less fat than control mice on a normal chow diet (Table 1) or on a high-fat diet (K.R., C.F.B., and M.A.R., unpublished observation). In contrast to mice that express the constitutively active form of PKB/Akt, lack of mTORC1 prevented the "translation" of PKB/Akt activation into muscle hypertrophy in RAmKO mice. Thus, RAmKO mice behave metabolically like mice that overexpress activated PKB/Akt but lack the hypertrophic effect on muscle. We hypothesize that the metabolic phenotype of being lean is due to the high need of muscles for glucose because of their high glycogen storage capability and their low capacity for oxidative phosphorylation. If the muscle of RAmKO mice acts as such a global glucose sink, non-muscle tissues may have to use alternative energy sources such as fatty acids. This, in turn, could result in an increased release and mobilization of fatty acids from adipose tissue. The high content of glycogen is probably based on the hyperactivation of PKB/Akt, which inhibits GSK3β, which in turn releases inhibition of glycogen synthase (Figure 5H). In addition, inhibition of GSK3β also lowers phosphorylation of NFATc and thus prolongs its activity in the nucleus (Beals et al., 1997). NFATc transcription factors, which are also targets of calcineurin (see above), are known to contribute to fiber type selection (reviewed in Wu et al., 2007). Thus, changes in NFATc activity may add to the expression of structural proteins indicative of slow-twitch muscle.

Hyperactivation of PKB/Akt Does Not Require rictor/mTORC2

Our data strongly indicate that the absence of the S6K-mediated inhibitory feedback caused phosphorylation of PKB/Akt on Thr308 and Ser473 in RAmKO mice. While phosphorylation on Thr308 is mediated by 3-phosphoinositide-dependent kinase (PDK1; Alessi et al., 1997), mTORC2 has been shown to phosphorylate PKB/Akt on Ser473 (Sarbassov et al., 2005). Consistent with such a role for mTORC2, we and others observed a

Figure 5. Biochemical Characterization

(A, B, D, and F) Western blot analysis of soleus muscle from 90-day-old RAmKO, RImKO, and control mice using antibodies directed against the proteins indicated (for details see Experimental Procedures). Equal amount of protein was loaded in each lane. Antibodies to α-actinin and PI3K were in addition used as loading controls.

(C and E) Relative mRNA levels of MuRF1, MAFbx, myoglobin (myogl.), and PGC1α in soleus muscle of 90-day-old RAmKO or control mice. Values obtained in controls were set to 100% (n = 3).

(G and I) Western blot analysis of soleus muscle from 60-day-old DmKO and control mice.

(H) PAS and NADH-TR staining on cross-sections of *triceps* muscles from 50-day-old DmKO and control mice.

(J) Immunostaining with antibodies specific for P-PKB/Akt^{S473} using cross-sections of 60-day-old DmKO and control mice.

(K) Schematic of the interactions contributing to the phenotype of RAmKO mice. Signaling pathway downstream of the insulin/IGF receptor is shown. Blue arrows with open arrowheads represent interactions that affect gene transcription; black symbols represent regulation on the protein level that activates or inhibits the targets. Abbreviations are as follows: atg: atrogenes (MuRF1 and MAFbx); GP: glycogen phosphorylase; GS: glycogen synthase; IGF-R: IGF receptor; Mb: myoglobin; slSP: slow structural proteins.

Data (C and E) represent means ± SEM. Scale bars (H and J): 50 μm. p values are $^{**}p < 0.01$; $^{*}p < 0.05$.

Cell Metabolism
Role of mTORC1 and mTORC2 in Skeletal Muscle

decrease in Ser473 phosphorylation in mice deficient for rictor (Figure 5; Shiota et al., 2006; Guertin et al., 2006; Kumar et al., 2008). We now show that, unexpectedly, muscles from mice lacking both mTORC1 and mTORC2 still showed a marked increase in PKB/Akt phosphorylation on both Thr308 and Ser473. Thus, mTORC2 is not required to phosphorylate PKB/Akt on Ser473 in vivo, indicating that skeletal muscles express a PDK2 distinct from mTORC2. A candidate for this kinase is DNA-dependent protein kinase (DNA-PK), which has been shown to phosphorylate PKBα/Akt1 in cells that are deficient for rictor in response to DNA damage (Bozulic et al., 2008). DNA-PK and PKB/Akt are localized in the nucleus of embryonic fibroblasts upon DNA damage (Bozulic et al., 2008). However, PKB/Akt phosphorylated on Ser473 in DmKO mice was expressed along the sarcolemma and not specifically localized in myonuclei. Several additional proteins have been postulated to act as PDK2, some of which are expressed in skeletal muscle and are localized to the sarcolemma (see Bayascas and Alessi, 2005 for a review).

In summary, our data show that mTORC1 is important for the function and maintenance of skeletal muscle. We provide evidence that the different aspects of the phenotype observed in RAmKO mice are probably based on the direct effect of mTORC1 on its downstream targets S6K and 4EBP1, on the function of mTORC1 to regulate mitochondrial biogenesis and function via PGC1α, or on an indirect effect on its upstream component PKB/Akt. Our data also suggest that long-term treatment with high doses of rapamycin may have detrimental effects on muscle function.

EXPERIMENTAL PROCEDURES

Antibodies

Rabbit polyclonal antibodies are as follows: 4E-BP1 (Phas-I) from Zymed, ERK1&2 pan and ERK1&2 (pTpY185/187) from Biosource, FoxO1a and FoxO1a (phospho S319) from Abcam, P-PKCα (Ser657) and Troponin T-SS (H-55) from Santa Cruz, Phospho-4E-BP1 (Ser65), PAN-actin, Akt, Phospho-Akt (Thr308), Pan-Calcineurin A, Phospho-FoxO1 (Thr24)/FoxO3a (Thr32), Phospho-GSK-3β (Ser9), Phospho-IRS-1 (S636/639), MEF2A, mTOR, PKCα, S6 Ribosomal Protein, Phospho-S6 Ribosomal Protein (Ser235/236), and p70 S6 kinase from Cell Signaling. Rabbit monoclonal antibodies are as follows: β-actin, Phospho-Akt (Ser473), Cox IV, FoxO3a (75D8), GSK-3β, IRS-1, PI3 Kinase p85, Raptor, and Rictor from Cell Signaling and PPARγ from Santa Cruz. Mouse monoclonal antibodies are as follows: α-actinin and myosin (skeletal, slow) from sigma and β-tubulin and Mef2D from BD Biosciences. Goat polyclonal antibody are as follows: GP from Santa Cruz.

Tissue Homogenization, Immunoprecipitation, SDS-PAGE, and Western Blot

Muscles frozen in liquid nitrogen were powdered on dry ice, then transferred to cold RIPA buffer supplemented with 1% Triton-X, 10% glycerol, protease inhibitor cocktail tablets (Roche), and phosphatase inhibitor cocktail I and II (Sigma). Cell lysates were incubated on ice for 2 hr, sonicated two times for 15 s and centrifuged at 13,600 g for 30 min at 4°C. Cleared lysates were then used to determine total protein levels (BCA Protein Assay, Pierce). After dilution with sample buffer, equal protein amounts were loaded onto SDS gels.

Histology and Immunohistochemistry

Muscles frozen in liquid nitrogen-cooled isopentane were fixed with 2% PFA and cut into 12 μm cross-sections. Cross-sections were permeabilized with 1% Triton/PBS for 5 min, washed with 100 mM glycine/PBS for 15 min, blocked with 1% BSA/PBS for 30 min, and incubated with specific primary antibody overnight at 4°C. Samples were subsequently washed with 1% BSA/PBS, three times for 1 hr, stained with appropriate fluorescently labeled secondary antibodies for 1 hr at room temperature. After washing with PBS, samples were mounted with Citifluor (Citifluor Ltd). General histology on cross-sections was performed using hematoxylin and eosin (H&E; Merck, Rayway, NJ, USA). NADH staining was done as described (Dunant et al., 2003). Periodic acid-Schiff staining (PAS staining system, Sigma) was performed according to the manufacturer's instruction. After H&E, NADH, and PAS staining, samples were dehydrated and mounted with DePeX mounting medium (Gurr, BDH).

SUPPLEMENTAL DATA

Supplemental Data include Supplemental Experimental Procedures, five figures, and one table and can be found with this article online at http://www.cellmetabolsim.org/supplemental/S1550-4131(08)00320-3.

ACKNOWLEDGMENTS

We thank people of the Transgenic Mouse Core Facility of the University of Basel, in particular D. Klewe Nebenius, for their help in generating the floxed mice. We are indebted to Drs. A. Felley and T. Pedrazzini at the Rodent Cardiovascular Assessment Facility of the University of Lausanne for echocardiography measurements and U. Sauder from the Microscopy Center of the University of Basel for assistance with electron microscopy. We thank Drs. D. Glass, T. Meier, and M. Sandri for reading the manuscript. This work was supported by the Cantons of Basel-Stadt and Baselland, grants from the Swiss National Science Foundation (M.N.H. and M.A.R.), the Association Francaise contres les Myopathies (F.Z.), and the Swiss Foundation for Research on Muscle Disease (M.A.R.). C.F.B. is a recipient of a fellowship from The Roche Research Foundation.

Received: June 8, 2008
Revised: August 15, 2008
Accepted: October 7, 2008
Published: November 4, 2008

REFERENCES

Alessi, D.R., James, S.R., Downes, C.P., Holmes, A.B., Gaffney, P.R., Reese, C.B., and Cohen, P. (1997). Characterization of a 3-phosphoinositide-dependent protein kinase which phosphorylates and activates protein kinase Balpha. Curr. Biol. *7*, 261–269.

Austyn, J.M., and Gordon, S. (1981). F4/80, a monoclonal antibody directed specifically against the mouse macrophage. Eur. J. Immunol. *11*, 805–815.

Bassel-Duby, R., and Olson, E.N. (2006). Signaling pathways in skeletal muscle remodeling. Annu. Rev. Biochem. *75*, 19–37.

Bayascas, J.R., and Alessi, D.R. (2005). Regulation of Akt/PKB Ser473 phosphorylation. Mol. Cell *18*, 143–145.

Beals, C.R., Sheridan, C.M., Turck, C.W., Gardner, P., and Crabtree, G.R. (1997). Nuclear export of NF-ATc enhanced by glycogen synthase kinase-3. Science *275*, 1930–1934.

Bodine, S.C., Stitt, T.N., Gonzalez, M., Kline, W.O., Stover, G.L., Bauerlein, R., Zlotchenko, E., Scrimgeour, A., Lawrence, J.C., Glass, D.J., and Yancopoulos, G.D. (2001). Akt/mTOR pathway is a crucial regulator of skeletal muscle hypertrophy and can prevent muscle atrophy in vivo. Nat. Cell Biol. *3*, 1014–1019.

Bozulic, L., Surucu, B., Hynx, D., and Hemmings, B.A. (2008). PKBalpha/Akt1 acts downstream of DNA-PK in the DNA double-strand break response and promotes survival. Mol. Cell *30*, 203–213.

Cunningham, J.T., Rodgers, J.T., Arlow, D.H., Vazquez, F., Mootha, V.K., and Puigserver, P. (2007). mTOR controls mitochondrial oxidative function through a YY1-PGC-1alpha transcriptional complex. Nature *450*, 736–740.

Dunant, P., Larochelle, N., Thirion, C., Stucka, R., Ursu, D., Petrof, B.J., Wolf, E., and Lochmuller, H. (2003). Expression of dystrophin driven by the 1.35-kb MCK promoter ameliorates muscular dystrophy in fast, but not in slow muscles of transgenic mdx mice. Mol. Ther. *8*, 80–89.

Cell Metabolism
Role of mTORC1 and mTORC2 in Skeletal Muscle

Glass, D.J. (2005). Skeletal muscle hypertrophy and atrophy signaling pathways. Int. J. Biochem. Cell Biol. *37*, 1974–1984.

Gollnick, P.D., Korge, P., Karpakka, J., and Saltin, B. (1991). Elongation of skeletal muscle relaxation during exercise is linked to reduced calcium uptake by the sarcoplasmic reticulum in man. Acta Physiol. Scand. *142*, 135–136.

Guertin, D.A., Stevens, D.M., Thoreen, C.C., Burds, A.A., Kalaany, N.Y., Moffat, J., Brown, M., Fitzgerald, K.J., and Sabatini, D.M. (2006). Ablation in mice of the mTORC components raptor, rictor, or mLST8 reveals that mTORC2 is required for signaling to Akt-FOXO and PKCalpha, but not S6K1. Dev. Cell *11*, 859–871.

Handschin, C., Chin, S., Li, P., Liu, F., Maratos-Flier, E., Lebrasseur, N.K., Yan, Z., and Spiegelman, B.M. (2007). Skeletal muscle fiber-type switching, exercise intolerance, and myopathy in PGC-1alpha muscle-specific knock-out animals. J. Biol. Chem. *282*, 30014–30021.

Harrington, L.S., Findlay, G.M., Gray, A., Tolkacheva, T., Wigfield, S., Rebholz, H., Barnett, J., Leslie, N.R., Cheng, S., Shepherd, P.R., et al. (2004). The TSC1–2 tumor suppressor controls insulin-PI3K signaling via regulation of IRS proteins. J. Cell Biol. *166*, 213–223.

Heitman, J., Movva, N.R., and Hall, M.N. (1991). Targets for cell cycle arrest by the immunosuppressant rapamycin in yeast. Science *253*, 905–909.

Izumiya, Y., Hopkins, T., Morris, C., Sato, K., Zeng, L., Viereck, J., Hamilton, J.A., Ouchi, N., LeBrasseur, N.K., and Walsh, K. (2008). Fast/Glycolytic muscle fiber growth reduces fat mass and improves metabolic parameters in obese mice. Cell Metab. *7*, 159–172.

Jacinto, E., Loewith, R., Schmidt, A., Lin, S., Ruegg, M.A., Hall, A., and Hall, M.N. (2004). Mammalian TOR complex 2 controls the actin cytoskeleton and is rapamycin insensitive. Nat. Cell Biol. *6*, 1122–1128.

Kumar, A., Harris, T.E., Keller, S.R., Choi, K.M., Magnuson, M.A., and Lawrence, J.C., Jr. (2008). Muscle-specific deletion of rictor impairs insulin-stimulated glucose transport and enhances Basal glycogen synthase activity. Mol. Cell. Biol. *28*, 61–70.

Laws, N., and Hoey, A. (2004). Progression of kyphosis in mdx mice. J. Appl. Physiol. *97*, 1970–1977.

Leone, T.C., Lehman, J.J., Finck, B.N., Schaeffer, P.J., Wende, A.R., Boudina, S., Courtois, M., Wozniak, D.F., Sambandam, N., Bernal-Mizrachi, C., et al. (2005). PGC-1alpha deficiency causes multi-system energy metabolic derangements: muscle dysfunction, abnormal weight control and hepatic steatosis. PLoS Biol. *3*, e101. 10.1371/journal.pbio.0030101.

Lin, J., Wu, H., Tarr, P.T., Zhang, C.Y., Wu, Z., Boss, O., Michael, L.F., Puigserver, P., Isotani, E., Olson, E.N., et al. (2002). Transcriptional co-activator PGC-1 alpha drives the formation of slow-twitch muscle fibres. Nature *418*, 797–801.

Manning, B.D. (2004). Balancing Akt with S6K: implications for both metabolic diseases and tumorigenesis. J. Cell Biol. *167*, 399–403.

Ohanna, M., Sobering, A.K., Lapointe, T., Lorenzo, L., Praud, C., Petroulakis, E., Sonenberg, N., Kelly, P.A., Sotiropoulos, A., and Pende, M. (2005). Atrophy of S6K1(−/−) skeletal muscle cells reveals distinct mTOR effectors for cell cycle and size control. Nat. Cell Biol. *7*, 286–294.

Pallafacchina, G., Calabria, E., Serrano, A.L., Kalhovde, J.M., and Schiaffino, S. (2002). A protein kinase B-dependent and rapamycin-sensitive pathway controls skeletal muscle growth but not fiber type specification. Proc. Natl. Acad. Sci. USA *99*, 9213–9218.

Polak, P., Cybulski, N., Feige, J.N., Auwerx, J., Ruegg, M.A., and Hall, M.N. (2008). Adipose-specific knockout of raptor results in lean mice with enhanced mitochondrial respiration. Cell Metab. *8*, this issue, 399–410.

Popovic, Z.B., Sun, J.P., Yamada, H., Drinko, J., Mauer, K., Greenberg, N.L., Cheng, Y., Moravec, C.S., Penn, M.S., Mazgalev, T.N., and Thomas, J.D. (2005). Differences in left ventricular long-axis function from mice to humans follow allometric scaling to ventricular size. J. Physiol. *568*, 255–265.

Potthoff, M.J., Wu, H., Arnold, M.A., Shelton, J.M., Backs, J., McAnally, J., Richardson, J.A., Bassel-Duby, R., and Olson, E.N. (2007). Histone deacetylase degradation and MEF2 activation promote the formation of slow-twitch myofibers. J. Clin. Invest. *117*, 2459–2467.

Ringelmann, B., Roder, C., Hallmann, R., Maley, M., Davies, M., Grounds, M., and Sorokin, L. (1999). Expression of laminin alpha1, alpha2, alpha4, and alpha5 chains, fibronectin, and tenascin-C in skeletal muscle of dystrophic 129ReJ dy/dy mice. Exp. Cell Res. *246*, 165–182.

Rodriguez, C.I., Buchholz, F., Galloway, J., Sequerra, R., Kasper, J., Ayala, R., Stewart, A.F., and Dymecki, S.M. (2000). High-efficiency deleter mice show that FLPe is an alternative to Cre-loxP. Nat. Genet. *25*, 139–140.

Rommel, C., Bodine, S.C., Clarke, B.A., Rossman, R., Nunez, L., Stitt, T.N., Yancopoulos, G.D., and Glass, D.J. (2001). Mediation of IGF-1-induced skeletal myotube hypertrophy by PI(3)K/Akt/mTOR and PI(3)K/Akt/GSK3 pathways. Nat. Cell Biol. *3*, 1009–1013.

Sakamoto, K., and Goodyear, L.J. (2002). Invited review: intracellular signaling in contracting skeletal muscle. J. Appl. Physiol. *93*, 369–383.

Sandri, M., Sandri, C., Gilbert, A., Skurk, C., Calabria, E., Picard, A., Walsh, K., Schiaffino, S., Lecker, S.H., and Goldberg, A.L. (2004). Foxo transcription factors induce the atrophy-related ubiquitin ligase atrogin-1 and cause skeletal muscle atrophy. Cell *117*, 399–412.

Sarbassov, D.D., Ali, S.M., Kim, D.H., Guertin, D.A., Latek, R.R., Erdjument-Bromage, H., Tempst, P., and Sabatini, D.M. (2004). Rictor, a novel binding partner of mTOR, defines a rapamycin-insensitive and raptor-independent pathway that regulates the cytoskeleton. Curr. Biol. *14*, 1296–1302.

Sarbassov, D.D., Guertin, D.A., Ali, S.M., and Sabatini, D.M. (2005). Phosphorylation and regulation of Akt/PKB by the rictor-mTOR complex. Science *307*, 1098–1101.

Schieke, S.M., Phillips, D., McCoy, J.P., Jr., Aponte, A.M., Shen, R.F., Balaban, R.S., and Finkel, T. (2006). The mammalian target of rapamycin (mTOR) pathway regulates mitochondrial oxygen consumption and oxidative capacity. J. Biol. Chem. *281*, 27643–27652.

Schwander, M., Leu, M., Stumm, M., Dorchies, O.M., Ruegg, U.T., Schittny, J., and Muller, U. (2003). Beta1 integrins regulate myoblast fusion and sarcomere assembly. Dev. Cell *4*, 673–685.

Sewry, C.A., Muller, C., Davis, M., Dwyer, J.S., Dove, J., Evans, G., Schroder, R., Furst, D., Helliwell, T., Laing, N., and Quinlivan, R.C. (2002). The spectrum of pathology in central core disease. Neuromuscul. Disord. *12*, 930–938.

Shiota, C., Woo, J.T., Lindner, J., Shelton, K.D., and Magnuson, M.A. (2006). Multiallelic disruption of the rictor gene in mice reveals that mTOR complex 2 is essential for fetal growth and viability. Dev. Cell *11*, 583–589.

Song, X.M., Ryder, J.W., Kawano, Y., Chibalin, A.V., Krook, A., and Zierath, J.R. (1999). Muscle fiber type specificity in insulin signal transduction. Am. J. Physiol. *277*, R1690–R1696.

Sorokin, L.M., Pausch, F., Frieser, M., Kroger, S., Ohage, E., and Deutzmann, R. (1997). Developmental regulation of the laminin alpha5 chain suggests a role in epithelial and endothelial cell maturation. Dev. Biol. *189*, 285–300.

Stitt, T.N., Drujan, D., Clarke, B.A., Panaro, F., Timofeyva, Y., Kline, W.O., Gonzalez, M., Yancopoulos, G.D., and Glass, D.J. (2004). The IGF-1/PI3K/Akt pathway prevents expression of muscle atrophy-induced ubiquitin ligases by inhibiting FOXO transcription factors. Mol. Cell *14*, 395–403.

Treves, S., Jungbluth, H., Muntoni, F., and Zorzato, F. (2008). Congenital muscle disorders with cores: the ryanodine receptor calcium channel paradigm. Curr. Opin. Pharmacol. *8*, 319–326.

Tsang, C.K., Qi, H., Liu, L.F., and Zheng, X.F. (2007). Targeting mammalian target of rapamycin (mTOR) for health and diseases. Drug Discov. Today *12*, 112–124.

Um, S.H., Frigerio, F., Watanabe, M., Picard, F., Joaquin, M., Sticker, M., Fumagalli, S., Allegrini, P.R., Kozma, S.C., Auwerx, J., and Thomas, G. (2004). Absence of S6K1 protects against age- and diet-induced obesity while enhancing insulin sensitivity. Nature *431*, 200–205.

Wende, A.R., Schaeffer, P.J., Parker, G.J., Zechner, C., Han, D.H., Chen, M.M., Hancock, C.R., Lehman, J.J., Huss, J.M., McClain, D.A., et al. (2007). A Role for the transcriptional coactivator PGC-1{alpha} in muscle refueling. J. Biol. Chem. *282*, 36642–36651.

Wiedmann, M., Wang, X., Tang, X., Han, M., Li, M., and Mao, Z. (2005). PI3K/Akt-dependent regulation of the transcription factor myocyte enhancer

factor-2 in insulin-like growth factor-1- and membrane depolarization-mediated survival of cerebellar granule neurons. J. Neurosci. Res. *81*, 226–234.

Winkel, L.P., Hagemans, M.L., van Doorn, P.A., Loonen, M.C., Hop, W.J., Reuser, A.J., and van der Ploeg, A.T. (2005). The natural course of non-classic Pompe's disease; a review of 225 published cases. J. Neurol. *252*, 875–884.

Wu, H., Naya, F.J., McKinsey, T.A., Mercer, B., Shelton, J.M., Chin, E.R., Simard, A.R., Michel, R.N., Bassel-Duby, R., Olson, E.N., and Williams, R.S. (2000). MEF2 responds to multiple calcium-regulated signals in the control of skeletal muscle fiber type. EMBO J. *19*, 1963–1973.

Wu, H., Peisley, A., Graef, I.A., and Crabtree, G.R. (2007). NFAT signaling and the invention of vertebrates. Trends Cell Biol. *17*, 251–260.

Wullschleger, S., Loewith, R., and Hall, M.N. (2006). TOR signaling in growth and metabolism. Cell *124*, 471–484.

ACKNOWLEDGMENTS

First of all, I am indebted to Prof. Markus Rüegg for granting me the opportunity to work on this exciting project. He gave me the freedom to explore my own ideas, kept me grounded and taught me not to jump to conclusions. His door was always open to spend some of his time discussing my data.

Secondly, I thank Prof. Christoph Handschin for being in my PhD committee and for his contribution to the first publication. Furthermore, I could always count on support from his group members. They helped me by providing materials and with technical advice which was very useful.

Several collaborators contributed to this thesis. Prof. Yann-Gael Gangloff and his group did a lot of work for the first publication. Prof. Thomas A. Lutz supplied equipment for the indirect calorimetry measurements, Melanie Wieland of the Universitätsspital Basel did part of the blood analysis and Dr. Anna Rostedt Punga provided medical advice. Also, I am very grateful to my former supervisor Dr. Florian Bentzinger who offered guidance for my projects and the publication process.

A warm thank you to my present and former colleagues. They provided a great working atmosphere and were always willing to sacrifice time to give me advice. I specifically have to thank my dear friend Dr. Alexander Kriz for his counsel and Dr. Regula “Mitzi” Lustenberger for proofreading this dissertation. I had the honor of supervising two very dedicated master students, Verena Albert and Barbara Kupr. Their extra hands were a great help and I thank them for their work and the time we spent together.

Last but definitely not least, I am deeply grateful for the support of my family and friends. Thank you for your patience and for listening to my moaning in the more demanding times. Fortunately, they are too many to name them all individually.